A PLASMA POLYMERIZATION INVESTIGATION AND LOW TEMPERATURE CASCADE ARC PLASMA FOR POLYMERIC SURFACE MODIFICATION

A Dissertation
presented to
the Faculty of the Graduate School
University of Missouri-Columbia

In Partial Fulfillment
of the Requirements for the Degree

Doctor of Philosophy

---

by

MARY A. GILLIAM

Dr. Qingsong Yu,
Faculty Advisor

AUGUST 2006

The undersigned, appointed by the Dean of the Graduate School, have examined the Dissertation entitled

A PLASMA POLYMERIZATION INVESTIGATION AND LOW TEMPERATURE CASCADE ARC PLASMA FOR POLYMERIC SURFACE MODIFICATION

Presented by MARY A. GILLIAM

A candidate for the degree of DOCTOR OF PHILOSOPHY

And hereby certify that in their opinion it is worthy of acceptance.

Prof. Qingsong Yu

Prof. David Retzloff

Prof. Scott Kovaleski

Prof. Stephen Lombardo

Prof. William Jacoby

To Ben, Alice, and Sam…

AKNOWLEDGEMENTS

I would like to express my sincere gratitude to both Dr. Yasuda and Dr. Yu for their support and guidance throughout my graduate career. I deeply appreciate the knowledge and experience I have gained from their vast insight in plasma technologies and interfacial engineering and I am honored to be their student.

Sincere thanks to Dr. Sunnyu Lee for serving as my co-advisor for some time and mostly for his friendship and encouragement as a mentor. I would also like to thank my distinguished PhD Committee members and I am honored to be considered worthy by them of a PhD.

Many thanks to my colleagues at the Surface Science and Plasma Technology Center for their friendship and collaboration: Kevin Young for helping me to become acclimated with the technologies, Bruce Huang for his friendship, encouragement, and insightful discussions, Andrew Ritts for his valuable contribution to the surface modification project, Jameel Feshitan for his helpful assistance with static contact angle and OES data, Yenfong Chan, and Young Jo Kim for their friendship and discussions.

Warm thanks go to Melina Young and Rita Preckshot for their friendship and support, whose tremendous assistance is deeply appreciated!

Finally, I would like to thank my parents, my husband, and my two children for their perpetual love and encouragement throughout my challenging and rewarding graduate education.

TABLE OF CONTENTS

LIST OF TABLES

LIST OF ILLUSTRATIONS

ABSTRACT

Plasma polymerization of fluorocarbon systems was investigated using the monomers C_3F_6, $C_2H_2F_4$, C_4F_{10} and C_3F_6O, which were compared to methane and butane. In fluorocarbon discharges, the luminous gas phase does not contain much polymer-forming species and the monomer deficient domain shifted to low W/FM and low GR/FM. Furthermore, for hydrocarbon systems, deposition rate was greater for RF than for AF, which was the opposite for the fluorocarbon discharges. These differences were attributed to the nature of fluorocarbons and the locations of the dissociation glow.

Surface modification treatments were performed on seven polymers using low temperature cascade arc torch (LTCAT) of Ar with or without adding reactive gas of O_2 or H_2O. Ar LTCAT treatments with low treatment times (2 s) resulted in stable, hydrophilic surfaces without surface degradation from oligomer formation, with the exception of nylon-6. The surface stability induced from Ar LTCAT treatments was attributed to the CASING effect (cross linking via activated species of inert gas). Addition of O_2 or H_2O vapor into Ar LTCAT resulted in greater wettability, but enhanced oligomer formation, which was more pronounced with H_2O. The surface oligomer formation was attributed to alkoxy degradation reactions and enhanced chain scission.

A stainless steel mesh was placed in LTCAT to remove ions and study the disturbance effects on LTCAT and on polymeric surface modification. The excited neutral species of Ar were greatly reduced by the mesh placement. In addition, grounding the mesh significantly altered the nature of the discharge. The dynamic surface characterization data indicated that while a decrease in surface damage was observed by placement of the mesh, the wettability achieved was also greatly reduced.

SECTION I

GENERAL INTRODUCTION

Low pressure plasmas are versatile, relatively environmentally-benign processes that can be used for interfacial engineering through 3 general mechanisms: (1) deposition of solid films, (2) etching of surface layers, or (3) chemical surface modification. Plasma polymerization, which involves the deposition of thin, organic films from plasma discharges, has been studied extensively over the past several decades[1-4]. The complex plasma polymerization mechanism has been described by Yasuda[1] as rapid step-growth polymerization (RSGP), in which molecular growth and subsequent deposition occurs by the recombination of free radicals in 2 simultaneous cycles. The plasma polymerization behavior of a system can be revealed by studying the locations of the energy domains for the polymerization system. The first part of this study involves an investigation into the plasma polymerization behavior of fluorocarbon systems, in comparison to hydrocarbon systems. Sections II and IV include a literature review and an experimental investigation, respectively, on fundamental aspects of the plasma polymerization behavior and locations of the energy domains of hydrocarbon and fluorocarbon plasma discharges.

Plasma processes are also useful for chemical surface modification, in which the surface layer of a material, such as a polymer, is chemically altered by the creation of new functional groups for applications involving adhesion, wettability, biocompatibility, reducing friction, etc. Although this type of modification involves the ablation of some material and the incorporation of new atoms to some extent, it is distinguished from etching and deposition processes in that only the very top surface layers are modified.

While plasma surface modification provides a unique method in tailoring surface characteristics of various polymers without affecting their bulk properties, plasma-induced degradation can be significant and the causes are not well understood, mainly due to the complex nature of the plasma environment.

In comparison with traditional plasma processes, a new and very different plasma technique, low-temperature cascade arc torch (LTCAT) plasma possesses many unique advantageous features in surface modification of polymeric materials. LTCAT consists of a beam of mainly electronically excited Ar neutrals, which provides an energetically milder source of polymeric surface treatment. Furthermore, LTCAT treatments are fast and effective and allow for ease of industrial scale-up. The literature review in Section III along with experimental investigations presented in Sections V, VI, and VII involve LTCAT surface modification of polymers. The effects of the treatments are presented and discussed, as well as the effects of a mesh disturbance in the system and comparisons among the treated polymers.

SECTION II

LITERATURE REVIEW OF PLASMA POLYMERIZATION

2.1 Domains of Plasma Polymerization

The polymerization rate in a plasma polymerization system is dependent on the energy density in the plasma phase[4]. The value of the power input, W, by itself does not have much meaning unless the medium to which the energy is applied is specified. In a plasma polymerization system, the energy supplied to the mass of monomer more accurately defines the energy domain. In practice, the energy density is calculated by W/FM (J/g), in which FM represents the mass flow rate of the monomer (F is the flow rate (mol/s) and M is the molecular weight). Studies have shown that the composite energy input parameter, W/FM, is very effective in describing the plasma polymerization behavior of a system and elucidating the different domains of plasma polymerization[4-7]. The energy deficient domain exists at low W/FM, in which the formation of polymer-forming species is dependent on the energy input rate, and additional energy input creates more polymer-forming species. In this domain, the deposition rate linearly increases with W/FM. The energy density of a system reaches an energy saturation point or critical energy input, $(W/FM)_c$, above which the addition of energy does not create more polymer-forming species. At higher values of $(W/FM)_c$, the creation of polymer-forming species is not dependent on the energy input rate, and this domain is termed the monomer deficient or more appropriately, the "polymer-forming species deficient domain".

The behavior of any plasma polymerization system and the value of $(W/FM)_c$ depend on the bond energies of the monomer molecules. In order to correlate the

molecular bond energies to W/FM, Yasuda and Wang[7] proposed that the normalized bond energy, Φ, can be obtained by dividing the total bond energy in a molecule by the molecular weight, M,

$$\Phi = \frac{\Sigma(bond\_energy)}{M} \tag{1}$$

Thus, $(W/FM)_c$ is proportional to the normalized bond energy, as shown below,

$$(W/FM)_c = \alpha\Phi \tag{2}$$

in which the dimensionless value of α is dependent on the reactor configuration.

2.2 Mass Balance and Deposition Rate in a Plasma Polymerization System

The mass balance in a plasma polymerization system can be performed as follows, using W_1 as the total mass flow rate of monomer into the system, W_2 as the total mass of the deposited monomer, and W_3 as the total mass flow rate of the monomer exiting the system[4].

$$W_1 - W_3 = W_2 \tag{3}$$

W_2 is related to the local mass deposition rate, k_1 (kg/m^2 s) by the following, in which S is the total surface area onto which deposition occurs.

$$W_2 = \oint_S k_1 ds \tag{4}$$

$$S = \oint ds \tag{5}$$

The local deposition rate on a substrate surface in a plasma polymerization system can be expressed by the mass deposition rate, k_1 (kg/m^2 s) and is proportional to the input power for any specified monomer and system[4]. However, the deposition rate is different for various monomer flow rates and the normalized deposition rate, k_0 (1/m^2) is more

useful in examining the plasma polymerization domains. The normalized deposition rate is obtained from:

$$k_0 = \frac{k_1}{M_i} \tag{6}$$

The deposition rate is more conveniently expressed in terms of film thickness growth rate, GR (m/s). A study by Miyama and Yasuda[6] has indicated that the plot of the normalized deposition rate using the thickness growth rate, GR/FM, versus W/FM for methane and butane data combined using various flow rates and operational times resulted in single, normalized curves for each RF and AF frequency.

2.3 The Effect of the Frequency on Plasma Polymerization

A different type of polymerization can occur on the cathode in DC discharges and on the electrodes in low frequency AF discharges, termed "cathodic polymerization"[6,8-12], which has been investigated for coating electrically conducting surfaces, such as for corrosion protection[13-15]. Recent discoveries have shown that cathodic polymerization differs from plasma polymerization in the negative glow, in that a dominant dissociation glow is present on the cathode, where most of the monomer activation and deposition is focused[4,9,12,16]. The dissociation glow is characterized by low energy electrons and other dissociated reactive species that possess enough energy to break typical molecular bonds present in organic discharges (~ 1-6 eV), but not ionize atoms and molecules (~ 10-25 eV). Cathodic deposition in DC discharges is controlled by the current density on the cathode, the mass of monomer, and the system pressure, not on W/FM.

In alternating frequency (AF) discharges with low frequency (<100 kHz), two different polymerization processes occur (1) cathodic polymerization on the electrodes, which is dependent on the current density (mA/cm^2)[6,10,17] and (2) plasma polymerization in the negative glow, which is controlled by W/FM[6,16]. In alternating glow discharges with a low frequency (<100 kHz), each electrode is a cathode in a half-cycle, and a core of dissociation glow is present on each electrode. The deposition rate on the electrode surfaces in a low frequency trimethylsilane (TMS) discharge has been shown to be half of the deposition rate on a cathode surface in DC discharge[8]. In radio frequency (RF, 13.56 MHz) discharges, cathodic deposition is eliminated, and the dissociation glow moves away from the electrode surfaces. Plasma polymerization in the negative glow regions is the dominant deposition mechanism in RF discharges[6].

2.4 Fluorocarbon Plasma Discharges

Fluorocarbon discharges, which are used extensively in the semiconductor industry for etching, can also deposit plasma polymers, depending on the F/C ratio and chemical features of the monomer and any additive gases. The characteristics of fluorocarbon films include extremely low surface energies, low friction coefficients and biocompatibility[3]. Iriyama and Yasuda[18] have shown that fluorocarbon monomers with F/C ratios of about 3 or greater are generally non-plasma polymerizing, while F/C ratio of 2 or less indicates that plasma polymerization is likely. Furthermore, the addition of H in a system reduces the presence of F by the formation of stable HF, which enhances the polymerizing capability of the fluorocarbon plasma[3,19]. The presence of oxygen in the system, except in an epoxide ring, decreases the deposition rate by quenching the

polymerizing carbon species into volatile gases that exit the plasma, thus limiting polymerization[3].

Many fluorocarbon gases can be used for etching or plasma polymerization, depending on some factors of the discharge. The relative occurrence of ablation and deposition can change with the density of highly electronegative F atoms dissociated from the monomer, in which electron attachment forms reactive F^-. Thus, as the W/FM of a fluorocarbon system increases, increased F^- in the discharge enhances the ablation effects[19,21,22] and a decrease in GR/FM may be observed at a W/FM value that is less than the actual onset of complete monomer fragmentation.

An investigation by Yasuda[23], et. al found that activation of fluorocarbon monomer begins at the tip of the glow and molecular fragmentation is greater inside the glow, where the F/C ratio of the deposited plasma polymer is low. In addition, as the energy density increases in an RF system, ablation effects become significant and the ratio of F/C in the plasma polymer decreases. For low frequency discharges, the F/C ratio in the plasma polymer on the substrate was reported to be higher than on the electrodes, and the situation was reversed for RF discharges[24].

2.5 References for Sections I and II

1. Yasuda, H., *Plasma Polymerization*, Academic Press, Inc., Orlando, Florida (1985).

2. Morosoff, N., in *Plasma Deposition, Treatment, and Etching of Polymers*, d'Agostino, R. (ed.), Academic Press, Inc., San Diego, CA (1990), Ch. 1.

3. d'Agostion, R., Cramarossa, F., and Fracassi, F., in *Plasma Deposition, Treatment, and Etching of Polymers*, d'Agostino, R. (ed.), Academic Press, Inc., San Diego, CA (1990), Ch. 2.

4. Yasuda, H., *Luminous Chemical Vapor Deposition and Interface Engineering*, Marcel Dekker, New York (2005).

5. Yasuda, H. and Hirotsu, T., *J. Polym. Sci., Polym. Chem. Ed.*, **16**, (1978) 743.

6. Miyama, M. and Yasuda, H. K., *J. Appl. Polym. Sci.*, **70**, (1998) 237.

7. Yasuda, H. and Wang, C.R., *J. Polym. Sci., Polym. Chem. Ed.*, **23** (1985) 87.

8. Yu, Q. S. and Yasuda, H. K., *J. Vac. Sci. and Tech., A-Vacuum Surfaces & Films*, **19**, no. 3 (2001) 773.

9. Yu, Q. S., Huang, C., and Yasuda, H. K., *J. Polym. Sci. A Polym. Chem.*, **42** 1042 (2004).

10. Yu, Q. and Yasuda, H. K., *Plasm. Polym.*, **7**, no. 1, (2002) 41.

11. Yu, Q., Yasuda, H., Moffitt, C.E., Wieliczka, D.M., and Yasuda, H., *J. Vac. Sci. and Tech., A-Vacuum Surfaces & Films*, **19**, no. 5 (2001) 2163.

12. Yasuda, H. and Yu, Q., *J. Vac. Sci. and Tech., A-Vacuum Surfaces & Films*, **22**, no. 3 (2004) 472.

13. Yu, Q., Deffeyes, J., and Yasuda, H.K., *Prog. Org. Coat.*, **42**, (2001) 100.

14. Yu, Q., Deffeyes, J., and Yasuda, H.K., *Prog. Org. Coat.*, **43**, (2001) 243.

15. Yu, Q., Deffeyes, J., and Yasuda, H.K., *Prog. Org. Coat.*, **44**, (2002) 37.

16. Yasuda, H. and Yu, Q., *Plasma Chem. Plasma Process.*, **24** (2004) 325.

17. W.-H. Tao and H. K. Yasuda, *Plasma Chem. Plasma Process.*, **22,** no. 2, (2004) 313.

18. Iriyama, Y. and Yasuda, H., *J. Polym. Sci. A Polym. Chem.*, **30** (1992) 1731.

19. Masuoka, T. and Yasuda, H., *J. Polym. Sci., Polym. Chem. Ed.*, **20** (1982) 2633.

20. Iriyama, Y., Yasuda, T., Cho, D.L., and Yasuda, H., *J. Appl. Polym. Sci.*, **39** (1990) 249.

21. Yanagihara, K. and Yasuda, H., *J. Polym. Sci., Polym. Chem. Ed.*, **20** (1982) 1833.

22. Yasuda, H. and Hsu, T., *Surf. Sci.*, **76** (1978) 232.

23. Yasuda, H., Morosoff, N., Brandt, E.S., Reilley, C.N., *J. Appl. Polym. Sci.*, **23** (1979) 1003.

24. Yasuda, H., *Luminous Chemical Vapor Deposition and Interface Engineering*, Marcel Dekker, New York (2005) p. 138.

SECTION III

LITERATURE REVIEW OF POLYMERIC SURFACE MODIFICATION USING LOW TEMPERATURE PLASMAS

3.1 Introduction to Polymer Surface Modification

Polymers cannot be selected for a particular application based solely on the bulk properties of the material. Surface characteristics play a vital role in the success of the application. Polymer surface modification techniques can be employed to improve adhesion of the polymer, wettability, biocompatibility, barrier properties, and optical reflection, susceptibility to harsh agents, and reducing friction, among other objectives[1-6]. Surface modification techniques include mechanical treatments, e.g., roughening by abrasion, wet-chemical treatments with strong acids or bases, exposure to flames or a corona discharge[7]. However, these treatment techniques have considerable drawbacks. For example, wet chemical treatment involves many additional processing steps such as washing, rinsing, and drying, and constitutes large amount of toxic waste disposal problem and cost. Low-temperature plasma treatment provides a versatile, reproducible, and environmentally benign method in modifying polymer surfaces while maintaining their desirable bulk properties[4,8]. However, bombardment of high-energy species in plasma, such as ions, accelerated electrons, and VUV/UV irradiations, can bring about significant damage on the polymer surfaces. In addition, the complex nature of the plasma makes it difficult to selectively isolate beneficial surface reaction mechanisms and minimize detrimental effects.

Plasma techniques can be used to modify a very thin surface layer of a polymer without altering the bulk characteristics of the polymer. In addition, plasma treatments can involve chemical modification of the surface, etching of the surface material, or plasma polymerization, in which a plasma polymer is deposited on the surface[9-11]. The first process is the focus of this investigation, which involves surface modification of polymers by chemically altering the surface properties without significant etching of polymer or deposition of new material. Several types of discharges that have been employed to modify polymeric surfaces include corona discharges, flame treatments, low-pressure non-equilibrium plasmas, and atmospheric non-equilibrium plasmas[7,12-14]. More recently, a discharge technique that involves a high flux of excited species of a noble gas directed at a polymer surface called low-temperature cascade arc torch (LTCAT) has demonstrated excellent results in improving adhesion and wettability of polymeric surfaces with minimal surface degradation[6,15-18].

Plasma discharges can chemically modify a polymer surface by surface functionalization using reactive gas plasma[9,13,14,19-35], in which new surface functional groups are produced, or by surface cross-linking, which includes the CASING process (Cross-linking via Activated Species of Inert Gases) with a plasma such as argon or helium[27,36-40]. The reactive plasmas of some gases (such as O_2, N_2, NH_3, CF_4, H_2O, CO_2, air, etc.) can result in the incorporation of some of the species of the gas into the surface functionalities of the polymer. The incorporation of such species in the polymer surface can be regarded as implantation of new moieties, which is distinguished from the deposition of plasma polymer film in a process called plasma polymerization[9]. The

reactions that occur on the polymer surface during a plasma treatment involve the production of free radical sites on the polymer surface that can react with the surrounding polymer molecules and the plasma-phase species. Radical sites that are not consumed during plasma exposure can be quenched by components in the ambient air, mainly oxygen, moisture, and to a less extent by nitrogen, upon exposure to atmosphere[13,19,21,28,39-42].

Although plasma techniques can be used to modify a polymer surface through surface functionalization and surface cross-linking, it should be pointed out that plasma treatment could result in polymer degradation and surface instability[7,23,43]. Many studies of the surface modification of polymers using conventional plasma techniques have shown certain degree of surface damage from vacuum ultraviolet (VUV) and ultraviolet (UV) radiation and continuous bombardment of high-energy, charged species[5,7,41,44]. Surface instability can result from the degradation of the top layer of macromolecules into low molecular weight oxidized material (LMWOM), which typically can be removed from the polymer surface with a polar solvent[5,6,13]. The LMWOM give rise to a weak boundary layer that is detrimental to many applications, including wettability and adhesion[5,14,45]. In addition, etching of the polymer macromolecules into volatile species can also create adverse effects on the polymer application. It is important to note that the extent of degradation of a polymer during a plasma surface modification process depends on the polymer's sensitivity to the plasma phase. Hence, the polymer structure, the energy levels and abundance of the reactive plasma species, and the wavelengths and

intensities of the photons present can determine the relative occurrences of surface functionalization, cross-linking, and degradation reactions.

This review outlines the effects of plasma constituents on the polymer surfaces from the standpoint of the beneficial consequences (surface functionalization and surface cross-linking) and degradation (etching of polymer into volatile species and the formation of LMWOM) on the polymer surface. Surface stability of the polymer after plasma treatment is vital for the application, which is an issue that is discussed in the section entitled "Surface dynamics of plasma treated surface & stability". Finally, the application of LTCAT to polymer surface modification is presented with regards to the characteristic features of the technique and the advantages offered over traditional plasma treatment of polymers.

3.2 Surface Treatment Effects of Plasma on Polymers

Low-temperature discharges contain many reactive species including photons, ions, high-energy electrons, free radicals, electronically excited molecular and atomic species, and ground-state neutrals. Once a polymeric material is placed in a plasma environment, the polymer surface is subject to continuous bombardment by these plasma species that can react with the surface structure, change the surface chemistry and modify the surface characteristics. Because of the plasma sheath formation around the polymer substrate, positive ions can be further accelerated by the sheath potential, and thus promote high-energy ion bombardment on the surface. Plasma surface modification treatments of polymers are aimed to bring about *surface functionalization*, which creates

new surface functional groups and thus new surface properties. Modification treatments typically involve the incorporation of some new atoms and the chemical abstraction of others present in the polymer, but are distinguished from deposition of new material and plasma etching, which involves the ablation of a significant amount of macromolecules into volatile species[9].

Figure 3.1 illustrates the interactions of the various plasma species with the polymer surface.

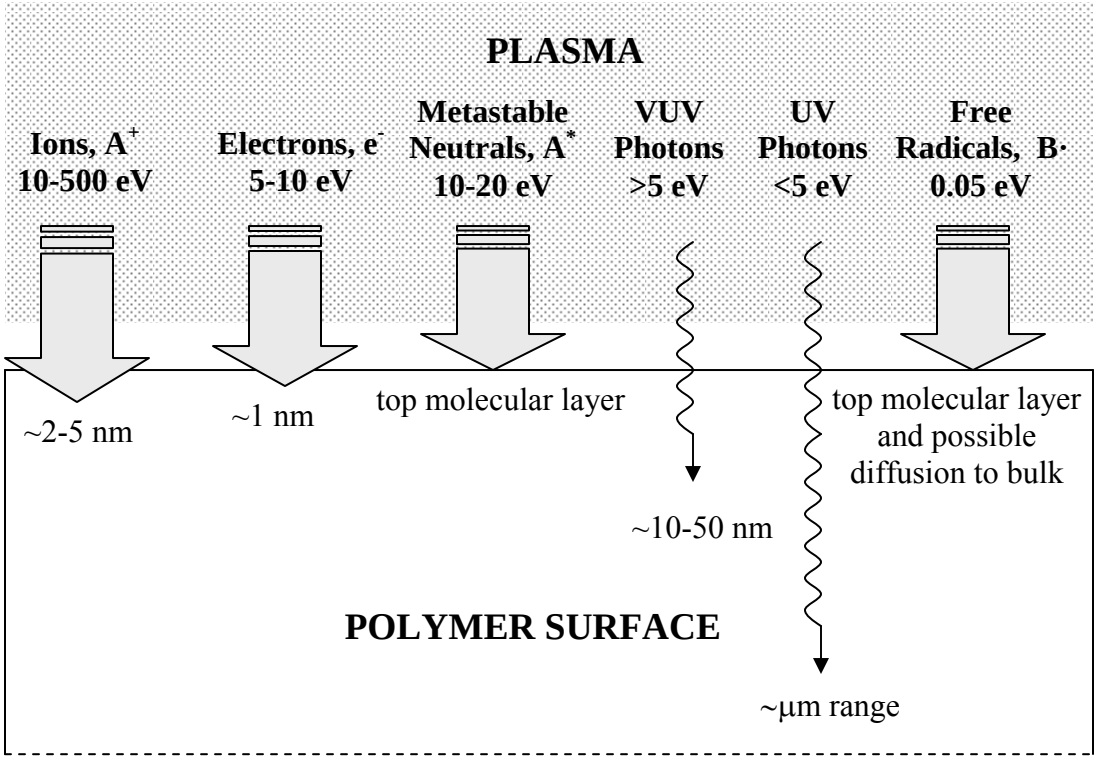

Figure 3.1. Schematic illustration of the interactions of the plasma phase species with the polymer surface (summarized from references 41, 61, and 104).

When a polymer is placed in plasma, a sheath is formed around the surface that accelerates nearby ions. Some electrons that contain high enough kinetic energy can overcome the sheath potential and impact the polymer surface. These charged species bombard the surface with high energy that allows them to react with the surface macromolecules or penetrate the surface and transfer their energy to the polymer. Energy transfers could also result from diffusion of metastable neutral species and irradiation by photons that absorb into the polymer surface layers. Energy transfers from the plasma species to the polymer can cause ablation of hydrogen or side-group species or chain scission, depending on the energy levels and the polymer structure. Free radicals that exist in reactive gas plasma can diffuse to the polymer surface and cause various chemical reactions, including abstraction of hydrogen or other side-group species and incorporation of chemical species into the polymer.

Much is still unknown about the complex reaction mechanisms that occur on the polymer surface during plasma treatment. Figure 3.2 presents possible reaction pathways that can occur at the plasma-polymer interface during plasma surface treatments of polymers and bring about various outcomes. Many plasma species including ions, photons, electrons, atoms, and free radicals can cause chain scission or hydrogen or side-group ablation, which results in the formation of surface radicals. However, high energy ions that are accelerated to the surface by the sheath potential have a greater tendancy for chain scission and subsequent degradation. The plasma-activated surface macromolecules can form covalent bonds with species in the plasma for surface functionalization, create a cross-linked or branched network with other surface

macromolecules, or further react to degrade into volatile etch products or LMWOM. However, the lack of selectivity during a plasma treatment makes it difficult to optimize specific reaction pathways.

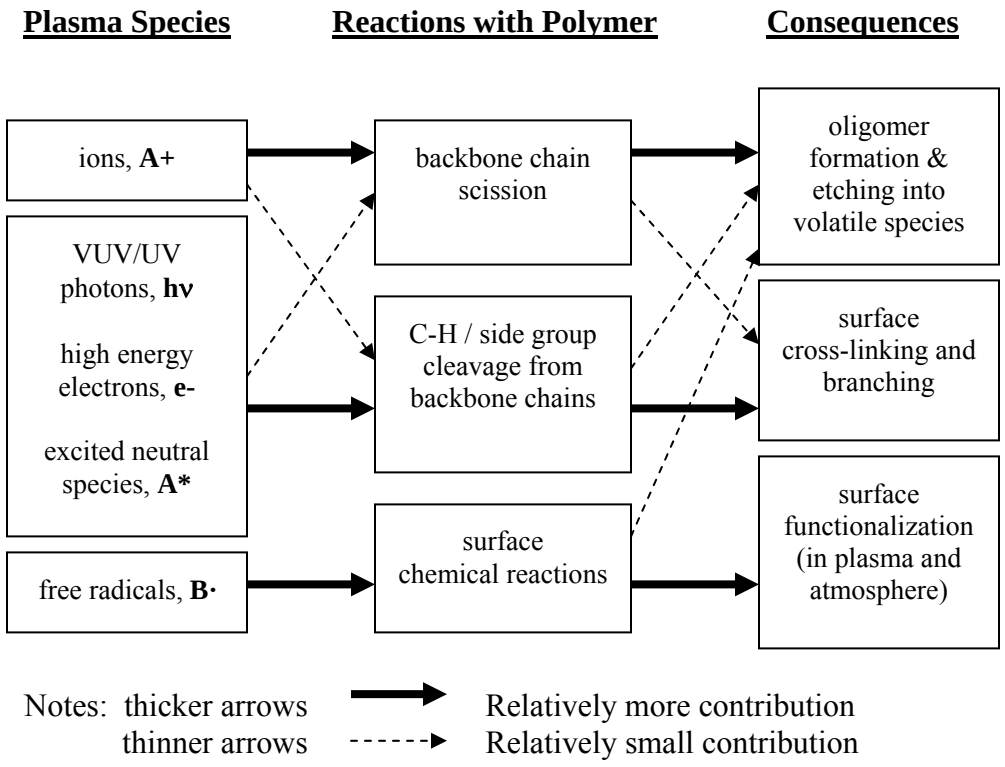

Figure 3.2. The chart shows the possible reaction pathways that could occur on a polymer surface in a plasma treatment process, which can lead to oligomer formation, material etching, cross-linking and branching, and surface functionalization.

3.2.1 Surface Functionalization

Plasma treatment of polymers can introduce a wide variety of functional groups on the polymer surface, which opens the door for numerous possible polymeric surface properties. Plasma surface oxidation can be applied to polymers, in which various oxygen groups are incorporated in the polymer to improve wettability and adhesion to metals[13,28,46]. Other surface modification techniques include fluorination[30-33,47] to

increase hydrophobicity of a polymer, and nitradation[19,22,29,35], for the introduction of basic groups for increasing dye-ability, printability, or biocompatibility.

Chemical functionalization reactions can occur after the creation of radical sites on the polymer surface from ablation of hydrogen or polymer chain side groups or from chain scission.

Hydrogen ablation: $RH \rightarrow R\bullet + H\bullet$

Side group ablation: $RX \rightarrow R\bullet + X\bullet$

Chain scission: $R_1R_2 \rightarrow R_1\bullet + R_2\bullet$

The radicals on the polymer surface can then react and form covalent bonds with plasma phase species that contain oxygen, nitrogen, fluorine, or other elements, and as a result, create stable side group functionalities on the surface. In addition, when the treated polymer is exposed to atmosphere, any radicals that remain on the surface may react with the air to incorporate oxygen, moisture, and to a less extent, nitrogen[13,19,21,28,39,40,42].

3.2.2 Surface Cross-linking and Branching

In the 1960s, Hansen and Schonhorn introduced the CASING effect (Cross-linking by Activated Species of INert Gases) on polymers surfaces exposed to ions and metastable species of inert gas plasmas[36,37]. In addition to noble gas plasma species, investigations have shown that VUV/UV photons[28,41,42,48,49] and electrons[50] that exist in a plasma can induce surface cross-linking on a polymer. Surface cross-linking produces many desirable effects on the polymer, including stability of the polymer surface, improved adhesion, improved surface bond strength and resistance to solvents, heat and

moisture[3,6,27,34,37-41,43]. Thus, surface cross-linking of a polymer is an important process that can be applied to many perturbable or mechanically weak polymers to improve their surface properties.

Cross-linking of a polymer surface from inert gas plasmas and VUV/UV irradiation occurs simply through ablation of hydrogen or side groups on polymer chains by bombardment of metastable noble gas atoms, noble gas ions, or photons to produce radical sites on the polymer surfaces. Photons can penetrate the polymer and induce cross-linking to depths where other plasma species are physically inhibited. Studies have shown that hydrogen abstraction is the dominant mechanism during VUV/UV irradiation of hydrocarbon polymers[51-54]. The radicals can form bonds with other radicals on nearby macromolecules, resulting in a cross-linked network of macromolecules on the surface layers of the polymer. In the absence of reactive species in the gas phase, the formation of new functionalities on the radical sites is inhibited and cross-linking with other polymer radicals is the significant consequence in noble gas plasmas or VUV/UV irradiation, as long as etching effects are minimal. Polymers treated with plasma always contain a certain amount un-reacted or residual surface free-radicals that can incorporate oxygen, moisture, and nitrogen upon exposure to atmosphere. Consequently, noble gas plasmas without reactive gas can result in a stable, cross-linked top layer with mainly oxygen and some nitrogen functional groups anchored at the surface, in an ideal situation.

It must be reiterated that ablation always occurs during a plasma treatment of a polymer and the extent of ablation depends on the structure of the polymer and its

sensitivity to the particular plasma conditions. In a noble gas plasma, positive ions that are accelerated by the sheath potential and VUV/UV photons can cause chain scission due to their high energy levels, and extensive chain scission can result in macromolecule "unzipping" or polymer degradation. On the other hand, in a noble gas plasma, the metastable species that cannot be accelerated by the sheath potential are more likely to cause hydrogen and side-group ablation, which results in surface cross-linking as the primary consequence. Ablation that brings about detrimental effects on the polymer application is discussed in more detail in the following section.

3.3 Surface Degradation Effects of Plasma on Polymers

Polymers are susceptible to degradation by a variety of sources, including high temperature, oxygen (and oxygen-containing species), radiation of VUV/UV photons and charged species, moisture, and chemical agents[5,7,55]. While the effects of energized species in a plasma discharge may generate desirable polymer surface properties, polymers that are exposed to plasma are subject to surface degradation reactions due to bombardment of high-energy ionic species, UV/VUV radiation, and oxygen plasma species. The surface degradation reactions can lead to etching of polymer fragments into volatile species and the formation of non-volatile LMWOM. There are ample data indicating that polymer surface degradation from plasma exposure can bring about many detrimental effects on their applications, such as loss of wettability, adhesion failure due to weak-boundary-layer (WBL) formation, and loss of tensile strength of polyethylene fibers resulting from plasma etching[5,7,44,56,57].

3.3.1 Chemical Etching and Photodegradation

Polymers subjected to a plasma discharges may undergo chemical etching from exposure to energetic charged and neutral species and electromagnetic radiation. In a low-temperature plasma, atomic oxygen is a prime instigator for polymer etching due to its electron count (number of electrons in the valence shell) and its high electronegativity[59]. With energies well above the covalent bond energies present in most polymers, the UV and VUV photons present in the plasma can also cause polymer etching[39,48,52-54,59-61]. While in some cases, such as applications in solid state electronic technologies, selective etching is a desirable outcome[59], significant material etching of a polymer surface during a surface modification treatment can be detrimental to the application.

Etching of polymer fragments into volatile material is preceded by the ablation of material on the side-group of a polymer chain and/or by chain scission of the polymer chain itself. Excessive ablation and chain scission can result in "un-zipping" of polymer macromolecules and thus the etching of the polymer material into volatile species. The reactions at the plasma-polymer surface are further complicated by the liberation of volatile species, which can react with other species in the plasma-polymer interface to bring about various outcomes. Hong et. al[54] found that one of the main fragments emitted from the polymer surface during plasma treatment was hydrogen, which is a strong VUV emitter that can cause surface etching.

The extent of etching depends on the polymer structure and the concentration of plasma etchants, such as atomic oxygen[59,62,63], and the wavelengths and intensities of VUV irradiated from the plasma[59,64]. The structure of a polymer can affect the polymer's vulnerability to plasma etching and photodegradation. For example, the presence of oxygen in the polymer backbone increases the polymer's susceptibility to plasma etching[5,59]. On the other hand, aromatic rings in the polymer (both in the backbone and in pendant groups) provide some resistance to etching reactions[28,54,59,62]. Organic polymers are susceptible to VUV/UV radiation in plasmas, mainly due to their ability to absorb photons in the VUV/UV wavelength range[3,65-67]. However, the absorption spectrum for a polymer depends on its structure, which results in different photochemical effects on the various polymers. Polymethylmethacrylate (PMMA) is a polymer that easily undergoes photodegradation and oxidative degradation in a plasma environment[62,68], while polystyrene (PS) is highly stable toward degradation[28,62,64]. Silicon-containing polymers are particularly resistant to photodegradation and oxidative degradation, yet degrade very easily in fluorine-containing plasmas, because of the formation of stable and volatile Si-F compounds[8].

3.3.2 The Formation of LMWOM

Polymer surface macromolecules that are subjected to a plasma environment can become fragmented from excessive ablation reactions, resulting in lower molecular weight, non-volatile oligomers. In addition, plasma treatments of polymers aimed at surface functionalization with oxygen-containing plasmas, such as O_2, air, H_2O, can result in polymer surface degradation and hence formation of LMWOM through alkoxy

degradation reactions that lead to chain scission[5,6,13,14,45,69,70]. The presence of significant amount of LMWOM on a polymer surface renders the plasma treated polymer impractical for applications, because the weak boundary layer formed by LMWOM on the treated surface is detrimental to adhesion and stability[5,14,45].

Most polymers are susceptible to oxidative degradation, which generally occurs by a free radical mechanism that is initiated by plasma ablation reactions and yields peroxy and hydroperoxy intermediates[55]. Some authors[7,62] cite the peroxy/hydroperoxy route to degradation as a major mechanism that leads to the formation of LMWOM on plasma-treated polymer surfaces. Figure 3.3 contains reaction pathways that can occur when a polymer is subjected to oxygen-containing plasma.

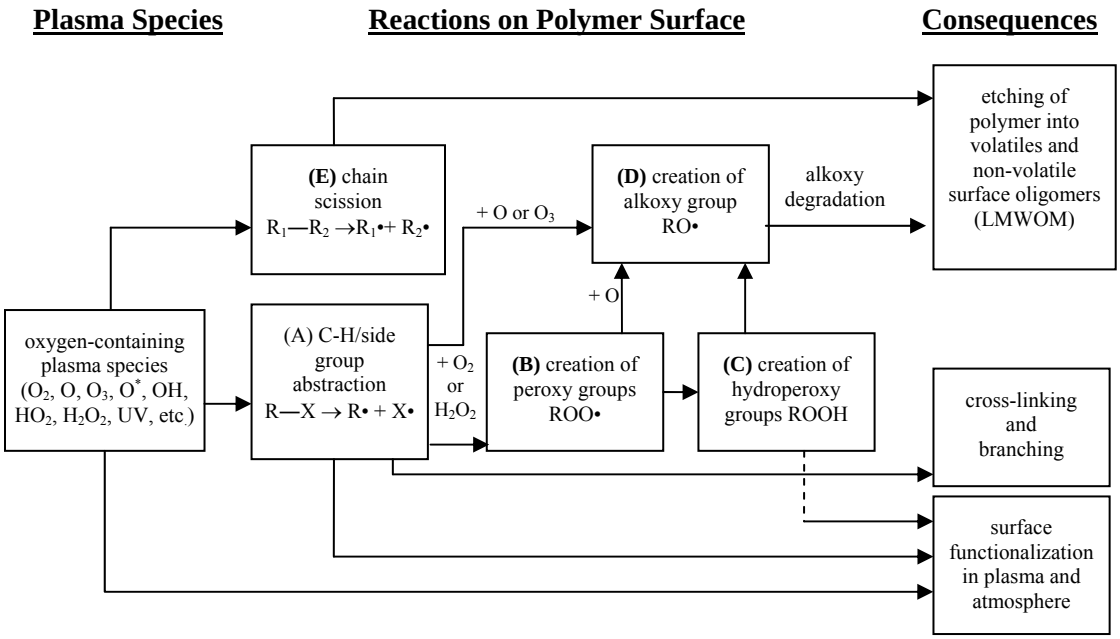

Figure 3.3. The chart shows the possible reaction pathways that could occur on a polymer surface in an oxygen-containing plasma treatment process, which can lead to material etching, the creation of LMWOM, cross-linking and branching, and surface functionalization.

The peroxy pathway to LMWOM formation is shown on Figure 3.3 as the route A→B→C→D that begins with the formation of a radical on the polymer surface, and then the surface free radical (a dangling bond) reacts with various plasma species to form peroxy intermediates.

Peroxy formation: $R\bullet + O_2\ (H_2O_2) \rightarrow ROO\bullet\ (+ H_2)$

Hydroperoxy formation: $ROO\bullet + R_1H \rightarrow ROOH + R_1\bullet$

$R\bullet + HO_2 \rightarrow ROOH$

Decomposition of the hydroperoxy group leads to the formation of an alkoxy radical, which degrade to form lower molecular weight oxidized molecules.

Hydroperoxy decomposition: $ROOH \rightarrow RO\bullet + OH$

Alkoxy degradation: $R_1—C—C(O\bullet)—R_2 \rightarrow R_1—C\bullet + R_2—C=O$

It is widely accepted that alkoxy radicals are the precursors to LMWOM[13,58,62]. However, Strobel et al.[13] have argued that the peroxy pathways to LMWOM are too slow to occur in the timeframe of a plasma treatment. Based on their study, they concluded that the reactions involving atomic oxygen and ozone to form alkoxy radicals are the major routes to the formation of LMWOM on polymer surfaces in plasma discharges. The atomic oxygen and ozone pathways are shown on Figure 3.3 as the routes C→D and A→B→D.

Direct alkoxy formation: $R\bullet + O \rightarrow RO\bullet$

$R\bullet + O_3 \rightarrow RO\bullet + O_2$

Alkoxy formation from peroxy and oxygen atom: $ROO\bullet + O \rightarrow RO\bullet + O_2$

The LMWOM layer is usually soluble in polar solvents. This allows for analysis of the LMWOM formation on a plasma-treated polymer surface. LMWOM products can be detected using several analytical techniques, including X-ray photoelectron spectroscopy (XPS)[13,14,28,45], atomic force microscopy (AFM)[13,14,71,72], static secondary ion mass spectrometry (SSIMS) [73] and contact angle measurement techniques[5,6,13,14,45]. Among these analysis methods, the Wilhelmy balance method is one of the simplest and the most effective technique that is extremely sensitive to the surface characteristic changes of a polymer, since it has the capability to examine the polymer surface before and after rinsing off the LMWOM in a liquid solvent in sequential cycles[5,6]. In this method, a tensionmeter is used to measure the force exerted on a plasma-treated polymer sample, which is immersed into a liquid to a preset depth and then emmersed out from the liquid in sequential cycles. Based on force loops measured, dynamic contact angles of the polymer surface can be then calculated. During immersion, LMWOM that may be present on the sample surface is washed off from the surface by dissolving into the liquid, which reveals the underneath intact polymer surface layer that is usually more hydrophobic. The exposure of a more hydrophobic surface is indicated by "overshooting" of the force loops in subsequent advancing cycles.

Figure 3.4 shows the Wilhelmy force loops obtained from a sheet of low density polyethylene (LDPE) that was treated with RF plasma of Ar + O_2 mixture. The force loop measured in the second immersion cycle shows significant overshooting from the first immersion cycle. The significant overshooting indicates that the plasma-treated LDPE surface during the second immersion was more hydrophobic than that in the first

immersion. This result clearly shows the presence of LMWOM on a plasma-treated LDPE surface, which can be removed by water in the first immersion to expose a more hydrophobic layer in the second immersion.

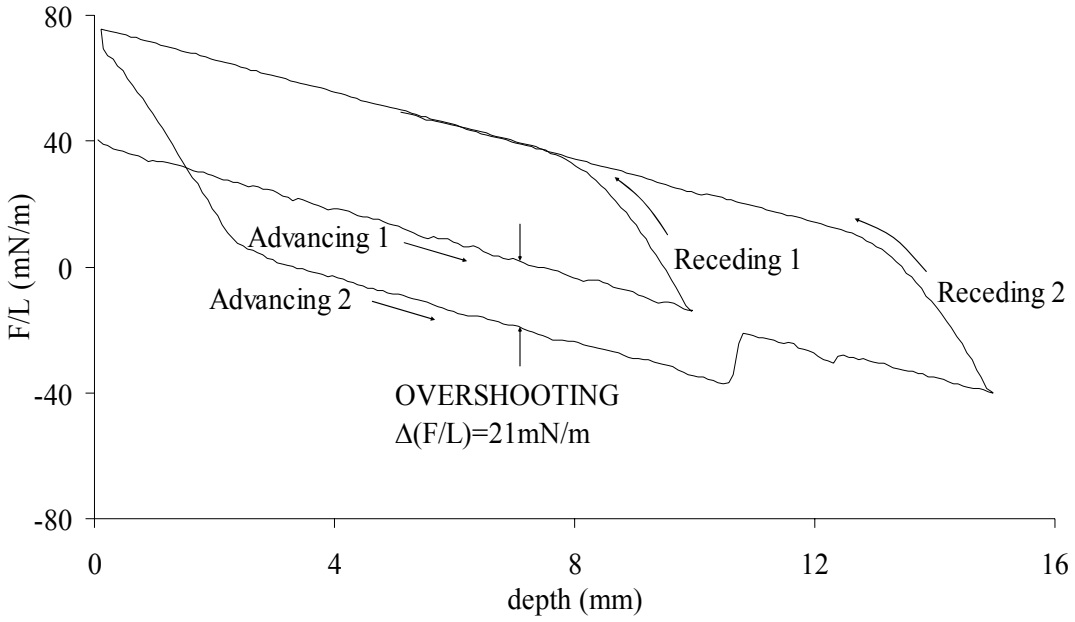

Figure 3.4. The Wilhelmy force loop obtained from RF plasma treatment of LDPE with two immersion cycles shows significant overshooting, indicating that LMWOM was created on the polymer surface during treatment. The conditions were as follows: 1 sccm Ar, 1 sccm O2, 25 W and 60 s exposure time[6].

Plasma treatments that result in LMWOM formation on a polymer surface are not useful for the purpose of incorporating oxygenated functional groups on the surface. To achieve a stable, oxygenated polymer surface, plasma processes that can minimize the formation of LMWOM and thus create stable, oxygenated functional groups are necessary. A discharge process that induces polymer surface cross-linking without the incorporation of oxygen during treatment can involve surface oxidation of the un-reacted surface radicals upon exposure to atmosphere. The consequence of such a technique

applied to polymers includes oxygen functional groups that are anchored to a stable, cross-linked surface network.

3.4 Surface Dynamics and Stability of Plasma Treated Polymers

The aim of any surface modification process includes a high surface stability with minimal aging effects. A good surface stability of a plasma treated polymer can usually be achieved by surface cross-linking and anchoring of the desired functional groups, since the cross-linking structure would limit the mobility of the surface functionalities. However, many plasma treatment processes bring about surface instabilities, such as hydrophobic recovery and long-term aging effects on the treated polymer surface, due to either excessive etching, the formation of LMWOM, or significant mobility of plasma-induced surface moieties. This section focuses on the mobility of plasma-induced surface moieties and surface hydrophobic recovery of a polymer, while the plasma etching and the creation of LMWOM due to plasma treatment was presented in the previous section.

3.4.1 Mobility of Surface Moieties

It is well recognized that the surface characteristics of polymers differ greatly from the polymer bulk properties. Langmuir first pointed out that the surface properties of a solid are determined by the *surface configuration* (orientation of the surface functional groups) rather than the chemical configuration of the bulk molecules[74]. In addition, much research has shown that the polymer surface is highly perturbable and polymers can undergo *surface configuration changes* with changing contacting

media[5,8,75-82]. Many applications require stable polymer surfaces with inhibited mobility of the surface moieties.

Surface dynamics deals with the changing surface characteristics due to variations in environmental conditions[8]. Surface configuration changes are driven by the thermodynamic requirement to minimize interfacial tension, whereby the interface changes to establish new equilibrium with a new set of conditions. A rotational change of functional groups about the polymer backbone involves less energy than the long-chain movement of the macromolecules. Factors that affect the surface dynamics include temperature, crystallinity and/or cross-linking of a polymer, and mainly, contacting medium. Yasuda[8] pointed out that rate of surface dynamic change depends on two major factors: (1) polymer chain mobility and (2) driving force to minimize interfacial tension, and thus the rate of surface dynamic change of a polymer can expressed by:

R (rate of surface dynamic change) = **F** (polymer chain mobility) x **G** (interfacial tension)

A variety of techniques have been utilized to characterize surface configuration changes, including XPS, SIMS, and contact angle measurements[5,6,77-88]. Among these, the Wilhelmy balance method is one of the best technique available for analyzing dynamic wettability and surface stability, because of its sensitivity to the surface state of the polymer[5,6,89]. Figure 3.5 shows a Wilhelmy force loop that was obtained for untreated nylon-6, which contains hydrophilic functional side-groups (carbonyl) on the macromolecule backbone. The apparent increase in hydrophilicity from the first advancing cycle to the next is a demonstration of intrinsic hysteresis, which is caused by

surface configuration changes of the hydrophilic moieties near the polymer surface. During the first immersion, the hydrophilic surface moieties are rearranged to bend toward the water-polymer interface, thus making the surface more wettable during the second advancing cycle.

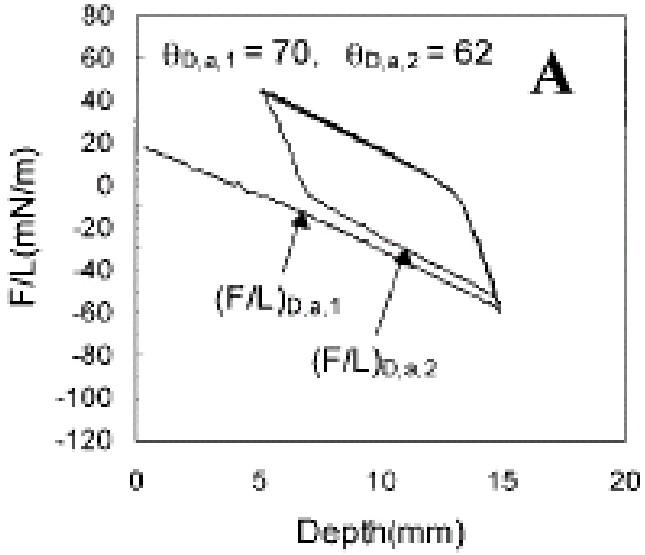

Figure 3.5. The Wilhelmy force loop obtained from untreated nylon 6 demonstrates *intrinsic hysteresis* by the apparent increase in hydrophilicity from the first immersion cycle to the second. This phenomenon is due to the *surface configuration changes* of hydrophilic functional groups in the polymer toward the polymer-water interface, causing the surface to be more wettable in the second immersion (from reference[5]).

On the other hand, a polymer that is imperturbable by water, such as low density polyethylene (LDPE), exhibits no intrinsic hysteresis in the Wilhelmy force loop, as shown by Figure 3.6.

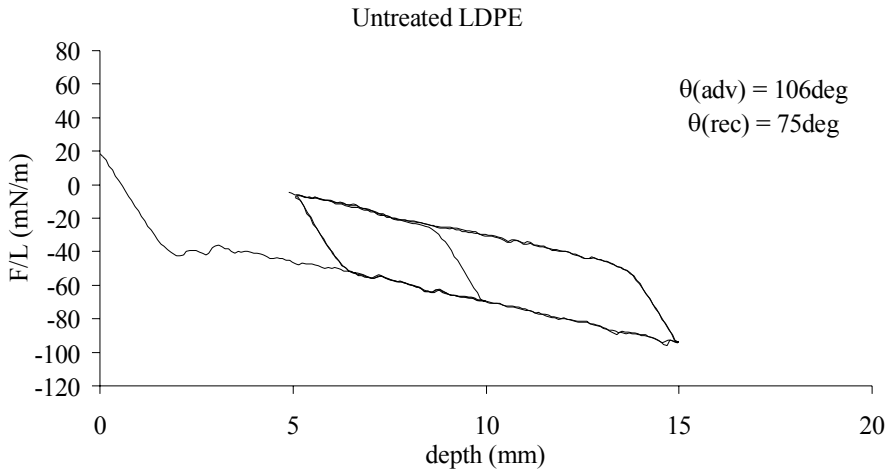

Figure 3.6. The Wilhelmy force loop of untreated LDPE shows a stable, hydrophobic surface with no intrinsic hysteresis (the second and third immersion lines trace the first immersion line)[6].

The discrepancy between the immersion and emersion lines of a Wilhelmy force loop demonstrates dynamic hysteresis, which depends on the meniscus shape during the immersion or emersion of the sample and does not indicate surface dynamic changes[8]. The dynamic contact angles measured from the Wilhelmy cycle (i.e. advancing, $\theta_{D,a}$, and receding, $\theta_{D,r}$) can be related to the static contact angle, θ_s, reasonably well by calculating the mean of $\cos(\theta_{D,a})$ and $\cos(\theta_{D,r})$, which has shown to approximate $\cos(\theta_s)$ [90]. In addition, a polymer may exhibit an ability to hold continuous films of water, which is demonstrated by the fluid holding time (FHT) measured by the Wilhelmy cycle[91].

3.4.2 Hydrophobic Recovery

Hydrophobic recovery and loss of adhesive properties can occur in plasma-treated polymers that are stored in ambient air for extended periods of time[5,6,13,14,41,43].

Hydrophobic recovery is an indication of polymer surface instability in which the hydrophilicity decreases with time stored in ambient air due to surface configuration changes. A plasma-treated polymer that undergoes aging effects could be useless for the desired application once the hydrophobic recovery is significant.

Weikart and Yasuda[5] demonstrated that, in some cases, long-term hydrophobic recovery can be reversed by immersing the treated sample in water for 24 hours. This indicates that over time, the hydrophilic surface moieties created from plasma treatment rearranged away from the polymer surface. Upon changing the surrounding conditions from air to water, the hydrophilic moieties re-oriented toward the polymer surface, thus making the surface wettable again.

3.5 Surface Treatment by a Low-Temperature Cascade Arc Torch (LTCAT)

Most plasma processes involve placement of the polymer directly in the electric field, which results in some extent of polymer surface degradation[5,6,45]. If a desirable surface modification is accomplished at the expense of degradation of the substrate, the value of such a modification is questionable, because ultimate success depends on the extent of the substrate damage. Therefore, a plasma treatment with minimized surface degradation is highly desirable for surface modification of polymeric materials. Investigations pioneered in our laboratory[6,15-18] using LTCAT for polymer surface treatment have demonstrated its many unique advantages in polymer surface modification with minimal surface damages.

The first cascade arc was developed by Maecker[92] in the 1950s, which involved a generator consisting of a tungsten needle cathode and several center-channeled metal disks separated by insulation with the last metal disk serving as a grounded anode. Such an electrode arrangement forces current to the gas, usually argon that is flowing through the disk channel, and ignites the gas discharge in the arc generator. Since the gas flows through the channel at an ultrasonic speed, the gas discharge created inside the arc generator is blown out of the arc generator and forms an arc jet (torch). The cascade arc torch has been used at atmospheric pressure as a heat source for cutting metals and welding[8]. However, when the cascade arc torch is injected into a vacuum chamber, the torch temperature decreases rapidly after expansion and our studies have shown that LTCAT can be used for plasma polymerization and surface modification of polymeric materials[6,15-18,93-102]. The length of the expanded plasma torch depends on the argon flow rate, input power, diameter of the cascade column, and the pressure of the expansion chamber.

The detailed description and operation procedures of the LTCAT reactor have been presented in our previous publications[16,100,103]. Figure 3.7 illustrates cascade arc torch generation in which the electric field confines most of charged species inside the arc generator. As a result, the plasma torch leaving the generator consists of mainly electronically excited argon neutral species, which has been verified by plasma diagnostic data[100,103].

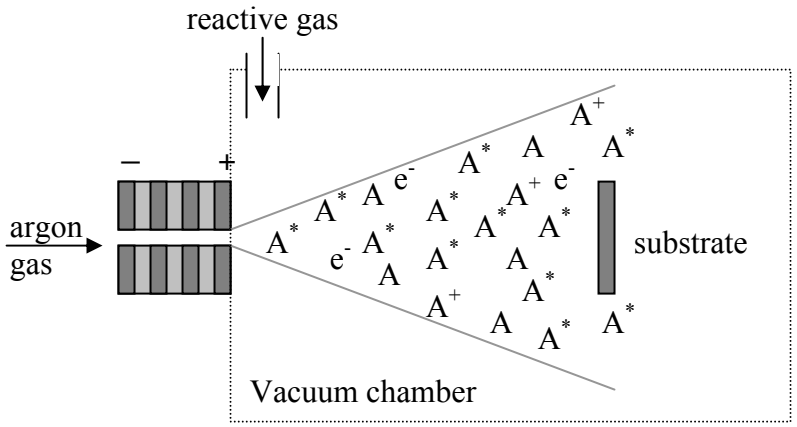

Figure 3.7. The illustration of the creation of plasma species in LTCAT process[6].

In LTCAT, the excited neutral species, rather than electrons, are the main energy carriers that are responsible for surface activation and modification. In LTCAT processes that involve the addition of a second gas into the expansion chamber, reactive gases are activated and transported to the target by the argon plasma torch, in which the second gas plasma species thus generated are energetically controlled by the electronic energy levels of the metastables[101,103]. In addition, the high flux of electronically excited argon neutrals directed to the polymer surface can prevent the possible contamination in LTCAT itself and at the polymer surface by the volatile byproducts released during plasma treatment.

In an LTCAT treatment process, because the reactive species are generated and energetically controlled by argon metastable neutrals, there are no high-energy electrons

and ions involved; hence the incisions in polymer chains and etching of macromolecules on polymer surfaces can be minimized. In addition, during LTCAT treatment, polymer samples are placed in the downstream of an LTCAT, where no external electrical field is present to further accelerate the charged plasma species, such as electrons and ionic species. Therefore, the application of LTCAT plasma in polymer surface treatment provides a unique opportunity to achieve a more controlled surface treatment of polymers, i.e., to introduce new and stable functionalities on polymer surfaces with minimum undesirable damages.

Metastable noble gas atoms in LTCAT discharges can induce the CASING effect on the polymer surface, resulting in a cross-linked surface containing some un-reacted radicals. Without the contribution of high-energy ions that are accelerated by electric fields in traditional plasma treatments, cross-linking of the polymer surface, rather than etching, is the major consequence in LTCAT. Upon exposure to atmosphere, the radicals on the cross-linked surface can incorporate oxygen to form stable surface functional groups. A comparison of polymer surfaces treated with conventional plasma treatment and LTCAT treatment is illustrated in Figure 3.8. While the conventional plasma treatment tends to result in an unstable, fragmented surface, LTCAT treatment produces hydrophilic moieties anchored to a stable, cross-linked top layer on a polymer.

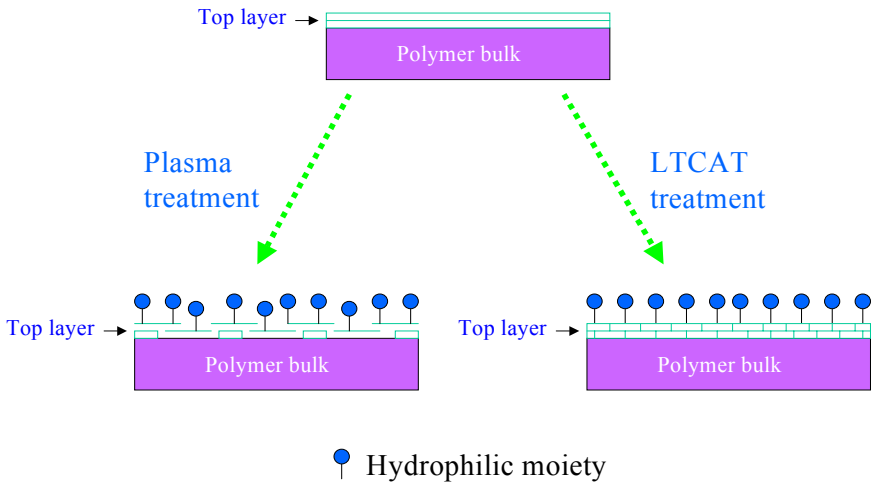

Figure 3.8. Schematic representation of the difference in the structures of polymer surfaces modified by traditional plasma techniques and LTCAT; the plasma treatment tends to modify the fragmented polymers, while LTCAT treatment strengthens top layer by surface cross-linking (from reference[18]).

Polymer surface modification studies have given evidence to the creation of a stable, cross-linked network at polymer surfaces treated with LTCAT [6,16]. A short treatment of a few seconds by argon LTCAT was very efficient in modifying the poly(tetrafluoroethylene) surface and provided a wettable surface that did not show any hydrophobic recovery over a 2-month aging period [16]. LTCAT treatments of thermoplastic olefins have resulted in much more durable and stable adhesion of paint than traditional plasma treatment[15,18]. A study involving LTCAT treatment of polypropylene fibers for concrete reinforcement showed improved strength of the composite that contained the LTCAT-treated fibers[102]. However, very slight surface damage was detected on the LDPE surface when treated with LTCAT without the addition of a second reactive gas [6]. The damage could possibly be from high energetic ions that escaped from the arc generator, or from VUV/UV radiation. Further detailed

studies are underway to examine the effects of the ions in the discharge and the VUV/UV radiation to determine the source of the slight damage.

The advantageous features offered by LTCAT over the conventional plasma processes in surface modification of polymeric materials can be summarized as follows:

(1) LTCAT provides a unique opportunity for individual optimization of the processes involved in plasma treatments, including plasma generation and activation (in arc generator) and deactivation of reactive species (in LTCAT down stream).

(2) LTCAT has a well-controlled energy (by electronically excited argon neutrals) and can be considered to be the mildest form of low-temperature plasmas due to the absence of high-energy electrons and ionic species.

(3) Because the plasma torch delivers a high flux of reactive species to the substrates, LTCAT offers a remarkable increase in plasma treatment rate and efficiency, e.g., within a few seconds, and has the capability of modifying polymer surfaces with a scanning mode.

(4) Since it can be automated as a scanning torch treatment process, LTCAT can be easily scaled-up and used to uniformly treat large pieces of materials with complex shapes in large-scale industrial applications.

The scanning treatment process has been demonstrated in our lab with a model LTCAT reactor for large-scale applications[15-16]. With this scanning treatment mode, reactor geometry has little effect on plasma properties, and therefore, the existing scale-up difficulty in the conventional plasma processes can be easily overcome by LTCAT

applications. Consequently, successful application of LTCAT to polymer surface modification will significantly reduce the plasma treatment cost and consequently lead to an acceptable production rate.

3.6 Summary

Low-temperature plasma treatment undoubtedly offers an effective and versatile surface modification method for various polymeric materials by generating new surface functionalities and thus introducing new surface properties necessitated for many applications. Plasma processes applied to polymers have the merits of being economically efficient, dry, and environmentally benign in tailoring surface characteristics while maintaining their desirable bulk properties. However, it should be pointed out that plasma treatment of polymers could result in significant surface damage through plasma degradation reactions, which depend on both the plasma sensitivity of a polymer structure and the extent of involvement of high-energy plasma species, such as ions and VUV/UV irradiation. Therefore, plasma treatment of polymers has to be practiced with care in order to meet the application needs. An appropriate plasma treatment of a polymer would deliver the desired surface functionalities with a strengthened surface layer through cross-linking, which would benefit many applications. On the other hand, an unsuitable plasma treatment for a polymer would lead to surface damage or degradation, weak boundary layer formation, and surface instability that will be detrimental to most applications.

As a very different plasma technique from conventional plasma processes, LTCAT has shown its many unique, advantageous features in surface treatment of polymers. With the presence of a relatively very small amount of high-energy ionic species, the LTCAT process directs a high flux of electronically excited argon species to the polymer surface, which is free of an external electrical field. As a result, LTCAT provides a rapid and effective surface modification method of polymers with more surface controllability and thus minimal surface damage effects, which have been evidenced by many of our pioneered studies. In addition, due to its automation capability as a scanning torch treatment process, LTCAT process can be easily scaled-up for large-scale industrial applications with an economically acceptable production rate.

3.7 References for Section III

1. Ratner, B.D.; Chilkoti, A.; Lopez, G.P.; "Plasma Deposition and Treatment for Biomedical Applications" in *Plasma Deposition, Treatment, and Etching of Polymers*, R. d'Agostino ed., Academic Press, Boston (1990) 463 – 516.

2. Penn, L.S.; Wang, H.; "Chemical Modification of Polymer Surfaces: A Review", *Polymers for Advanced Technologies* **5** (1994) 809-917.

3. Wertheimer, M.R.; Martinu, L.; and Liston, E.M.; "Plasma Sources for Polymer Surface Treatment" in *Handbook of Thin Film Process Technology, Volume 2*, Glocker, D.A. ed., Institute of Physics Publishing, Bristol (2002) E3.0:1-E3.0:38.

4. Durand, A.M.; "The Practical Application of Plasma Treatment to Polymer Surfaces for Improved Adhesion", *LE VIDE, Science, Technique, et Applications* **53** (1997) 242 – 252.

5. Weikart, C.M.; Yasuda, H.K.; "Modification, Degradation, and Stability of Polymeric Surface Treated with Reactive Plasmas", *J. Polym. Sci.* A **38** (2000) 3028-3042.

6. Gilliam, M.A.; Yu, Q.; "Surface Modification of Low Density Polyethylene Using a Low-Temperature Cascade Arc Torch", accepted by the *J. of Appl. Polym. Sci.* (2005).

7. Wertheimer, M.R.; Bartnikas, R.; "Degradation effects of plasma and corona on polymers" in *Plasma Processing of Polymers*, R. d'Agostino et al. eds., Kluwer Academic Publishers, Netherlands (1997) 435 – 450.

8. Yasuda, H.K.; *Luminous Chemical Vapor Deposition and Interface Engineering*, Marcel Dekker, New York (2005).

9. Yasuda, H.K.; Cho, D.L.; Yeh, Y.-S.; "Plasma-Surface Interactions in the Plasma Modification of Polymer Surfaces" in *Polymer Surfaces and Interfaces*, Feast, W.J.; Munro, H.S.; eds., John Wiley & Sons, New Jersey (1987) 149-162.

10. Strobel, M.; Walzak, M.J.; Hill, J.M.; Lin, A.; Karbashewski, E.; Lyons, C.S.; "A Comparison of Gas-Phase Methods of Modifying Polymer Surfaces", *J. Adhesion Sci. Technol*. **9** (1995) 365 - 383.

11. Shishoo, R.; "Plasma Treatment – Industrial Applications and its Impact on the C&L Industry", *J. Coated Fabrics* **26** (1997) 26 - 35.

12. Shenton, M.J.; Stevens, G.C.; "Surface Modification of Polymer Surfaces: Atmospheric Plasma versus Vacuum Plasma Treatments", *J. Phys. D: Appl. Phys.* **34** (2001) 2761-2768.

13. Strobel, M.; Jones, V; Lyons, C.S.; Ulsh, M.; Kushner, M.J.; Dorai, R.; Branch, M.C.; "A Comparison of Corona-Treated and Flame-Treated Polypropylene Films", *Plasma Polym.* **8**, No. 1 (2003) 61-95.

14. Guimond, S.; Wertheimer, M.R.; "Surface Degradation and Hydrophobic Recovery of Polyolefins Treated by Air Corona and Nitrogen Atmospheric Pressure Glow Discharge", *J. Appl. Polym. Sci.* **94** (2004) 1291-1303.

15. Yasuda, H.K.; Lin, Y.-S.; "Low-Temperature Cascade Arc Torch Treatments for Enhanced Adhesion of Primer to Thermoplastic Olefins", *J. Appl. Polym. Sci.* **67** (1998) 855-863.

16. Yu, Q.S.; Reddy, C.M.; Meives, M.F.; Yasuda, H.K.; "Surface Modification of Poly(tetrafluoroethylene) by a Low-Temperature Cascade Arc Torch and Radio-Frequency Plasma", *J. Polym. Sci.: Part A: Polym. Chem.* **37** (1999) 4432 – 4441.

17. Yu, Q.; Deffeyes, J.; Yasuda, H; "Engineering the Surface and Interface of Parylene C Coatings by Low-Temperature Plasmas", *Prog. Org. Coat.* **41** (2001) 247-253.

18. Yasuda, H.K.; Lin, Y.-S.; Yu, Q.S.; "Durable Bonding Characteristics of Thermoplastic Olefins Plasma-Treated by Low-Temperature Cascade Arc Torches", *Prog. Org. Coat.* **42** (2001) 236-243.

19. Hollahan, J.R.; Stafford, B.B.; "Attachment of Amino Groups to Polymer Surfaces by Radiofrequency Plasmas", *J. Appl. Polym. Sci.* **13** (1969) 807-816.

20. Kogoma, M.; Turban, G.; "Mechanism of Etching and of Surface Modification of Polyimide in RF and LF SF_6-O_2 Discharges", *Plasma Chem. Plasma Proess.* **6**, No. 4 (1986) 349-380.

21. Momose, Y.; Noguchi, M.; Okazaki, S.; "Ar, O_2 and CF_4 Plasma Treatment of Poly-(vinylidene fluoride), Polyimide and Polyamidoimide and its Relationship to Wettability", *Nucl. Instrum. Meth. Phys. Res. B* **39** (1989) 805-808.

22. Klemberg-Sapieha, J.E.; Kuttel, O.M.; Martinu, L.; Wertheimer, M.R.; "Dual-Frequency N_2 and NH_3 Plasma Modification of Polyethylene and Polyimide", *J. Vac. Sci. Technol. A* **9** (1991) 2975-2981.

23. Morra, M.; Occhiello, E.; Garbassi, F.; "Chemical Reactions on Plasma-Treated Polyethylene Surfaces", *J. Adhesion Sci. Technol.* **7**, No. 10 (1993) 1051-1063.

24. Behnisch, J.; Hollander, A.; Zimmermann, H.; "Controlled Functionalization of Polymer Surfaces by Low Pressure Plasma Treatment", *Intern. J. Polymeric Mater.* **23** (1994) 215-224.

25. Meichsner, J.; Nitschke, Rochotzke, R.; Zeuner, M.; "Fundamental Investigations in Plasma Modification of Polymers", *Surf. Coat. Technol.* **74-75** (1995) 227-231.

26. Behnisch, J.; "Plasmachemical Modification of Natural Polymers" in *Plasma Processing of Polymers*, d'Agostino, R.; Favia, P.; Fracassi, F.; eds.; Kluwer, Dordrecht (1997) 345.

27. Placinta, G.; Arefi-Khonsari, F.; Gheorghiu, M.; Amouroux, J.; Popa, G.; "Surface Properties and the Stability of Poly(ethylene Terephtalate) Films Treated in Plasmas of Helium-Oxygen Mixtures", *J. Appl. Polym. Sci.* **66** (1997) 1367-1375.

28. France, R.M.; Short, R.D.; "Plasma Treatment of Polymers: The Effects of Energy Transfer from an Argon Plasma on the Surface Chemistry of Polystyrene and Polypropylene. A High-Energy Resolution X-Ray Photoelectron Spectroscopy Study", *Langmuir* **14** (1998) 4827-4835.

29. Deslandes, Y.; Pleizier, G.; Poire, E.; Sapieha, S.; Wertheimer, M.R.; Sacher, E.; "The Surface Modification of Pure Cellulose Paper Induced by Low-Pressure Nitrogen Plasma Treatment", *Plasma Polym.* **3**, No. 2 (1998) 61-76.

30. Jama, C.; Quensierre, J.-D.; Gengembre, L.; Moineau, V.; Grimblot, J.; Dessaux, O.; Goudrnand, P.; "Characterization of Polyethylene Surface Heated after Plasma Fluorination", *Surf. Interface Anal.* **27** (1999) 653-658.

31. Zhang, L.; Chin, W.S.; Huang, W.; Wang, J.Q.; "Investigation of the Surface Structures and Dynamics of Polyethylene Terephthalate (PET) Modified by Fluorocarbon Plasmas" *Surf. Interface Anal.* **28** (1999) 16-19.

32. McCord, M.G.; Hwang, Y.J.; Qiu, Y.; Hughes, L.K.; Bourham, M.A.; "Surface Analysis of Cotton Fabrics Fluorinated in Radio-Frequency Plasma" *J. Appl. Polym. Sci.* **88** (2003) 2038-2047.

33. Rangel, E.C.; Bento, W.C.A.; Kayama, M.E.; Schreiner, W.H.; Cruz, N.C.; "Enhancement of Polymer Hydrophobicity by SF_6 Plasma Treatment and Argon Plasma Immersion Ion Implantation", *Surf. Interface Anal.* **35** (2003) 179-183.

34. Laurens, P.; Petit, S.; Arefi-Khonsari, F.; "Study of PET Surfaces After Laser or Plasma Treatment: Surface Modification and Adhesion Properties Towards Al Deposition" *Plasma Polym.* **8**, No. 4 (2003) 281-295.

35. Tatoulian, M.; Bouloussa, O; Moriere, F.; Arefi-Khonsari, F.; Amouroux, J.; Rondelez, F.; "Plasma Surface Modification of Organic Materials: Comparison Between Polyethylene Films and Octadecyltrichlorosilane Self-Assembled Monolayers" *Langmuir* **20** (2004) 10481-10489.

36. Hansen, R.H.; Schonhorn; "A New Technique for Preparing Low Surface Energy Polymers for Adhesive Bonding" *J. Polym. Sci. Part B: Polym. Letters* **4**, No. 3 (1966) 203-209.

37. Schonhorn, H.; Hansen, R.H.; "Surface Treatment of Polymers for Adhesive Bonding" *J. Appl. Polym. Sci.* **11** (1967) 1461-1474.

38. Hall, J.R.; Westerdahl, C.A.L.; Devine, A.T.; Bodnar, M.J.; "Activated Gas Plasma Surface Treatment of Polymers for Adhesive Bonding" *J. Appl. Polym. Sci.* **13** (1969) 2085-2096.

39. Momose, Y.; Tamura, Y.; Ogino, M.; Okazaki, S.; "Chemical Reactivity between Teflon Surfaces Subjected to Argon Plasma Treatment and Atmospheric Oxygen" J. *Vac. Sci. Technol. A* **10** (1992) 229-238.

40. Liston, E.M.; Martinu, L.; Wertheimer, M.R.; "Plasma Surface Modification of Polymers for Improved Adhesion: A Critical Review" in *Plasma Surface Modification of Polymers: Relevance to Adhesion* Strobel, M.; Lyons, C.S.; Mittal, K.L.; Eds., VSP: Utrecht, The Netherlands (1994) 3-39.

41. Egitto, F.D.; Matienzo, L.J.; "Plasma Modification of Polymer Surfaces for Adhesion Improvement" *IBM J. Res. Develop.* **38**, No. 4 (1994) 423-439.

42. Matienzo, L.J.; Zimmerman, J.A.; Egitto, F.D.; "Surface Modification of Fluoropolymers with Vacuum Ultraviolet Irradiation" J. *Vac. Sci. Technol. A* **12** (1994) 2662-2671.

43. Arefi-Khonsari, F.; Tatoulian, M.; Shahidzadeh, N.; Amouroux, J.; "Study of the Plasma Treated Polymers and the Stability of the Surface Properties" in *Plasma Processing of Polymers*, R. d'Agostino et al. eds., Kluwer Academic Publishers, Netherlands (1997) 165-207.

44. Arefi, F.; Andre, V.; Montazer-Rahmati, P.; Amouroux, J.; "Plasma Polymerization and Surface Treatment of Polymers", *Pure & Appl. Chem.* **64** (1992) 715 – 723.

45. Inagaki, N.; Tasaka, S.; Shimada, S.; "Comparative Studies on Surface Modification of Poly(ethylene terephthalate) by Remote and Direct Argon Plasmas" *J. Appl. Polym. Sci.* **79** (2001) 808-815.

46. Bernier, M.H.; Kemberg-Sapieha, J.E.; Martinu, L.; Wertheimer, M.R.; "Polymer Surface Modification by Dual-Frequency Plasma Treatment" in *Metallization of Polymers*, Sacher, E. et al. eds., American Chemical Society, Washington, DC (1990) 147-160.

47. Klausner, M.; Baddour, R.F.; Cohen, R.E.; "Surface Modification of Polymers with Fluorine-Containing Plasmas: Deposition Versus Replacement Reactions", *Polym. Eng. Sci.* **27**, No. 11 (1987) 861-868.

48. Fozza, A.C.; Kemberg-Sapieha, J.E.; Wertheimer, M.R.; "Vacuum Ultraviolet Irradiation of Polymers", *Plasma Polym.* **4**, No. 2/3 (1999) 183-206.

49. Tamai, T.; Ichinose, N.; Kawanishi, S.; Mizuno, K.; "Photochemical Oxygenation and Cross-Linking of Poly(4-trimethylsilymethylstyrene) Thin Film by UV Irradiation", *Macromolecules* **33** (2000) 2881-2886.

50. Sessler, G.M.; West, J.E.; Ryan, F.W.; Schonhorn, H.; Increase of Gold-Teflon FEP Joint Strength by Electron Bombardment", *J. Appl. Polym. Sci.* **17** (1973) 3199-3209.

51. Rabek, J.F.; *Photodegradation of Polymers: Physical Characteristics and Applications*, Springer, New York (1996).

52. Wilken, R.; Hollander, A.; Behnisch, J.; "Quantitative Comparison between Vacuum Ultraviolet Irradiation and Remote Hydrogen Plasma Treatment of Polymers", *Plasma Polym.* **3** (1998) 165-175.

53. Wilken, R.; Hollander, A.; Behnisch, J.; "Vacuum Ultraviolet Photolysis of Polyethylene, Polypropylene, and Polystyrene", *Plasma Polym.* **7** (2002) 185-205.

54. Hong, J.; Truica-Marasescu, F.; Martinu, L.; Wertheimer, M.R.; "An Investigation of Plasma-Polymer Interactions by Mass Spectrometry", *Plasma Polym.* **7** (2002) 245-260.

55. Fried, J.R.; *Polymer Science and Technology*, Prentice Hall PTR, New Jersey (1995).

56. Bettge, D.J.; Hinrichsen, G.; "Continuous Manufacturing of Composites of High-Performance Polyethylene Fibers", *Compos. Sci. Technol*. **47** (1993) 131 – 136.

57. Ameen, A.P.; "An Investigation of the Surface Chemical Homogeneity of Plasma Oxidized Poly(ether Etherketone)", *Polymer Degradation and Stability* **51** (1996) 179 – 84.

58. Egitto, F.D.; Vukanovic, V.; Taylor, G.N.; "Plasma Etching of Organic Polymers" in *Plasma Deposition, Treatment, and Etching of Polymers*, R. d'Agostino ed., Academic Press, Boston (1990) 321-422.

59. Hollander, A.; Kemberg-Sapieha, J.E.; Wertheimer, M.R.; "The Influence of Vacuum Ultraviolet Radiation on Poly(ethylene Terephthalate)", *J. Polym. Sci.* A **34** (1996) 1511-1516.

60. Fozza, A.C.; Roch, J.; Klemberg-Sapieha, J.E.; Kruse, A.; Hollander, A.; Wertheimer, M.R.; "Oxidation and Ablation of Polymers by Vacuum-UV Radiation from Low Pressure Plasmas", *Nucl. Instrum. Meth. Phys. Res. B* **131** (1997) 205-210.

61. Wertheimer, M.R.; Fozza, A.C.; Hollander, A.; "Industrial Processing of Polymers by Low-Pressure Plasmas: The Role of VUV Radiation", *Nucl. Instrum. Meth. Phys. Res. B* **151** (1999) 65-75.

62. Moss, S.J.; Jolly, A.M.; Tighe, B.J.; "Plasma Oxidation of Polymers", *Plasma Chem. Plasma Process.* **6**, No. 4 (1986) 401-416.

63. Joubert, O.; Pelletier, J.; Arnal, Y.; "The Etching of Polymers in Oxygen-Based Plasmas: A Parametric Study", *J. Appl. Phys.* **65**, No. 12 (1989) 5096-5100.

64. Marasescu, F.-E.T.; Wertheimer, M.R.; "Vacuum Ultraviolet Photolysis of Hydrocarbon Polymers", *Macromol. Chem. Phys.* **206** (2005) 744-757.

65. Partridge, R.H.; "Vacuum-Ultraviolet Absorption Spectrum of Polyethylene", *J. Chem. Phys.* **45**, No. 5 (1966) 1685-1690.

66. Partridge, R.H.; "Vacuum-Ultraviolet Absorption Spectrum of Polysyrene", *J. Chem. Phys.* **47**, No. 10 (1967) 4223-4227.

67. Partridge, R.H.; "Exciton Interpretation of Vacuum-Ultraviolet Absorption Spectra of Saturated Organic Polymers", *J. Chem. Phys.* **49**, No. 8 (1968) 3656-3668.

68. Hozumi, A.; Masuda, T.; Hayashi, K.; Sugimura, H.; Takai, O.; Kameyama, T.; "Spatially Defined Surface Modification of Poly(methylmethacrylate) Using 172 nm Vacuum Ultraviolet Light", *Langmuir* **18** (2002) 9022-9027.

69. Foerch, R.; Kill, G.; Walzak, M.J.; "Plasma Surface Modification of Polyethylene: Short-Term vs. Long-Term Plasma Treatment" in *Plasma Surface Modification of Polymers*, VSP, Utrecht (1994) 99-111.

70. Callen, B.W.; Ridge, M.L.; Lahooti, S.; Neumann, A.W.; Sodhi, R.N.S.; "Remote Plasma and Ultraviolet-Ozone Modification of Polystyrene", *J. Vac. Sci. Technol. A* **13**, No. 4 (1994) 2023-2029.

71. Boyd, R.D.; Kenwright, A.M.; Badyal, J.P.S.; Briggs, D.; "Atmospheric Nonequilibrium Plasma Treatment of Biaxially Oriented Polypropylene", *Macromolecules* **30** (1997) 5429-5436.

72. Mahlberg, R.; Niemi, H.E.-M.; Denes, F.S.; Rowell, R.M.; "Application of AFM on the Adhesion Studies of Oxygen-Plasma Treated Polypropylene and Lignocellulosics" *Langmuir* **15** (1999) 2985-2992.

73. van Ooij, W.J.; Michael, R.S.; "Plasma- and Corona- Modified Polymer Surfaces: Characterization by Static Secondary Ion Mass Spectrometry" in *Metallization of Polymers*, Sacher, E. et al. eds., American Chemical Society, Washington, DC (1990) 60-87.

74. Langmuir, I.; "Overturning and Anchoring of Monolayers", *Science* **87**, No. 2266 (1938) 493-500.

75. Holly, F.J.; Refojo, M.F.; "Wettability of Hydrogels I. Poly(2-hydroxyethyl methacrylate)", *J. Biomed. Mater. Res.* **9** (1975) 315-326.

76. Ratner, B.; Weatherby, P.; Hoffman, A.; Kelly, M.; Scharpen, L.; "Radiation-Grafted Hydrogels for Biomaterial Applications as Studied by the ESCA Technique", *J. Appl. Polym. Sci.* **22** (1978) 643-664.

77. Yasuda, T.; Okuno, T.; Yoshida, K.; Yasuda, H.; "A Study of Surface Dynamics of Polymers. II. Investigation by Plasma Surface Implantation of Fluorine-Containing Moieties", *J. Polym. Sci. B* **26** (1988) 1781-1794.

78. Yasuda, H.; Charlson, E.J.; Charlson, E.M.; "Dynamics of Surface Property Change in Response to Changes in Environmental Conditions", *Langmuir* **7** (1991) 2394-2400.

79. Yasuda, T.; Miyama, M.; Yasuda, H.; "Dynamics of the Surface Configuration Change of Polymers in Response to Changes in Environmental Conditions. 2. Comparison of Changes in Air and in Liquid Water", *Langmuir* **8** (1992) 1425-1430.

80. Yasuda, T.; Miyama, M.; Yasuda, H.; "Effect of Water Immersion on Surface Configuration of an Ethylene-Vinyl Alcohol Copolymer", *Langmuir* **10** (1994) 583-585.

81. Yasuda, T.; Okuno, T.; Yasuda, H.; "Contact Angle of Water on Polymer Surfaces", *Langmuir* **10** (1994) 2435-2439.

82. Yasuda, H.; Okuno, T.; Sawa, Y.; Yasuda, T.; "Surface Configuration Change Observed for Teflon-PFA on Immersion in Water", *Langmuir* **11** (1995) 3255-3260.

83. Cuthrell, R.E.; "Environment-Influenced Surface Layer in Polymers", *J. Appl. Polym. Sci.* **11** (1967) 1495.

84. Gagnon, D.R.; McCarthy, T.J.; "Polymer Surface Reconstruction by Diffusion of Organic Functional Groups from and to the Surface", *J. Appl. Polym. Sci.* **29** (1984) 4335.

85. Lavielle, L.; Schultz, J.; "Surface Properties of Graft Polyethylene in Contact with Water I. Orientation Phenomena", *J. Colloid Interface Sci.* **106** (1985) 438.

86. Ruckenstein, E.; Gourisankar, S.V.; "Environmentally Induced Restructuring of Polymer Surfaces and Its Influence on Their Wetting Characteristics in an Aqueous Environment", *J. Colloid Interface Sci.* **107** (1985) 488.

87. Van Damme, H.S.; Hogt, A.H.; Feijen, J.; "Surface Mobility and Structural Transitions of Poly(n-alkyl methacrylates) Probed by Dynamic Contact Angle Measurements", *J. Colloid Interface Sci.* **114** (1986) 167.

88. Parker, J.L.; Claesson, P.M.; Wang, J.-H.; Yasuda, H.K.; "Surface Forces between Plasma Polymer Films", *Langmuir* **10** (1984) 2766-2773.

89. Miyama, M.; Yasuda, H.K.; "Surface Dynamics of Plasma Polymers Studied by the Wilhelmy Force Measurement", *Langmuir* **14** (1998) 960-964.

90. Weikart, C.M.; Miyama, M.; Yasuda, H.K.; "Surface Modification of Conventional Polymers by Depositing Plasma Polymers of Trimethylsilane and of Trimethylsilane + O_2", *J. Colloid Interface Sci.* **211** (1999) 28-38.

91. Weikart, C.M.; Miyama, M.; Yasuda, H.K.; "Fluid-Holding Time Parameter and Fluid Holding Capability of Polymeric Materials", *Langmuir* **16** (2000) 5169-5177.

92. Maecker, H.; *Z. Naturforsh.* **11a** (1956) 457.

93. Kroesen, G.M.W., Ph.D. Thesis, Eindhoven University of Technology, Eindhoven, The Netherlands (1988).

94. Beulens, J.J.; Kroesen, G.M.W.; Schram, D.C.; Timmermans, C.J.; Crouzen, P.C.N.; Vasmel, H.; Schuurmans, H.J.A.; Beijer, C.B.; Werner, J.; *J. Appl. Polym. Sci.: Appl. Polym. Symp.* **46** (1990) 527.

95. Kroesen, G.M.W.; Schram, D.C.; van de Sande, M.J.F.; *Plasma Chem. Plasma Process.* **10** (1990) 49.

96. De Graaf, M.J.; Dahiya, R.P.; Jauberteau, J.L.; De Hoog, F.J.; van de Sande, M.J.F.; Schram, D.C.; *Colloq. Phys.* **51** (1990) c5-387.

97. Beulens, J.J., Ph.D. Thesis, Eindhoven University of Technology, Eindhoven, The Netherlands (1992).

98. Buuron, A.J.M.; Otorbaev, D.K.; van de Sande, M.C.M.; Schram, D.C.; *Phys. Rev. E* **50** (1994) 1383.

99. Krentsel, E.; Fusselman, S.; Yasuda, H.; Yasuda, T.; Miyama, M.; "Penetration of Plasma Surface Modification. II. CF4 and C2F4 Low-Temperature Cascade Arc Torch", *J. Polym. Sci.: Part A: Polym. Chem.* **32** (1994) 1839 – 1845.

100. Fusselman, S.P. and Yasuda, H.K.; "Particle Densities and Non-Equilibrium in a Low-Pressure Argon Plasma Jet", *Plasma Chem. Plasma Process,* **14** (1994) 251 - 275.

101. Yu, Q.S. and Yasuda, H.K.; "Deposition Behavior in a Low-Temperature Cascade Arc Torch (CAT) Polymerization Process", *J. Polym. Sci. A.* **37** (1999) 967-982.

102. Zhang, C.; Gopalaratnam, V.S.; Yasuda, H.K.; "Plasma Treatment of Polymeric Fibers for Improved Performance in Cement Matrices", *J. Appl. Polym. Sci.* **76** (2000) 1985-1996.

103. Yu, Q.S. and Yasuda, H.K.; "An Optical Emission Study on Expanding Low-Temperature Cascade Arc Plasmas", *Plasma Chem. Plasma Process.* **18** (1998) 461 - 485.

104. Meichsner, J.; "Low-Temperature Plasmas for Polymer Surface Modification" in *Low Temperature Plasma Physics*, Hippler, R. et al. eds., Wiley-VCH, Berlin (2001) 453-472.

SECTION IV

THE PLASMA POLYMERIZATION BEHAVIOR OF FLUOROCARBON MONOMERS IN LOW FREQUENCY AND HIGH FREQUENCY DISCHARGES

4.1 Introduction

This study involves the investigation and comparison of the plasma polymerization behavior of several hydrocarbon and fluorocarbon systems utilizing AF and RF frequency power. The fluorocarbon monomers include C_3F_6, with F/C ratio of 2 and a C=C bond that enhances polymerization by formation of a di-radical, $C_2F_4H_2$, in which the presence of H depletes the system of F to enhance polymerization, and C_3F_6O, which contains an epoxide ring that can easily open to create a di-radical. C_4F_{10} was also used, which is a saturated fluorocarbon with a high F/C ratio of 2.5 and no chemical feature to enhance polymerization.

4.2 Experimental

4.2.1 Materials

Methane CH_4, 99.0 %, and butane C_4H_{10}, 99.5 %, were purchased from Matheson, Inc. Oxygen, 99.5 %, was supplied by MU General Stores and Praxair. Perfluorobutane C_4F_{10} was obtained from PCR Incorporated. Lancaster Synthesis supplied hexafluoropropene C_3F_6, 98 %, tetrafluoroethane $C_2F_4H_2$, 99 %, and hexafluoropropene oxide C_3F_6O, 97 %. All gases were used without additional purification. The substrates used were pieces of silicon wafers (1 × 1 cm) that were cut from a 125 mm diameter silicon wafer with a primary flat edge. The silicon pieces were cleaned with acetone prior to placing them in the reactor.

4.2.2 Reactor System

Polymerization was carried out in a glass bell jar plasma reactor (PlasmaCarb) surrounded by a cage. The radius of the largest section of the bell jar was about 23 cm and the height of the bell jar was about 60 cm. The total volume of the reactor was about 80 L. Refer to previous publications for the schematics and flow system of the plasma reactor[1,2].

Two parallel titanium electrodes (18 x 18 x 0.1 cm) were placed in the reactor at a distance of 8.5 cm apart. Magnetic enhancement was placed on the back sides of each electrode using bar magnets. Six bar magnets (8 x 1 x 1 cm) were affixed on the back of each electrode with the south poles facing outward. A stainless steel rotating disk (36 cm diameter) was centered between the electrodes. The disk held the silicon substrates using copper clips at a radial distance of about 14 cm from the disk center. The disk rotated at a speed of 15 rpm to achieve uniform deposition.

The reactor was evacuated using a system of a rotary pump and a mechanical booster pump in series. The base pressure of the reactor was approximately 1 mtorr and the pressure was measured using a MKS Baratron pressure transducer. For the hydrocarbon systems, the flow rate was controlled using a Tylan mass flow controller and was determined by applying the ideal gas law to pressure measurements taken at different times after closing the exit stream of the system. For the fluorocarbon systems, the flow rate was controlled using a Tylan mass flow controller and a Whitey manual needle valve. It was determined that some of the fluorocarbon gases were not compatible with the

Viton® O-ring in the mass flow contollers, so the stainless steel manual valve was attached. For each experiment, the pressure was set at 50 mtorr prior to igniting the plasma.

The power sources used for the hydrocarbon discharges included a 15 kHz (Plasma Carb) current-controlled power source, a 40 kHz (Advanced Energy PE-100) power-controlled source, and a RF (13.56 MHz, Advanced Energy RFX-600) power-controlled source, each used separately. In the fluorocarbon systems, the 40 kHz and 13.56 MHz power sources were used for separate experiments. Both of the electrodes were powered and the base of the reactor was grounded. The composite energy input parameter, W/FM, was determined by dividing the input power (W) by the mass flow rate FM (g/min) and converting to units of GJ/kg.

After each fluorocarbon experiment, the reactor was treated with oxygen plasma to remove any remaining fluorocarbon contaminants in the reactor. For cleaning, the flow rate of oxygen was controlled using a MKS mass flow controller and set at 8 sccm and 7-9 W power using the 13.56 MHz power source and 1 W using the 40 kHz power source. The oxygen cleaning time was 5 min.

4.2.3 Ellipsometer Measurements

The thickness and refractive index of the plasma polymer films were measured using a null-seeking Rudolph Research/Auto EL ellipsometer, which uses a 632.8 nm helium-neon laser. The maximum thickness of the films for all of the trials was 130 nm.

The refractive indexes of all of the samples ranged from about 1.2 to 1.7. The average thickness and average refractive index of four substrates were used for data analysis in each trial. The normalized deposition rate was calculated for each trial by dividing the deposition rate GR (μm/min), by the mass flow rate FM (g/min).

4.3 Results and Discussion

4.3.1 Plasma Polymerization in Hydrocarbon Systems

Methane and butane discharges using 15 kHz, 40 kHz, and 13.56 MHz frequencies separately were used to deposit films on silicon substrates attached to the rotating substrate disk in the center of the electrodes. The values of the operational conditions range as follows for the hydrocarbon trials: 0.7-5.2 sccm flow rate, 6-75 W input power, and 5-60 min operation time. The film thicknesses on 4 silicon substrates for each experiment were recorded and averaged. The local deposition rate on a substrate surface in a plasma polymerization system can be expressed by the mass deposition rate, k_0 (kg/m^2 s) and is proportional to the input power for any specified monomer and system[3]. However, the deposition rate is different for various monomer flow rates and the normalized deposition rate is more useful in examining the plasma polymerization domains, which is obtained by k_0/FM ($1/m^2$).

The deposition rate is more commonly expressed in terms of film thickness growth rate, GR (m/s). A study by Miyama and Yasuda[1] has indicated that the plot of the normalized deposition rate, GR/FM, versus W/FM for methane and butane data combined using various flow rates and operational times resulted in single, normalized

curves for each RF and AF frequency. The hydrocarbon plasma polymerization behavior observed in this investigation is presented in Figure 4.1, which contains the plot of GR/FM (μm/g) versus W/FM (GJ/kg), and is similar to the results previously presented by Miyama and Yasuda[1].

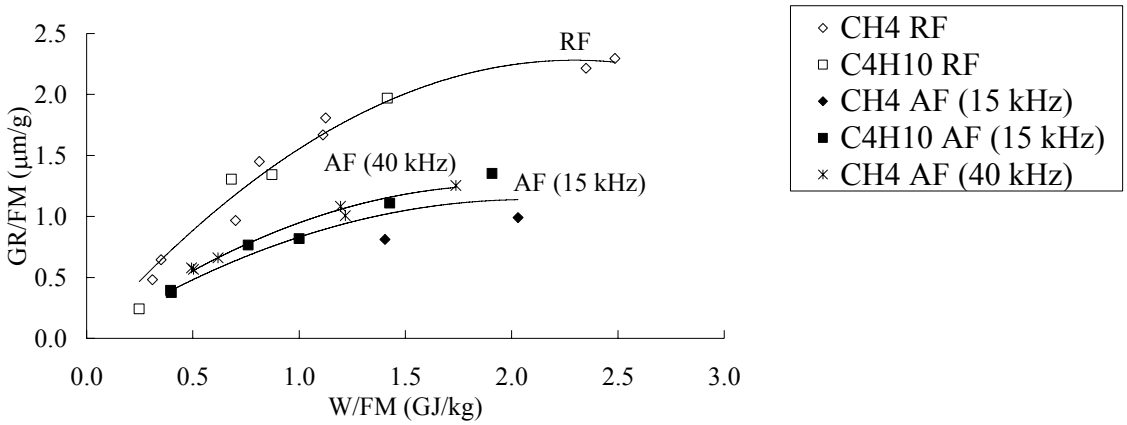

Figure 4.1. The dependence of normalized deposition rate, GR/FM (μm/g), on W/FM (GJ/kg) is shown for methane and butane flow system discharges with 15 kHz, 40 kHz, and 13.56 MHz frequencies.

The graph in Figure 4.1 reveals the energy deficient and polymer-forming species deficient domains of the hydrocarbon plasma polymerization systems. The energy deficient domain is observed by an increase in GR/FM with increasing W/FM, in which more polymer-forming species are created with increasing energy input. At the observed critical energy value, $(W/FM)_c$, which is estimated between 1.9-2.2 GJ/kg, the luminous gas phase is saturated with energy and increasing W/FM does not enhance the production of polymer-forming species. Thus, in the polymer-forming species deficient region, the normalized deposition rate, GR/FM, is constant with increasing W/FM. Another important observation is that the combined data for both methane and butane resulted in single normalized curves for each frequency system. The hydrocarbon systems consisted

of similar monomer structures (saturated hydrocarbons), and thus, the plasma polymerization behavior was very similar.

4.3.2 Plasma Polymerization of Fluorocarbon Systems

The plasma polymerization behavior of fluorocarbon discharges was investigated, and the values of the operational conditions range as follows for the fluorocarbon trials: 0.9-5.0 sccm flow rate, 2-60 W input power, and 0.5-10 min operation time. The normalized bond energies of fluorocarbon monomers are much lower than the values of hydrocarbon monomers, due to the greater mass of fluorine. As described earlier, $(W/FM)_c$ is proportional to the normalized bond energy with α constant for a given reactor system. Thus, for the reactor system used, $(W/FM)_c$ for fluorocarbons is expected to be much lower than for hydrocarbons. The dependence of GR/FM on W/FM was plotted for C_4F_{10}, C_3F_6, C_3F_6O, and $C_2F_4H_2$ and the data did not result in normalized curves for each power frequency with all of the gases combined. This is not surprising, however, because the monomer gases used have various chemical features and thus, exhibit different plasma polymerization behavior. Individual plots of film growth as a function of W/FM were separated from the others and are given in Figure 4.2 for $C_2H_2F_4$, Figure 4.3 for C_3F_6, Figure 4.4 for C_3F_6O, and Figure 4.5 for C_4F_{10}.

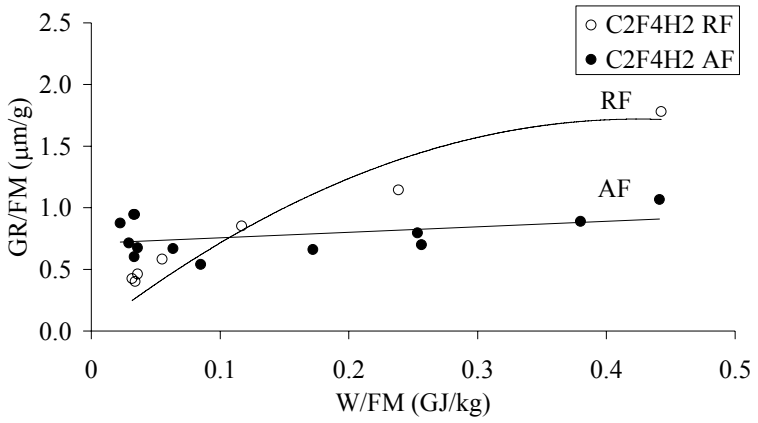

Figure 4.2. The dependence of normalized deposition rate, GR/FM (μm/g), on W/FM (GJ/kg) is shown for $C_2H_2F_4$ flow system discharges using AF (40 kHz), and RF (13.56 MHz) frequencies.

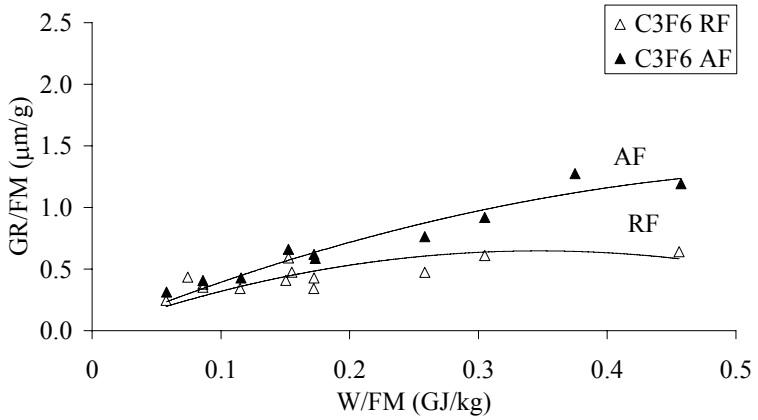

Figure 4.3. The dependence of normalized deposition rate, GR/FM (μm/g), on W/FM (GJ/kg) is shown for C_3F_6 flow system discharges using AF (40 kHz), and RF (13.56 MHz) frequencies.

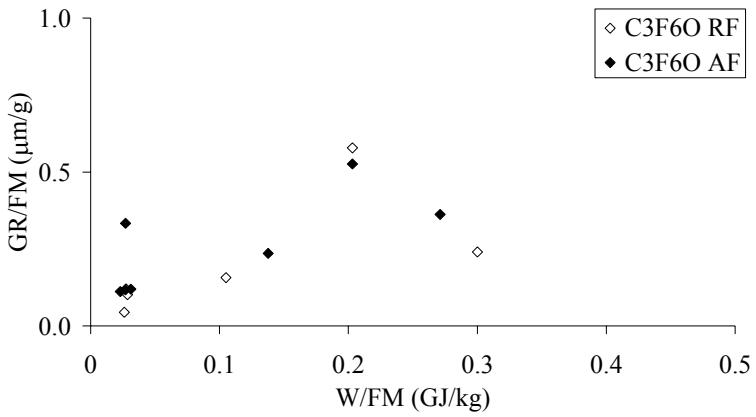

Figure 4.4. The dependence of normalized deposition rate, GR/FM (μm/g), on W/FM (GJ/kg) is shown for C_3F_6O flow system discharges using AF (40 kHz), and RF (13.56 MHz) frequencies.

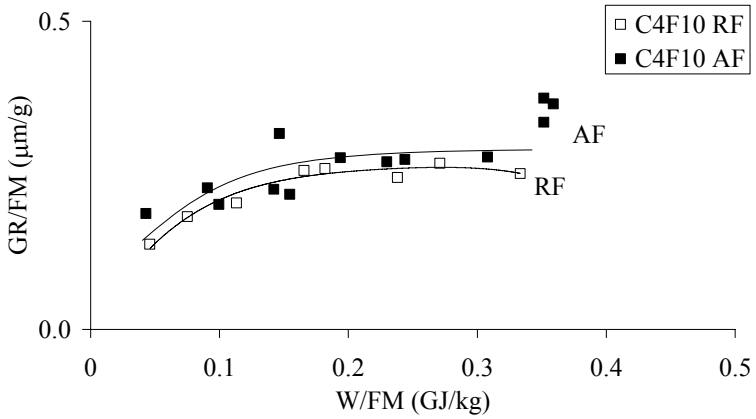

Figure 4.5. The dependence of normalized deposition rate, GR/FM (μm/g), on W/FM (GJ/kg) is shown for C_4F_{10} flow system discharges using AF (40 kHz), and RF (13.56 MHz) frequencies.

Each type of fluorocarbon monomer exhibited different plasma polymerization behavior, due to their various chemical structures. Table 4.1 contains the normalized bond energies, the estimated $(W/FM)_c$ values, and the maximum observed DP/FM for each monomer.

Table 4.1. Normalized Bond Energies, Estimated Critical Energy Input, and Maximum GR/FM for Monomers

Monomer	Bond Energy (kJ/mol)	Molecular Weight	Normalized Bond Energy (GJ/kg)	Estimated (W/FM)c (GJ/kg)	Maximum GR/FM (μm/kg)
C_4F_{10}	5,891	238	2.475E-02	0.20	0.4
C_3F_6O	4,320	166	2.602E-02	0.20	0.6
C_3F_6	3,871	150	2.581E-02	0.40	1.3
$C_2H_2F_4$	3,113	102	3.052E-02	0.45	1.8
CH_4	1,652	16	1.033E-01	2.00	2.3
C_4H_{10}	5,171	58	8.916E-02	2.00	2.3

The presence of H in $C_2F_4H_2$ can enhance the polymerizing ability of the system by removal of HF from the system. Thus, the $C_2F_4H_2$ system was more conducive to plasma polymerization than the other fluorocarbon monomers, and an energy deficient region was observed at low W/FM. C_3F_6 contains a C=C bond, in which monomer activation results in the production of a polymerizing di-radical. An energy deficient region was also revealed for this monomer at low W/FM, in which the creation of polymer-forming species increased with increasing energy density. The C_3F_6O monomer contains an epoxide ring, which easily opens to remove O and form the same polymerizing di-radical as with C_3F_6. Thus, the deposition rate of this monomer was expected to be higher than the saturated fluorocarbon monomer, which it was. However, the maximum deposition rate for C_3F_6 was about 2 times greater than for C_3F_6O, which indicates that the double-bond feature is more effective for fluorocarbon plasma polymerization than the epoxide ring. The saturated fluorocarbon, C_4F_{10}, is a good etching agent, which exhibited the lowest deposition rates among all of the monomers used in this study (note the smaller scale of GR/FM for C_4F_{10}).

Although different chemical features in fluorocarbon monomers affected the deposition rates of the various fluorocarbon systems, some general trends were observed regarding the plasma polymerization behavior of fluorocarbons. The plots of GR/FM vs. W/FM reveal that the locations of the polymer-forming species deficient domains were generally located at lower values of W/FM for fluorocarbon systems than for hydrocarbon systems. It was expected that the polymer-forming species deficient domain and the $(W/FM)_c$ values would shift to low values of W/FM due to the low normalized bond energies of the fluorocarbons. The $(W/FM)_c$ values that were estimated for each monomer were plotted with the normalized bond energies for each monomer and given in Figure 4.6.

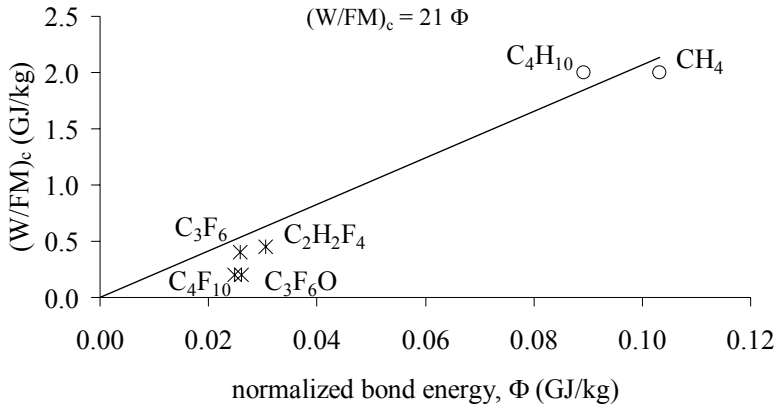

Figure 4.6. Critical energy input value $(W/FM)_c$ (GJ/kg) versus the normalized bond energies, Φ (GJ/kg), for each hydrocarbon and fluorocarbon gas used.

The slope of the line corresponds to the value of α, according to (2) in the Literature Review, which was estimated from the hydrocarbon systems to be 21. Although the values of $(W/FM)_c$ are estimates, all of the fluorocarbon monomers were consistently located well below the regression line and the expected $(W/FM)_c$ values from the value of α were, in general, significantly greater than the observed values of

$(W/FM)_c$ for the fluorocarbons. Thus, the shift in energy deficient domain to lower W/FM is not entirely due to the lower normalized bond energies and is also likely related to the nature of fluorocarbon discharges. The shift in location of the polymer-forming species deficient domain to low GR/FM for the fluorocarbon systems shed more light on the behavior of the fluorocarbon discharges.

Figure 4.7 illustrates the general locations of the polymer-forming species deficient domains for hydrocarbon and fluorocarbon systems.

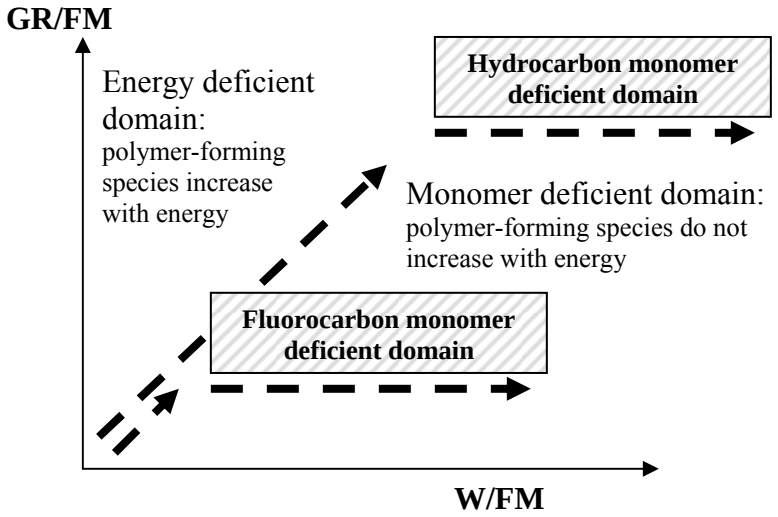

Figure 4.7. Illustrative depiction of the polymer-forming species deficient domains for hydrocarbon (HC) and fluorocarbon (FC) plasma polymerization systems with respect to the relationship between the normalized deposition rate, GR/FM, and the energy density of the systems W/FM.

For hydrocarbon systems in the energy deficient region, additional energy in the dissociation glow creates more polymer-forming species. In fluorocarbon discharges, however, the luminous gas phase created by dissociation glow does not contain much polymer-forming species and additional energy does not enhance the production of polymer-forming species. Consequently, the polymer-forming species deficient domain

is shifted to low W/FM and low GR/FM. Although the causes of the energy domain shift for fluorocarbon systems needs to be thoroughly investigated, it is possible that the electronegativity of the fluorocarbon monomer fragments inhibits recombination.

4.3.3 The Effects of Frequency on Polymerization

Another important observation should be discussed regarding the differences observed between the AF and RF discharges. In hydrocarbon systems, the normalized deposition rate in the gas phase between the two parallel electrodes is greater in the RF discharges than the AF discharges for similar W/FM as shown in Figure 4.1, which is due to the location of the dissociation glows in the different systems[4]. In low frequency AF discharges, the dissociation glows are focused on each electrode, with DC cathodic polymerization on the electrodes dominating over plasma polymerization in the negative glow[5]. The density of polymer-forming species is greater in the core of dissociation glow and decreases around the core in the fainter areas of glow. In higher frequency discharges, the dissociation glows move away from the electrode surfaces and plasma polymerization occurs throughout the more expansive negative glow. For hydrocarbon systems, greater energy density corresponds to enhanced production of polymer-forming species. Thus, greater deposition occurred in the luminous gas phase of the RF discharges with greater energy density than in the AF discharges, in which deposition was primarily focused on the electrodes.

The results of this investigation show that for fluorocarbon systems of C_3F_6, C_3F_6O and C_4F_{10}, GR/FM in the luminous gas phase was generally higher for AF than for

RF systems. For AF, the substrate position corresponds to the low intensity glow region, where a greater production of polymer-forming species occurred. For RF, however, the substrate location is in a more intense region of negative glow, where the energy density was greater and the production of polymer-forming species was lower than AF. The exception is $C_2H_2F_4$, which behaved like a fluorocarbon system for low W/FM, while at higher W/FM, the system more closely resembled a hydrocarbon discharge.

4.4 Conclusions

For successful application of any plasma polymerization system, it is important to analyze the energy domains of the system and the critical energy input values, $(W/FM)_c$, which are different for each type of monomer. The plasma polymerization behavior of fluorocarbon systems is much different from hydrocarbon systems and the luminous gas created by the dissociation glow in a fluorocarbon system does not contain much polymer-forming species. Consequently, the location of the polymer-forming species deficient domain was shifted to low W/FM and low DP/FM for the fluorocarbon systems used.

Regardless of the fluorocarbon monomer used, all of the fluorocarbons exhibited a shift in polymer-forming species domain to low W/FM and low DP/FM. However, some differences were observed among the fluorocarbon systems, which were attributed to the various chemical features of the monomers. The fluorocarbon monomer containing special chemical features for enhancement of polymerization, such as H in $C_2H_2F_4$, a double bond in C_3F_6, and an epoxide ring in C_3F_6O, exhibited an increase in

the production of polymer-forming species at very low W/FM. The saturated fluorocarbon, C_4F_{10}, did not exhibit much enhancement of polymer-forming species with increasing energy density for the range of W/FM used and the normalized deposition rate was mostly flat.

The frequency of the power input to the electrodes affects the locations of the dissociation glow and the behavior of a plasma polymerization system. In low frequency AF discharges, the dissociation glow is concentrated on the electrode surfaces, which corresponds to high energy density. In RF frequency, however, the dissociation glows move away from the electrode surfaces, where the energy density is greater. For hydrocarbon systems, greater energy density corresponds to higher production of polymer-forming species, and the normalized deposition rate in the center of the electrodes was greater for RF than for AF. On the other hand, the normalized deposition rate in the center of the electrodes in fluorocarbon systems was generally higher for AF than for RF discharges. Thus, a higher energy density corresponds to a lower production of polymer-forming species in a fluorocarbon discharge. The exception was the $C_2H_2F_4$ monomer, in which the plasma polymerization behavior was similar to fluorocarbon systems for low W/FM and hydrocarbon systems for higher W/FM.

4.5 References for Section IV

1. Miyama, M. and Yasuda, H. K., *J. Appl. Polym. Sci.*, **70**, (1998) 237.
2. Iriyama, Y., Yasuda, T., Cho, D.L., and Yasuda, H., *J. Appl. Polym. Sci.*, **39** (1990) 249.
3. Yasuda, H., *Luminous Chemical Vapor Deposition and Interface Engineering*, Marcel Dekker, New York (2005).
4. Yasuda, H. and Yu, Q., *Plasma Chem. Plasma Process.*, **24** (2004) 325.
5. Yu, Q. S. and Yasuda, H. K., *J. Vac. Sci. and Tech., A-Vacuum Surfaces & Films*, **19**, no. 3 (2001) 773.

SECTION V

SURFACE CHARACTERIZATION OF LOW-TEMPERATURE CASCADE ARC PLASMA-TREATED LOW-DENSITY POLYETHYLENE USING CONTACT ANGLE MEASUREMENTS

5.1 Introduction

Polymeric materials cannot be selected for a given application only on the basis of their bulk properties. Surface characteristics usually play a critical role in their successful applications. Many methods have been developed and used to modify polymer surfaces for improved adhesion, and other related surface characteristics. These methods include mechanical treatments, e.g., roughening by abrasion, wet-chemical treatments with strong acids or bases, exposure to flames or corona discharge. However, these treatment techniques have considerable drawbacks. For example, wet chemical treatment involves many additional processing steps such as washing, rinsing, and drying, and constitutes large amount of toxic waste disposal problem and cost. On the other hand, low-temperature plasma treatment provides a versatile, reproducible, and environmental benign method in modifying polymer surfaces while maintaining their desirable bulk properties.[1]

Low-temperature plasma that can be simply created by electrical glow discharge contains many reactive species including ions, high-energy electrons, free radicals, and electronically excited molecular and atomic species. Once a polymeric material is subjected to plasma environments, these highly reactive plasma species can react with the polymer surface, change the surface chemistry and thus modify their surface

characteristics. Low-temperature plasma has been widely used to treat polymeric materials in order to improve their surface energy, barrier properties, optical reflection, biocompatibility, and adhesion to other materials. One of the most important features of plasma treatments is that they can modify the outermost surface of polymers without changing their desirable bulk properties.[2,3] In addition, since plasma processes are "dry" and "clean", plasma treatments of polymers are becoming favorable and popular in industrial applications as they avoid the environmental restrictions of wet chemical processes.

Although plasma treatment is one favorable method in modifying polymer surfaces, its large-scale industrial applications have not been very successful to date. One of the main reasons is due to the difficulty in achieving controllable plasma treatment on polymer surface with conventional plasma sources, in which polymer surfaces are exposed to many reactive species simultaneously and the processes involved cannot be optimized separately. There are ample data indicating that this "uncontrollable" plasma treatment can bring about many undesirable changes/damages on the surface of polymers, such as degradation of polymer chains and etching of the surface materials.[4,5] These undesirable changes/damages on polymer surfaces have many detrimental effects on their applications, such as loss of wettability, adhesion failure due to weak-boundary-layer (WBL) formation, and loss of tensile strength of polyethylene fibers resulting from plasma etching.[6,7] If a desirable surface modification is accomplished at the expense of degradation of the substrate, the value of such a modification is questionable. Ultimate success depends on the extent of the substrate damage. Therefore, a plasma system with

lower production cost and easily optimized and controllable treatment processes could lead to a rapid growth in the utilization of plasma technologies on an industrial scale.

LTCAT offers an alternative plasma method for polymeric surface modification by providing a high flux of excited species of a noble gas, usually argon, directed to the polymer surface. In LTCAT plasma process, discharge of argon is created in an arc generator and emanated from the generator as a stable luminous plasma torch. The luminous plasma torch can be used to directly treat a surface or to activate a second reactive gas added into the plasma torch. When the LTCAT plasma torch is injected into a vacuum chamber, the torch temperature decreases rapidly after expansion and can be used as a low-temperature plasma source for plasma polymerization and surface modification on polymeric materials.[8,9] In this process, most of the charged plasma species including ions and electrons are confined inside the arc generator. Plasma diagnostic data has verified that the luminous plasma torch emanated from the arc generator consists of mainly electronically excited argon metastable atoms, which distinguish LTCAT from the rest of conventional plasma processes in which ions and electrons play dominant roles.[10,11] Since a high flux of electronically excited argon atoms whose energy are well determined are directed to the surface, rapid surface treatment and less surface damage on polymeric materials by LTCAT treatment are anticipated than conventional plasma treatment processes.

In this study, LTCAT plasma treatment is used to modify LDPE polymer surface in order to improve its surface wettability, which is directly related its successful

applications such as adhesion, paintability, and printability. Plasma treatment effects, including surface wettability changes, surface stability, and possible surface damages, are investigated by both static and dynamic surface contact angle measurements, i.e., sessile droplet method and Wilhelmy balance method. The dynamic analysis using Wilhelmy balance method on the LTCAT treated LDPE provides many important information, including the possible surface damages in the form of low molecular oligomers formation on the treated surfaces and surface stability of hydrophilic moieties to undergo surface configuration changes.

5.2 Experimental

5.2.1 Materials

The polymeric substrates that were used for the LTCAT treatments consisted of 1 mm thick, low density polyethylene (LDPE) sheets, purchased from Goodfellow Cambridge Limited. The LDPE sheets were cut into 1 × 2 cm pieces and used as the substrates for plasma treatments. In order to eliminate the effects of various contaminants possibly presented on the surface, all the LDPE samples were cleaned in an ultrasonic bath solution consisting of 5 % detergent in de-ionized water for 30 minutes. The samples were then thoroughly rinsed in de-ionized water, dried in ambient air for 1 day, then stored in a dry dessicator. The Ar and O_2 gases were obtained from Praxair, with purities of 99.997 % and 99.5 %, respectively. The water vapor consisted of de-ionized water obtained from a Culligan de-ionizing system attached to in-house distilled water.

5.2.2 RF Plasma Reactor

RF plasma treatments were performed in a bell jar reactor (80 L), which contains a pair of parallel electrodes made of titanium plates (18 × 18 × 0.1 cm) with spacing of 8.5 cm. The vacuum system consisted of a rotary pump (E2M-12, Edwards High Vacuum, Great Britain) and a mechanical booster pump (MB-100F, Shimadzu Corporation, Japan), which evacuated the reactor to a base pressure of 1.4 mtorr. Plasma gases were introduced into the reactor to reach a preset system pressure of 50 mtorr. RF power was supplied to the electrodes using a power-controlled RF power supply with a matching network (RFX-600, Advanced Energy Industries, Inc., United States). Both electrodes were powered and the base of the reactor was grounded. The gas flow rates, input power, and exposure times varied for each trial. The polymer samples were placed in the plasma glow on an aluminum disk centered between the electrodes that rotated at a speed of 15 RPM.

5.2.3 LTCAT Reactor

The detailed description and operation procedures of the LTCAT reactor is presented in earlier publications.[9-11] The major components of the LTCAT reactor include an arc generator, a Pyrex glass cross vacuum chamber, an Edward High-Vacuum EH500A/E2M80 combination pump. The arc generator was mounted onto one port of the Pyrex glass cross. The arc generator consisted of a narrow channel (3 mm) formed by a series of copper disks that are separated by silicone rubber insulators. The arc generator was cooled to 10 ^{o}C before starting each experiment using an ethylene glycol-water mixture that flowed inside the copper disks. Ar flowed through the narrow channel of the

arc generator at a rate of 500-3000 sccm. An MDX-5K direct current magnetron power supply was used to ignite and sustain the argon discharge inside the arc generator. Due to the high speed of argon passing through the generator, the argon discharge was then blown out of the arc generator to form a luminous plasma torch into the glass chamber. As shown in Figure 3.7, the electric field confined most of charged species inside the arc generator, and as a result the plasma torch leaving the generator consisted of mainly electronically excited argon neutral species.[10,11]

The LTCAT treatment of LDPE was operated using the Ar plasma torch with or without addition of a reactive gas. The reactive gas was introduced to the reactor chamber through an inlet next to the torch inlet into the chamber. A LDPE sheet was placed on the substrate clip at the end of a sliding bar that could be moved into and out of the torch through another port of the glass cross chamber. The position of the polymer substrate was 22 cm away from the torch inlet. The reactor was pumped down to the base pressure of 10 mtorr before each experiment. When the torch was steady, the sample was immersed inside the torch for the preset exposure time. The gas flow rates, input current, and exposure times were the variables studied.

5.2.4 Surface Contact Angle Measurements

The wettabililty of the polymeric surfaces was determined using static and dynamic contact angle measurements. The Sessile droplet method with a surface contact angle measurement system (VCA 2500XE, Advanced Surface Technologies, Inc., United States) was used to measure static contact angle , in which a 0.3 μL droplet of de-ionized

water was placed on the surface of the polymer and computer software supplied with the equipment was used to obtain a photograph of the image. With the aid of the software, the computer users were able to manually trace the droplet arc and the computer program calculated the two angles of contact at the water/air/solid interface.

Dynamic measurements were obtained by using the Wilhelmy balance method, in which a tensiometer (Sigma 70, KSV Instruments, Ltd., Finland) measured the total force exerted on the polymer sample plate while immersing in water. Illustrations of hydrophobic and hydrophilic sample plates immersing into and withdrawing out the water is presented elsewhere,[12] showing the meniscus changes during the advancing and receding cycles. The immersion and withdrawing speed of the samples was fixed at 5 mm/min, which is low enough to minimize the dependence of dynamic contact angles on immersion velocity.

The forces exerted on the sample include a gravitational force, buoyancy force, and an interfacial force between the sample and the water. Before the sample touch the water surface, the computer user zeroed the balance so the gravitational force could be neglected. The following equation describes the actual sum of the forces measured by the tensiometer:

$$F = L\gamma_L \cos\theta - \rho gtHd \qquad (1)$$

where $\boldsymbol{F}$ is the total force measured, $\boldsymbol{L}$ is the perimeter of the plate, $\boldsymbol{\gamma_L}$ is the surface tension of the water, $\boldsymbol{\theta}$ is the contact angle at the solid/liquid/air line, $\boldsymbol{\rho}$ is the mass density of the sample, $\boldsymbol{g}$ is the acceleration of gravity, $\boldsymbol{t}$ is the plate thickness, $\boldsymbol{H}$ is the

plate width, and ***d*** is the depth of immersion in the water. The surface tension of water was obtained using the Wilhelmy plate method. The measured force, ***F***, was divided by the plate perimeter, ***L***, to obtain the Wilhelmy balance loops, which plot ***F/L*** at the depths of immersion. The results were extrapolated to 0 immersion depth to obtain the advancing and receding contact angles for each immersion cycle.

Wettability analysis was performed immediately after each treatment. Some samples were used to examine aging effects on the treatments. These samples were then submerged in de-ionized water and placed in an ultrasonic bath for 10 minutes to wash away any possible surface oligomers that would have been created during the treatments. The samples were then allowed to dry in ambient air and subsequent analyses were performed at various stages of aging.

5.3 Results and Discussion

In this study, plasma treatments of LDPE was performed using LTCAT of argon only, argon LTCAT with O_2 addition, and argon LTCAT with H_2O vapor addition. Plasma treatment effects including surface wettability changes, surface stability, and possible surface damages were investigated with comparison to conventional RF plasma treatments.

5.3.1 RF Plasma Treatment

Many studies of the surface modification of polymers using conventional RF plasma techniques have shown certain degree of surface damages because of the

continuous bombardment of high-energy species.[4,5,13] Weikart and Yasuda[13] reported that plasma induced surface damage of polymers resulted in the formation of a certain amount of low molecular oligomers, which were washed away after immersion in water. As a comparison to LTCAT treatments, RF plasma treatments of LDPE were investigated by varying plasma exposure time, while RF power, system pressure, and flow rates were fixed in this study.

Figure 5.1 shows the surface contact angle change of LDPE measured by static sessile drop method with different exposure time in RF plasmas of Ar, Ar + O_2, and Ar + H_2O vapor.

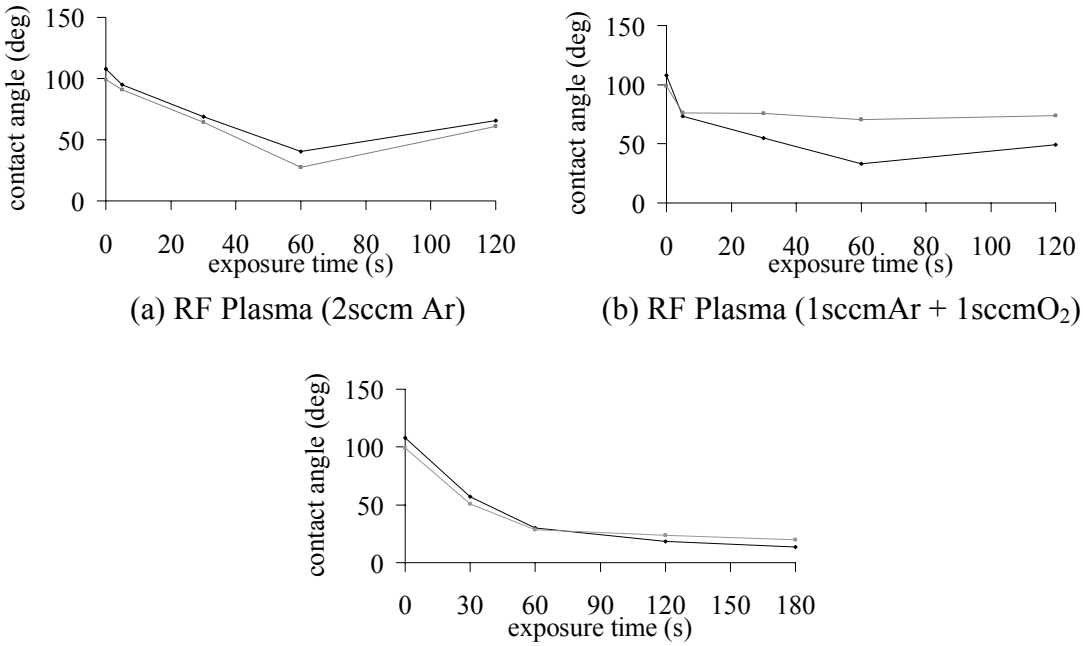

Figure 5.1. The change of static surface contact angle of LDPE with plasma exposure time in (a) Ar, (b) Ar + O2, and (c) Ar + H2O RF plasmas. The dark lines show water contact angles of freshly treated samples without washing, and the gray lines show water contact angles of treated samples after washing. The plasma conditions are 8 W RF power and 50 mtorr system pressure.

The black lines show the static contact angle measurements immediately after treatment, while the gray lines indicate the contact angles of the samples washed in an ultrasonic bath of de-ionized water for 10 min, then blotting dried with Kimwipes® (Kimberly Clark, United States) and left in the air for 2 min.

As seen from Figure 5.1, the untreated LDPE samples (0 s exposure time) showed a ~ 8^{o} decrease in contact angle after washing. It should be noted that, after kept in a dry dessicator for 5 min, the washed samples showed the same contact angle value as the unwashed samples. A decrease in surface contact angle after exposure to water could be an indication of a surface configuration change or water adsorption or penetration. Untreated LDPE, however, has shown to possess a high surface stability and does not undergo surface configuration changes upon exposure of water.[12] Therefore, the decrease in static contact angle after washing is likely due to water adsorption on the surface. It was presumed that the treated samples would also experience some water adsorption during the timeframe of the washing and drying process. For the Ar RF plasma treated samples as shown in Figure 5.1 (a), the contact angles decreased slightly after washing and the extent of the effects of surface configuration change and water adsorption cannot be distinguished by static contact angle measurement. The treatments required an exposure time of 60 s to reduce surface water contact angle to 40^{o} and further increase in exposure time resulted in higher contact angles.

The results of the Ar + O_2 RF plasma treatments shown in Figure 5.1 (b), however, showed a significant increase from 3^{o} to 38° in static contact angle after washing.

Hydrophobicity recovery after washing the samples is a clear indication of washing away of surface oligomers that were formed due to cleavage of surface polymer chains during the plasma treatment and thus exposing a more hydrophobic layer underneath. The results of the Ar + H_2O vapor RF plasma treatments shown in Figure 5.1 (c) also showed slight increases (5-6°) in static contact angle measurements after washing with exposure times greater than 60 s, but much less than the Ar + O_2 RF plasma treatments.

From Figure 5.1, it can be seen that, in general, RF plasma treatments require about 1 min treatment time to improve the surface wettability of LDPE. The lowest surface contact angle after water washing achieved by RF plasma treatments included 41° by Ar plasma, 71° by Ar + O_2 plasma, and 17° for Ar + H_2O plasma. The RF plasma-treated samples also exhibited hydrophobic recovery after aging in ambient air, and the results are described and discussed in a later section as compared with LTCAT treated samples.

5.3.2 LTCAT Plasma Treatments

In LTCAT process, electric power input into the system can be well expressed by arc current because of very little variation in voltage when argon was used as the carrier gas through the arc generator. In addition, the argon flow rate passing through the arc generator is an indication of the amount of energy that is carried by the luminous plasma torch.[14] In this study, therefore, arc current, argon flow rate, and plasma exposure time are the three major operating variables examined in LTCAT treatment of LDPE.

When a reactive gas is added to argon LTCAT plasma torch, collisions between excited argon metastable species with the reactive gas molecules occur, resulting in an energy transfer to the reactive gas molecules. The direct outcome of such energy transfers is the production of new reactive plasma species from the added reactive gases. These plasma species thus formed can also react with the polymer surface, and achieve surface modification of organic materials. In the present study, argon LTCAT without adding any reactive gases, as well as that with addition of oxygen and water vapor were used to modify the LDPE surfaces and the resulted plasma treatment effects were investigated.

5.3.3 Sessile Droplet Method

Figure 5.2 shows the surface contact angle changes of argon LTCAT treated LDPE with Ar flow rate, arc current, and exposure time. It should be noted that the surface contact angles of LTCAT treated LDPE were measured without and with water washing, but no significant difference were found from the data as was the case of RF plasma treatments shown in Figure 5.1. In Figure 5.2, therefore, the contact angles after washing the LTCAT treated samples are not presented.

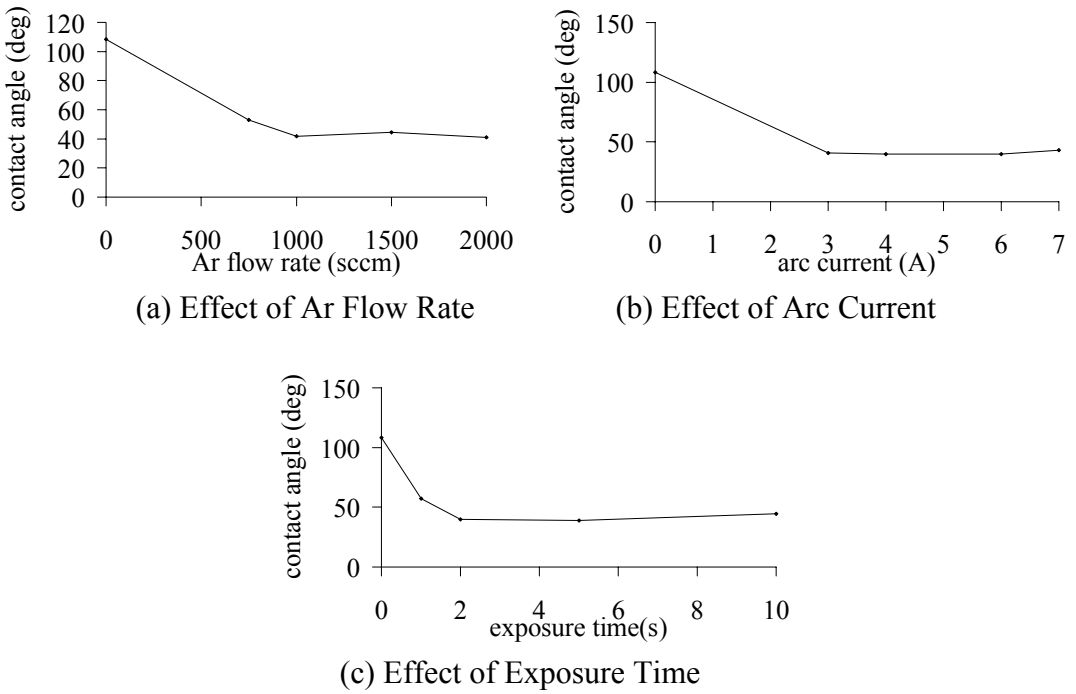

Figure 5.2. The surface contact angle changes of Ar LTCAT treated LDPE with (a) Ar flow rate, (b) arc current, and (c) exposure time. The LTCAT conditions are, if not specified in the plots, 1500 sccm Ar, 4.0 A arc current, and 2.0 s exposure time.

The data show that good wettability was achieved with very short treatment time of only 2.0 s, as compared to the 60 s with RF plasma. Other operating conditions to achieve good surface wettability (with water contact angle of ~ 40°) included 1000 sccm Ar flow rate and 3 A current. It should be noted that further increasing argon flow rate and arc current, within the ranges that were examined, did not contribute much in improving the surface wettability.

Figure 5.3 shows the plasma treatment effects of argon LTCAT with addition of O_2 on LDPE surfaces.

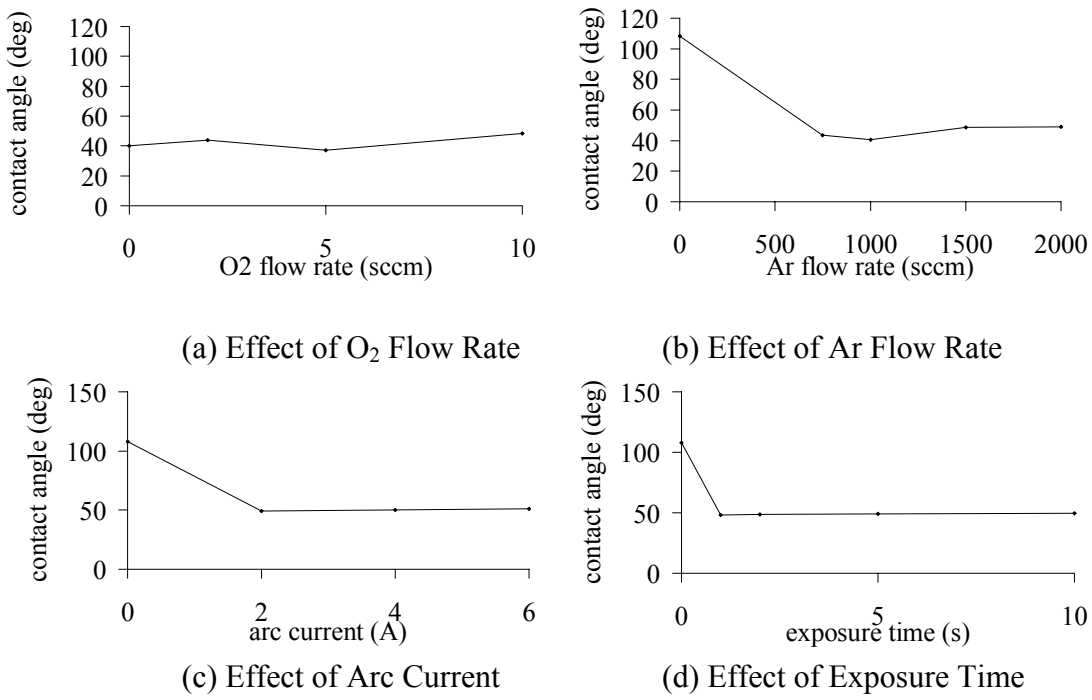

Figure 5.3. The surface contact angle changes of Ar+O_2 LTCAT treated LDPE with (a) O_2 flow rate, (b) Ar flow rate, (c) arc current, and (d) exposure time. The other LTCAT conditions are, if not specified in the plots, 1500 sccm Ar, 4.0 A arc current, 2.0 s exposure time, 10 sccm O_2.

The LTCAT conditions that produced the lowest contact angle (49°) included 1000 sccm Ar, 4.0 A arc current, and 2.0 s exposure time. It should be noted that, from Figure 5.3 (a), addition of oxygen into argon LTCAT did not show any advantages in improving the surface wettability of LDPE as compared with argon LTCAT treatment.

Figure 5.4 shows the plasma treatment effects of argon LTCAT with addition of water vapor on LDPE surfaces.

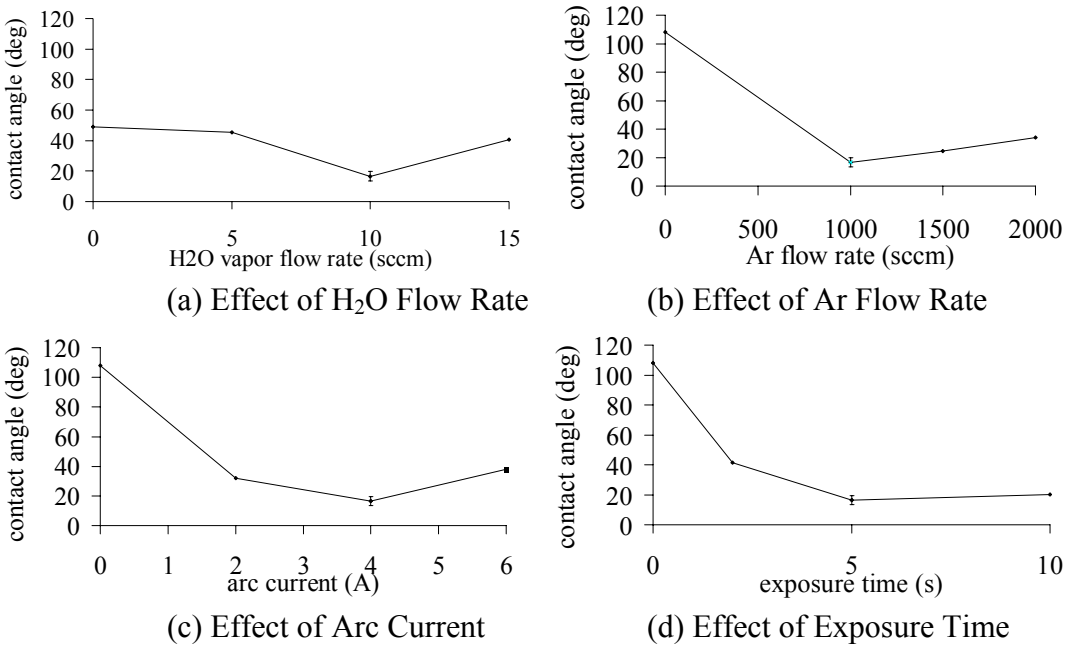

Figure 5.4. The surface contact angle changes of Ar+H_2O LTCAT treated LDPE with (a) H_2O flow rate, (b) Ar flow rate, (c) arc current, and (d) exposure time. The other LTCAT conditions are, if not specified in the plots, 1500 sccm Ar, 4.0 A arc current, 5.0 s exposure time, 10 sccm H_2O.

Based on the static contact angle data, the conditions that produced the best wettability were found to be 10 sccm H_2O, 1000 sccm Ar, 4 A current, and 5 s exposure time, which resulted in a static contact angle of 17°. At such low contact angles, spreading of the water droplets is significant.

5.3.4 Wilhelmy Balance Method

Wilhelmy force loops were obtained using Wilhelmy balance method for LDPE samples treated with LTCAT to examine dynamic wettability, surface damage in the form of ***overshooting***,[13] and surface configuration changes in the form of ***intrinsic hysteresis***.[12,15] The dynamic contact angles were determined for advancing (immersion)

and receding (emersion) phases of the cycles by using ***Equation 1*** and extrapolating each force trend to the intercept (0 depth) where the buoyancy term is zero. A force trend that has an intercept of 0 mN/m corresponds to a contact angle of 90°. An increase in the force trend corresponds to an increase in hydrophilicity, while a decrease in the force trend corresponds to an increase in hydrophobicity.

The stability of a surface can be examined by observing *overshooting* and *intrinsic hysteresis* between two Wilhelmy cycles. Overshooting in Wilhelmy cycles occurs when the advancing force trend in a second Wilhelmy immersion cycle shows a more hydrophobic surface than the first advancing immersion cycle. It is believed that *overshooting* is due to the presence of surface oligomers, which were formed from polymer degradation or bond cleavage of surface macromolecules during treatment and washed away during the Wilhelmy cycle exposing a more hydrophobic layer underneath. Surface configuration changes, on the other hand, are shown by an increase in the force trend from the first immersion cycle to the next, which is called *intrinsic hysteresis*. These configuration changes involve hydrophilic groups re-orienting toward the surface while the sample is immersed in water, thus making the surface more hydrophilic. After longer exposure in air, the hydrophilic surface groups may re-orient toward the bulk sample, making the sample surface more hydrophobic.

During the first cycle, the sample was immersed 10 mm into water and then withdrawn back to zero and allowed to dry for 5 minutes in ambient air. The purpose of drying in air was to allow the reversal of the possible surface configuration changes that

would have occurred during the first wetting. The second cycle involved immersing the sample to 15 mm, in which *overshooting* could be observed at 0-10 mm and the section from 10-15 mm would undergo its first wetting. After the sample was withdrawn back to 5 mm in the second cycle, the third cycle was allowed to begin immediately, which immersed the sample from 5-15 mm and then withdrew it to 0 mm. During the third cycle, both *overshooting* from surface damages and *intrinsic hysteresis* due to surface configuration changes could affect the outcome of Wilhelmy force loop, because the sample was not allowed to dry in ambient air. Therefore, the changes observed at 10-15 mm between the immersion phases of cycle 2 and cycle 3 could be a result of both *overshooting* and *intrinsic hysteresis*. When *overshooting* occurs, the difference in the degree of *overshooting* from 0-10 mm and 10-15 mm immersion phases can provide some indication of surface configuration changes.

Figure 5.5 shows the Wilhelmy force loop for a pre-cleaned, untreated LDPE sample with a hydrophobic surface, as exhibited by the dynamic contact angles.

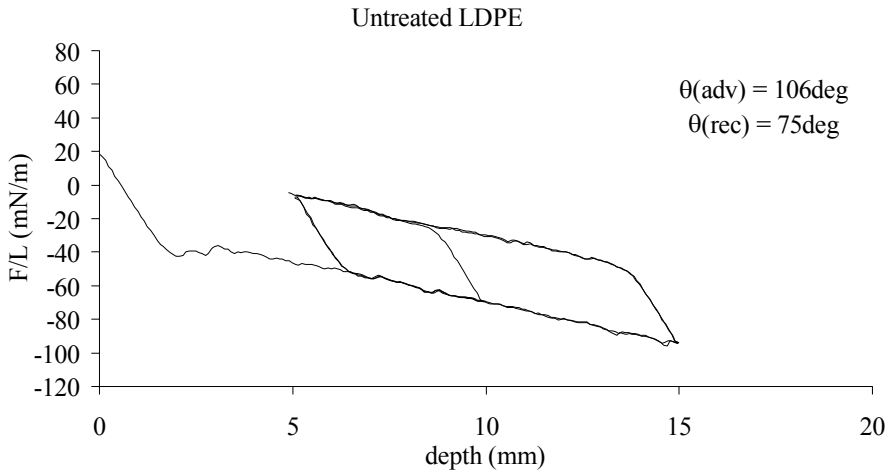

Figure 5.5. The Wilhelmy force loop of untreated LDPE shows a stable, hydrophobic surface with no intrinsic hysteresis (the second and third immersion lines trace the first immersion line).

The sample exhibits no *intrinsic hysteresis* from the first to the second immersion and the second to the third immersion, which indicates that the sample surface is very stable.

Figure 5.6 shows the Wilhelmy force loops Ar LTCAT treated LDPE samples with different exposure times.

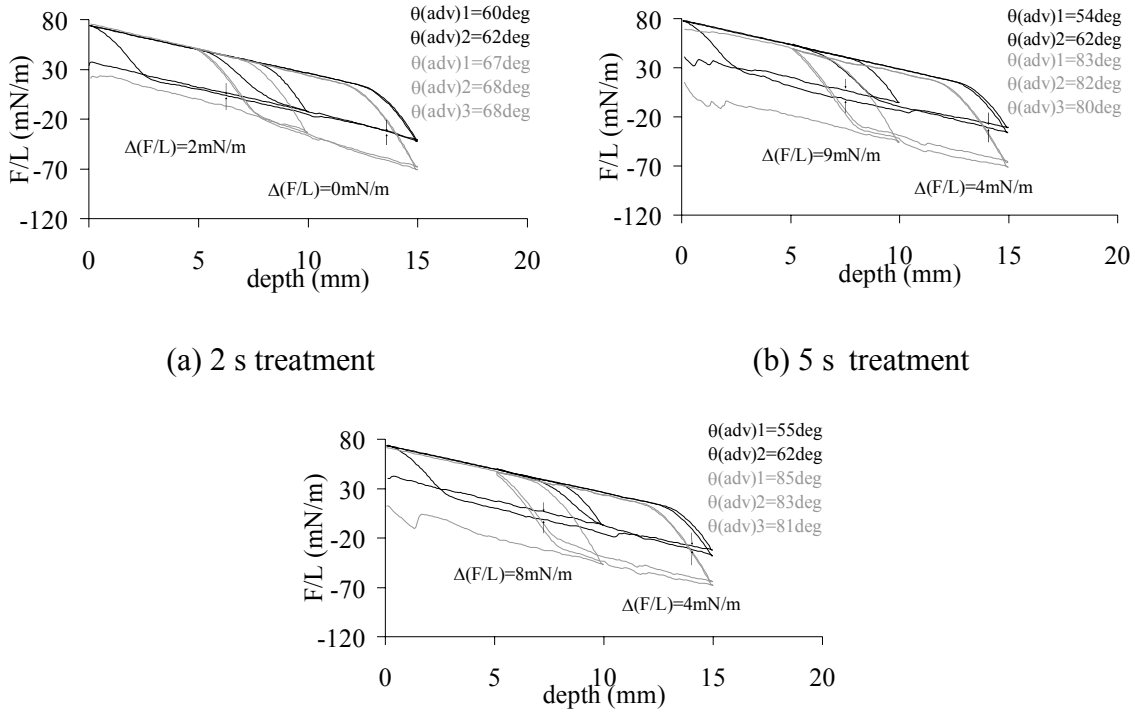

(a) 2 s treatment

(b) 5 s treatment

(c) 10 s treatment

Figure 5.6. The Wilhelmy force loops of Ar LTCAT treated LDPE samples with different treatment time. The black lines show the force loops obtained immediately after treatment, and the grey lines show the force loops obtained after 2 weeks of aging in air. The other LTCAT conditions include 1000sccm Ar and 4.0 A arc current.

It can be seen that all treated samples exhibited some degree of *overshooting*. The *overshooting* was minimized with a short exposure time of 2.0 s, as shown by a difference in force trends of 2 mN/m at 0-10 mm immersion. The *overshooting* from 10-15 mm immersion was reduced to 0 mN/m, which was less than the *overshooting* of 2 mN/m from 0-10 mm. This data indicates that the sample also underwent some degree of surface configuration changes when shifting the contacting medium from air to water. Wilhelmy loops were obtained after aging the samples in air for 2 weeks, as shown in Figure 5.6 by the gray loops. The aged samples showed no *overshooting*, which indicates that the surface oligomers were washed away after obtaining the first Wilhelmy force

loop and washing in de-ionized water. At the same time, all the aged samples in Figure 5.6 showed some degrees of *intrinsic hysteresis* further confirming surface configuration changes for argon LTCAT treated LDPE. It should be noted that, after 2 weeks aging, the sample treated with a shorter exposure time of 2.0 s showed the greatest surface stability, as shown by both the least amount of hydrophobic recovery and the minimal *intrinsic hysteresis*.

Figure 5.7 shows the Wilhelmy force loops obtained with LDPE samples treated by argon LTCAT plasma torch with addition of different amount of oxygen at 1 sccm, 2 sccm, and 7 sccm.

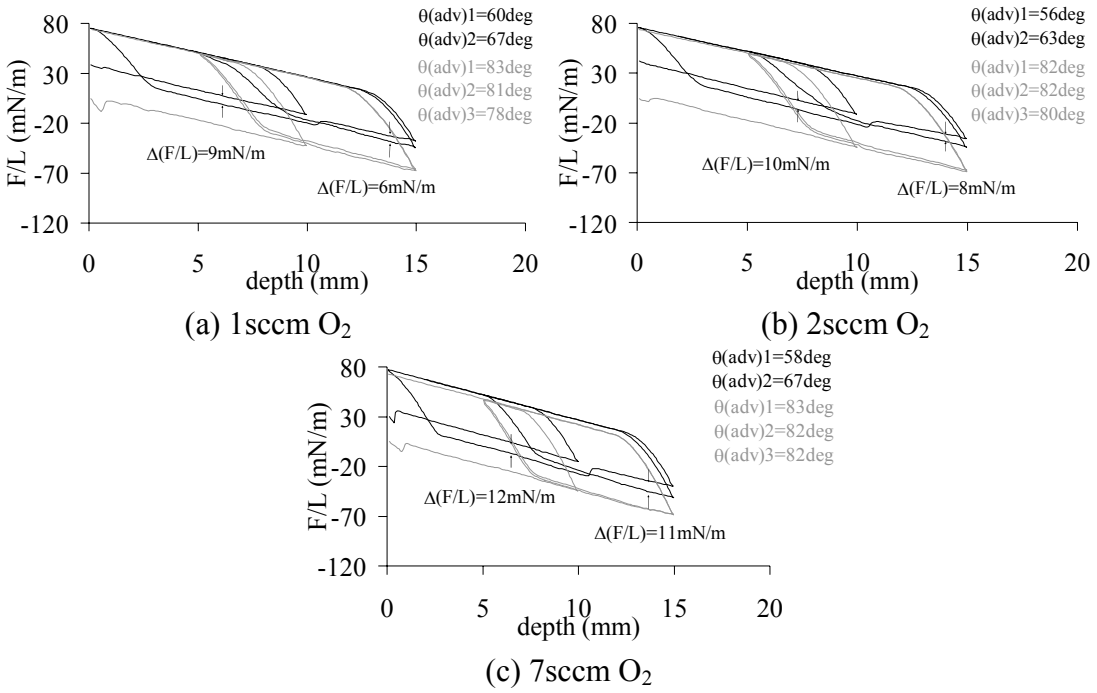

Figure 5.7. The Wilhelmy force loops of Ar+O_2 LTCAT treated LDPE samples with different O_2 flow rates. The black lines show the force loops obtained immediately after treatment, and the grey lines show the force loops obtained after 2 weeks of aging in air. The other LTCAT conditions are 1000sccm Ar, 4.0 A arc current, 2.0 s exposure time.

As can be seen in Figure 5.7, all of the treatments resulted in *overshooting*, which was significantly higher than that from the Ar LTCAT treatments. It should be noted for each condition, the overshooting from 10-15 mm immersion is less than the overshooting from 0-10 mm immersion. This indicates that all of the treated samples also exhibited some degree of surface configuration change.

The conditions involving 1sccm O_2, which resulted in the lowest *overshooting*, were used to examine the effects of exposure time on LDPE using Wilhelmy force loops. As shown in Figure 5.8, the loops show that *overshooting* decreased with increasing exposure time, up to 15 s, when the *overshooting* was 3 mN/m for both 0-10 mm and 10-15 mm immersions. Further increasing the treatment time to 20 s increased the degree of *overshooting* indicating more surface damages occurred. For all of the treatments, the loops showed *intrinsic hysteresis* after aging in ambient air for 2 weeks, indicating significant mobility of hydrophilic moieties on Ar + O_2 LTCAT treated LDPE surfaces.

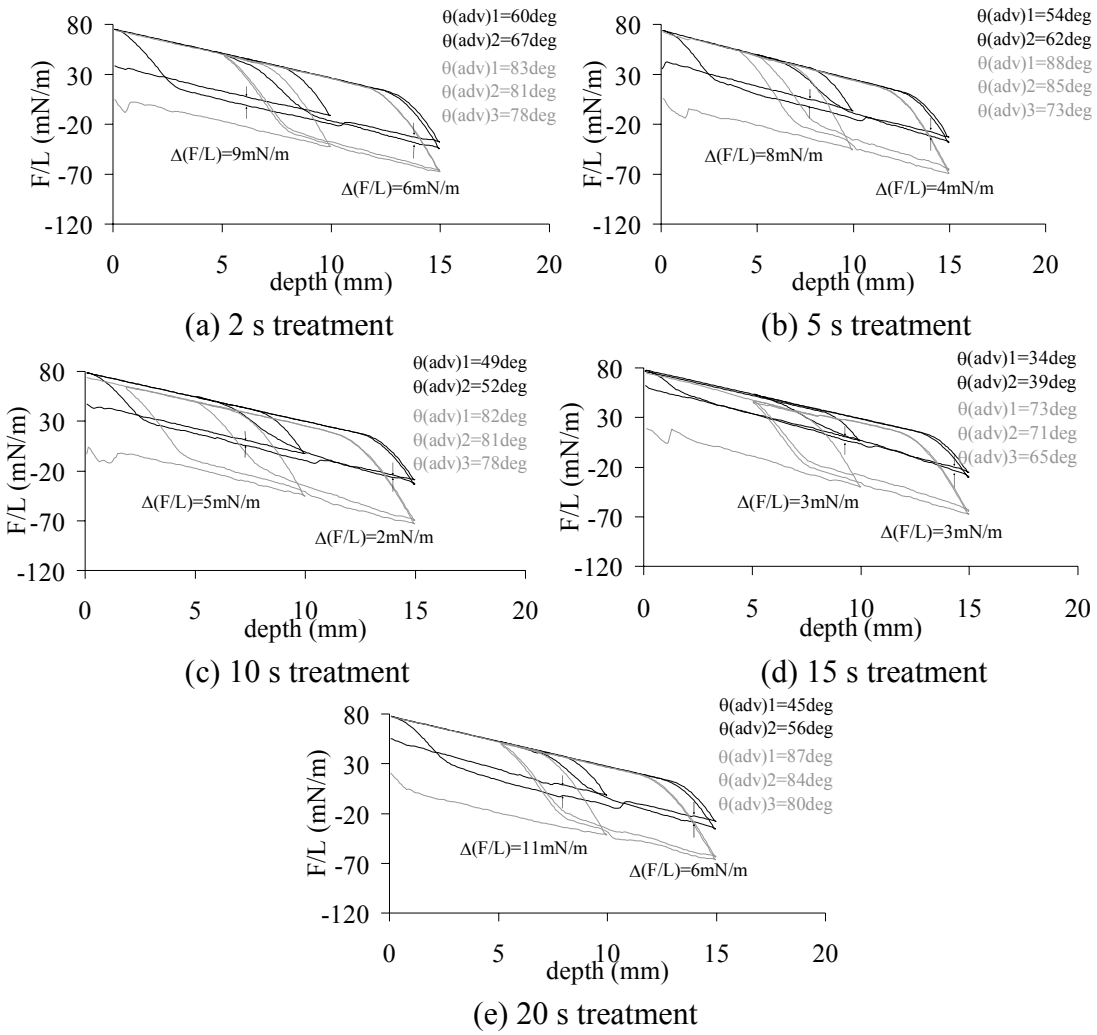

Figure 5.8. The Wilhelmy force loops of Ar+O_2 LTCAT treated LDPE samples with different treatment time. The black lines show the force loops obtained immediately after treatment, and the grey lines show the force loops obtained after 2 weeks of aging in air. The constant conditions include 1000 sccm Ar, 1 sccm O_2, 4.0 A arc current.

Figure 5.9 shows the Wilhelmy force loops obtained with LDPE samples treated by argon LTCAT plasma torch with addition of different amount of water at 1 sccm, 2 sccm, and 10 sccm.

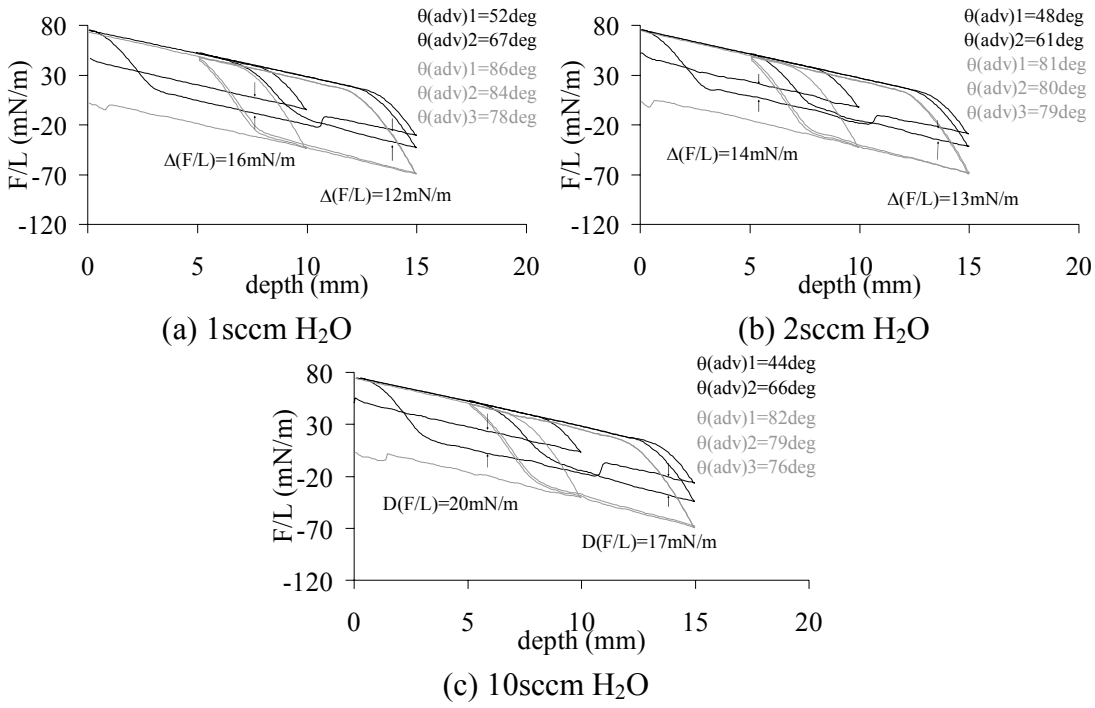

Figure 5.9. The Wilhelmy force loops of Ar+H_2O LTCAT treated LDPE samples with different H_2O flow rates. The black lines show the force loops obtained immediately after treatment, and the grey lines show the force loops obtained after 2 weeks of aging in air. The other LTCAT conditions include 1000sccm Ar, 4.0 A arc current, 3.0 s exposure time.

All of the treatments resulted in a high degree of ***overshootings*** in the range of 13 to 20 mN/m, which was even greater than the treatments involving Ar LTCAT with addition of O_2. These data clearly indicated that LTCAT treatment with addition of water vapor resulted more damages on LDPE surfaces. It was also noted that, from Figure 5.9, more addition of water vapor resulted higher degree of ***overshooting***. When H_2O vapor was added, the LTCAT torch became fainter than the case with O_2 addition, which indicates a greater consumption of the argon torch by H_2O molecules than the O_2 molecules. In other words, the energy carriers (excited Ar atoms in this case) in the LTCAT torch are

more favorably to transfer their energy to the H_2O molecules than to the O_2 molecules. It is well known that argon plasma treatment of polymers usually causes surface CASING effect (cross-linking via activated species of inert gases),[16] which helps to stabilize the hydrophilic moieties and minimize the formation of low molecular oligomers on the surface. Therefore, one of the possible reasons for the high degree of surface damages on LDPE by LTCAT treatment with water addition could be the reduction of argon plasma species in the LTCAT due to their energy transfer to the added water molecules. As a result, the CASING effects due to argon plasma species diminished.

The Ar LTCAT treatments with 2 sccm H_2O vapor showed the greatest wettability, the least amount of ***overshooting***, and the minimum surface configuration changes, as shown by the lowest difference in ***overshooting*** between 0-10 mm and 10-15 mm. This condition was used to investigate the effects of LTCAT exposure time on LDPE surface, as shown in Figure 5.10. The data shows that the 3.0 s treatment time gave rise to the least amount of ***overshooting***, but no clear trends developed with increase in exposure time. The Wilhelmy force loops of the aged samples show that most of the LTCAT treatments of LDPE with water vapor addition resulted in relatively stable surfaces after aging in ambient air, as shown by the very small degrees of ***intrinsic hysteresis***.

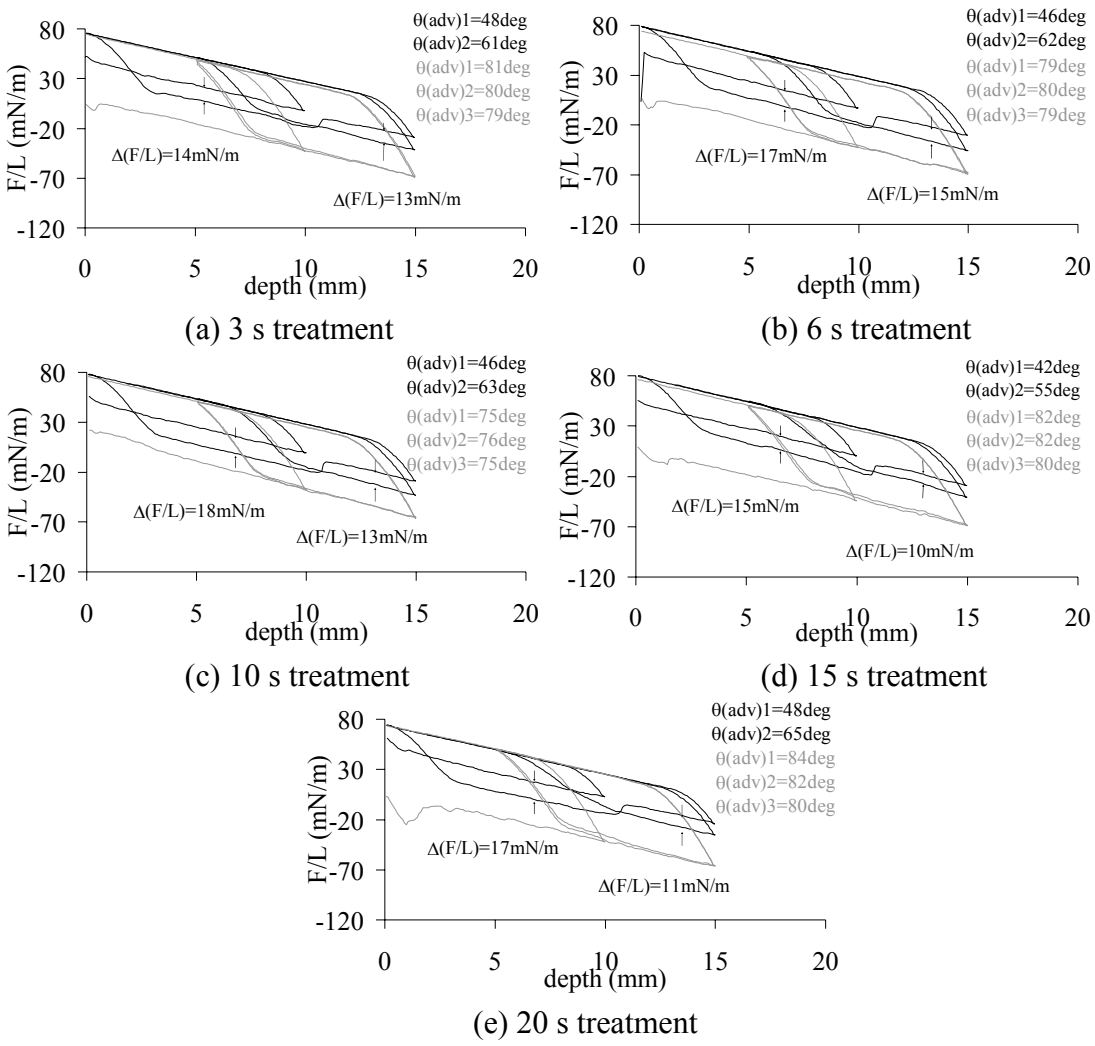

Figure 5.10. The Wilhelmy force loops of Ar+H_2O LTCAT treated LDPE samples with different treatment time. The black lines show the force loops obtained immediately after treatment, and the grey lines show the force loops obtained after 2 weeks of aging in air. The constant conditions include 1000sccm Ar, 2 sccm H_2O, 4.0 A arc current.

5.3.5 Surface Stability of the Treated Surface upon Aging

Aging effects on LTCAT and RF plasma treated LDPE samples were investigated with storing the samples in ambient air for over a 2 week period. Figure 5.11 shows the static contact angle changes of these samples upon aging.

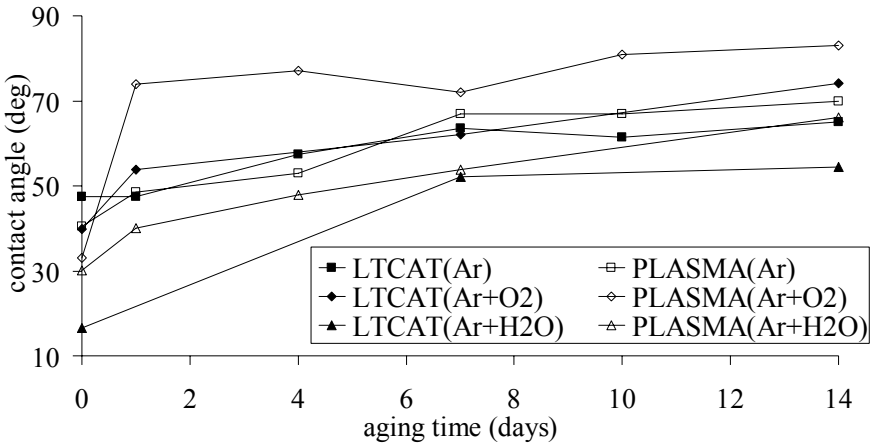

Figure 5.11. Aging effects on the static surface contact angles of LTCAT and RF plasma treated LDPE samples, which were prepared under plasma conditions that gave the lowest static surface contact angles.

After 2-week aging, the sample treated by Ar LTCAT with H_2O vapor addition showed the best wettability results, while the samples treated by Ar + O_2 RF plasma showed the most hydrophobic recovery. In overall, the LTCAT treatments for each gas combination resulted in better wettability on LDPE surfaces than the RF plasma counterparts.

As a comparison, Figure 5.12 shows the Wilhelmy force loops measured from LTCAT and RF plasma treated LDPE samples, which were prepared under conditions that gave the best wettability for each gas combination.

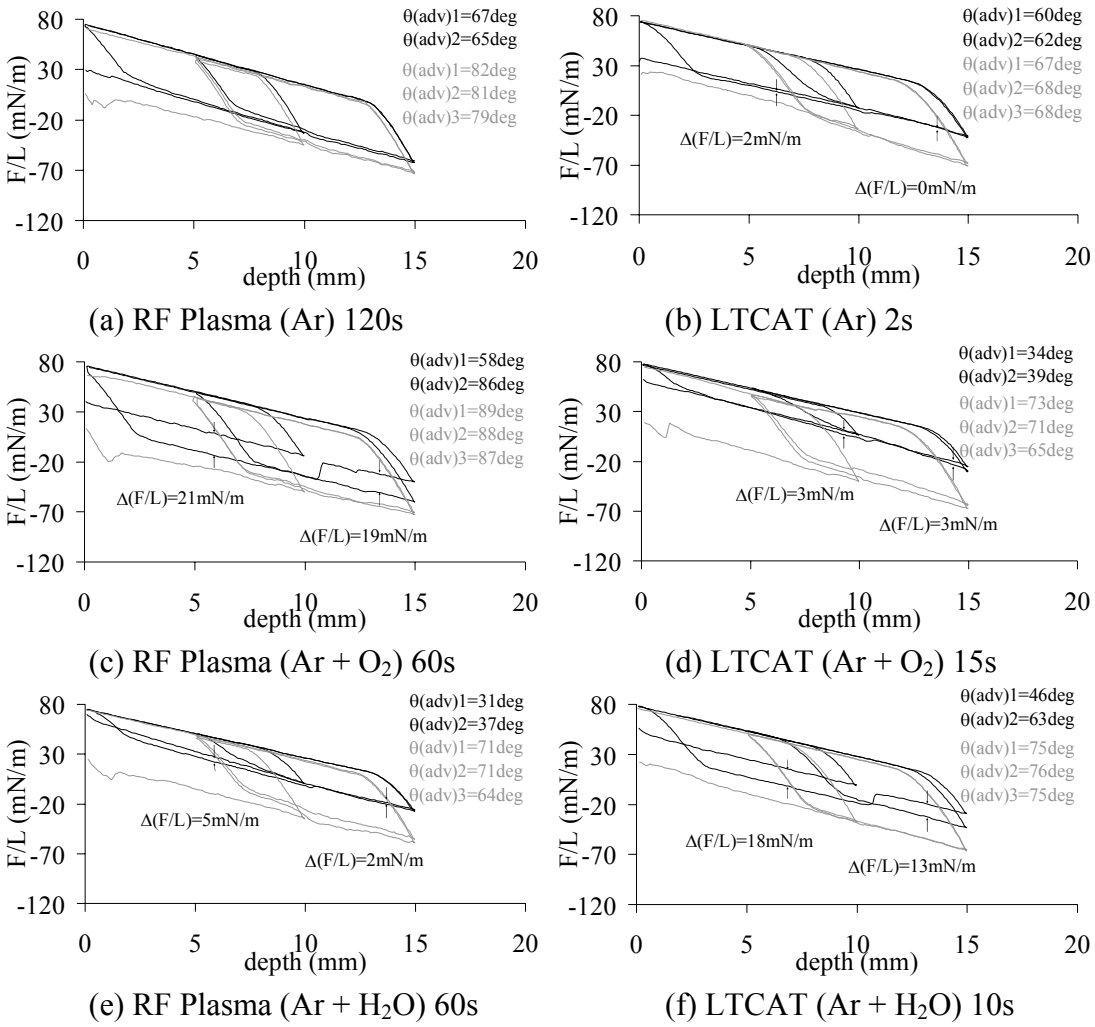

Figure 5.12. Wilhelmy force loops measured from LTCAT and RF plasma-treated LDPE samples, which were prepared under conditions that gave the best wettability for each gas combination.

Most of the treatments by LTCAT and RF plasmas resulted in certain surface damages shown as the ***overshooting*** on the Wilhelmy force loops. One exception is the Ar RF plasma treated sample (Figure 5.12 (a)), which did not show any ***overshooting*** but significant mobility of surface moieties shown by the high degree of ***intrinsic hysteresis***. The Ar LTCAT treatment without reactive gas addition (Figure 5.12 (b)) produced the best wettabiltiy after 2 week aging, the least hydrophobic recovery, the slightest ***intrinsic***

hysteresis indicating the most stable surface. In addition, the treatment time of 2.0 s is the shortest and thus the most rapid and efficient treatment process. It was expected that the Ar LTCAT without reactive gas addition would result in a stable surface due to the CASING effect. The freshly treated samples, however, showed slight *overshooting* (2 mN/m), which points to a small degree of surface damage. The damage induced during treatment is possibly due to a significant presence of residual air in the reactor background because of the high base pressure of 10 mtorr.

The Ar LTCAT treatments with O_2 addition produced more wettable surfaces with less damage than the Ar + O_2 RF plasma treatments, as indicated by significantly less *overshooting*. In addition, the treatment time was much shorter with LTCAT, which was 15 s, compared to RF plasma, which required 60 s. After aging in air for 2 weeks, the immersion force trends and the *intrinsic hysteresis* show that LTCAT-treated sample exhibited greater wettability, but also higher mobility of surface functionalities than the RF plasma-treated sample.

The LDPE samples treated by LTCAT involving H_2O vapor showed lower wettability and greater overshooting than the Ar + H_2O vapor RF plasma treated samples immediately after treatment. This trend is opposite to the case of oxygen addition. In RF plasma, the energy is carried by both the Ar and reactive gas, while in LTCAT the energy is carried by the excited Ar atoms and transferred to the reactive gas. Previous study in surface modification of polymers using RF plasma treatments has indicated a high degree of surface damage in H_2O vapor plasma using a low frequency input.[13] It is possible that

the Ar plasma species in Ar + H_2O RF plasma could remedy some of the damages induced by H_2O plasma species. In LTCAT process, however, the addition of H_2O vapor consumes the excited Ar atoms to a greater extent than addition of O_2 and causes greater surface damage of LDPE.

Continuous studies are currently underway to examine the energy transfer processes involved in Ar LTCAT with reactive gas addition, the plasma constituents created in the LTCAT and RF plasmas, and the reactions induced on the polymeric surfaces during the LTCAT and RF plasma treatments. The results thus achieved are expected to provide a deep insight into the plasma surface modification process of polymers in order to elucidate how the damage is induced on the polymeric surfaces and how surface stability is created by LTCAT and RF plasma treatments.

5.4 Conclusions

Application of LTCAT to surface modification of LDPE polymer sheets has been studied by surface contact angle measurements, including static sessile droplet method and dynamic Wilhelmy balance methods. Combination of static and dynamic surface contact angle measurements enabled a comprehensive investigation of the plasma treatment effects, which include surface wettability changes, surface stability, and possible surface damages induced by the LTCAT plasma. The experimental results thus achieved clearly indicate that LTCAT treatment is a very rapid, effective and efficient technique in surface modification of LDPE polymers.

Without adding reactive gases, plasma treatment using LTCAT of argon only significantly improved the LDPE surface wettability to 40^{o} within a very short treatment time of 2.0 second. Dynamic analysis of Wilhelmy force loops of the treated LDPE samples indicated that such a short Ar LTCAT treatment produced a stable hydrophilic surface with slight surface damage, as shown by a very low initial *overshooting* (2 mN/m) and little *intrinsic hysteresis* after 2 weeks of aging. The excellent surface stability was attributed to CASING effects on LDPE surface resulted from argon plasma species existing the Ar LTCAT plasma torch.

The experimental data showed that addition of reactive gases of oxygen or water vapor into the Ar LTCAT resulted in a greater surface damage on LDPE surface, as shown by the increased *overshooting* in the Wilhelmy force loops measured with the treated samples. Surface treatment of LDPE by Ar LTCAT with oxygen addition did not further improve the surface wettability. On the other hand, it gave a less stable surface as shown by a significant *intrinsic hysteresis* in the Wilhelmy force loops measured with the treated samples upon 2 weeks of aging in air. Plasma treatment of LDPE by Ar LTCAT with H_2O vapor addition produced an extremely wettable surface with water contact angle of 17^{o}. However, it caused greater damage on LDPE surface as observed by the pronounced *overshooting* in the Wilhelmy force loops.

In comparison with RF plasma treatments, LTCAT treatments are much more rapid and efficient in surface modification of LDPE. LTCAT treatment usually requires a few seconds to achieve a significant improvement in surface wettability of LDPE, while

RF plasma treatment takes a couple of minutes. The Wilhelmy analysis showed greater wettability was obtained with LDPE samples treated with Ar LTCAT alone and Ar LTCAT with O_2 addition than the samples treated with the corresponding RF plasmas. Despite the small degree of initial surface damage, Ar LTCAT treated surface was more wettable and stable than the Ar RF plasma-treated surface, for both the freshly treated and aged samples for 2 weeks in air. The Ar + O_2 RF plasma treatment resulted in much more damage on LDPE surface than the Ar LTCAT treatment with O_2 addition.

5.5 References for Section V

1. Durand, A.M.; "The practical application of plasma treatment to polymer surfaces for improved adhesion", *LE VIDE, Science, Technique, et Applications*, 1997, **53**, 242 - 252.

2. Strobel, M.; Walzak, M.J.; Hill, J.M.; Lin, A.; Karbashewski, E.; Lyons, C.S.; "A comparison of gas-phase methods of modifying polymer surfaces", *J. Adhesion Sci. Technol*., 1995, **9**, 365 - 383.

3. Shishoo, R.; "Plasma treatment – industrial applications and its impact on the C&L industry", *J. Coated Fabrics*, 1997, **26**, 26 - 35.

4. Wertheimer, M.R. and Bartnikas, R.; "Degradation effects of plasma and corona on polymers" in *Plasma Processing of Polymers*, R. d'Agostino et al. eds., Kluwer Academic Publishers, Netherlands, 1997, 435 – 450.

5. Arefi, F.; Andre, V.; Montazer-Rahmati, P.; Amouroux, J.; "Plasma polymerization and surface treatment of polymers", *Pure & Appl. Chem.*, 1992, **64**, 715 - 723.

6. Bettge, D.J.; Hinrichsen, G.; "Continuous manufacturing of composites of high-performance polyethylene fibers", *Compos. Sci. Technol*., 1993, **47**, 131 - 136.

7. Ameen, A.P.; "An investigation of the surface chemical homogeneity of plasma oxidized poly(ether etherketone)", *Polymer Degradation and Stability*, 1996, **51**, 179 - 84.

8. Krentsel, E.; Fusselman, S.; Yasuda, H.; Yasuda, T.; Miyama, M.; "Penetration of plasma surface modification. II. CF4 and C2F4 low-temperature cascade arc torch", *J. Polym. Sci.: Part A: Polym. Chem.*, 1994, **32**, 1839 - 1845.

9. Yu, Q.S.; Reddy, C.M.; Meives, M.F.; Yasuda, H.K.; "Surface modification of poly(tetrafluoroethylene) by a low-temperature cascade arc torch and radio-frequency plasma", *J. Polym. Sci.: Part A: Polym. Chem.*, 1999, **37**, 4432 – 4441.

10. Fusselman, S.P. and Yasuda, H.K.; "Particle densities and non-equilibrium in a low-pressure argon plasma jet", *Plasma Chem. Plasma Process.,* 1994, **14**, 251 - 275.

11. Yu, Q.S. and Yasuda, H.K.; "An optical emission study on expanding low-temperature cascade arc plasmas", *Plasma Chem. Plasma Process.,* 1998, **18**, 461 - 485.

12. Weikart, C.M.; Miyama, M.; Yasuda, H.K.; "Surface modification of conventional polymers by depositing plasma polymers of trimethylsilane + O_2. Part II: Dynamic wetting properties", *J. Colloid and Interface Sci.* 1999, **211**, 28-38.

13. Weikart, C.M.; Yasuda, H.K.; "Modification, degradation, and stability of polymeric surface treated with reactive plasmas", *J. Polym. Sci.* A, 2000, **38**, 3028-3042.

14. Yu, Q.S. and Yasuda, H.K.; "Deposition behavior in a low-temperature cascade arc torch (CAT) polymerization process", *J. Polym. Sci. A.,* 1999, **37**, 967-982.

15. Miyama, M.; Yang, Y.; Yasuda, T.; Okuno, T.; Yasuda, H.K.; "Static dynamic contact angles of water on polymer surfaces", *Langmuir*, 1997, **13**, 5494-5503.

16. Liston, E.M.; Martinu, L.; Wertheimer, M.R.; "Plasma surface modification of polymers for improved adhesion: a critical review", In *Plasam Surface Modification of Polymers: Relevance to Adhesion*, Strobel, M.; Lyons, C.S.; Mittal, K.L.; Eds.; VSP: Utrecht, The Netherlands, 1994, p3.

SECTION VI

THE MESH DISTURBANCE EFFECTS IN A LOW TEMPERATURE CASCADE ARC TORCH (LTCAT) FOR SURFACE MODIFICATION OF LOW DENSITY POLYETHYLENE (LDPE)

6.1 Introduction

Surface modification treatments are often applied to polymeric surfaces for the enhancement of adhesion, wettability, biocompatibility, printability, barrier properties, susceptibility to harsh agents, and other interfacial characteristics[1-6]. Surface modification treatments can involve deposition of thin films or chemical changes in the top molecular layers. Among the surface modification treatments applied to polymers, plasma processes, including low-pressure plasma, present advantages over other treatments, such as wet chemical treatments and mechanical roughening. Plasma processes are versatile and environmentally benign methods for polymeric surface modification[5].

Plasma treatments of polymers that involve chemical surface modification can induce surface functionalization, in which new surface functional groups are created, surface cross-linking, and degradation. Plasma processes can have significant drawbacks for polymer surface treatment, though, due to the difficulties in optimization of certain desirable reactions and in minimization of undesired consequences, such as surface degradation[7]. Many species exist in low pressure plasmas, including high-energy ions, electrons, vacuum ultraviolet (VUV) and ultraviolet (UV) photons, excited neutral species, reactive free radicals, and neutrals. Bombardment from high energy species,

such as ions, can result in significant ablation of surface moieties, chain scission, and surface degradation[8-10]. Degradation can occur in the form of etching into volatile species, which could be desirable or tunable to fit the application, or the scission of surface macromolecular chains into oligomers or low molecular weight oxidized material (LMWOM), which form a weak boundary layer on the surface that is detrimental to adhesion and stability.

Recent studies[1,11] have demonstrated the many unique advantages of low temperature cascade arc torch (LTCAT) over traditional plasma techniques, including significant reduction of degradation on polymer surfaces and enhanced surface stability. In addition, LTCAT treatment is fast and effective, in the case of Ar LTCAT, 2 s exposure time was reported to be sufficient for the surface modification of low density polyethylene (LDPE), which was much faster than the 120 s that was required for Ar RF plasma treatment (see Section V). LTCAT consists of a beam of mainly excited neutral species of a noble gas, while most of the ions and electrons are contained in a DC arc generator[12,13]. However, some ions and low energy electrons (0.3 – 1.5 eV)[14] escape the discharge generator and remain in the beam that expands into the substrate chamber. It was reported that Ar LTCAT treatments applied to LDPE surfaces induced some surface damage from LMWOM formation[1]. In Ar LTCAT without reactive gas addition, the likely sources of surface degradation include effects from high energy Ar ions (>15 eV) that escape the arc generator and the effects of VUV/UV radiation.

An investigation by Fisher, et. al[10] has indicated that placing a grounded metal mesh in the path of a RF discharge beam successfully removed the ions from the beam. In this study, we chose to place a stainless steel mesh in the LTCAT beam in an attempt to remove ions from the discharge before interacting with the polymer substrates and to study the disturbance effects of the mesh. Furthermore, the mesh was placed in the reactor chamber which is absent of an external electric field and thus, no ion regeneration occurred between the mesh and the substrate. The treatment conditions included Ar LTCAT, Ar LTCAT + O_2, and Ar LTCAT + H_2O with the mesh placed at grounded or floating potential for each experiment. The changes in light emitting species were examined by optical emission spectroscopy (OES) and the treatment effects were observed by dynamic surface characterization of the treated polymer samples using the Wilhelmy balance method. The treated samples in this investigation were compared with the results reported in Section V, which were conducted without any disturbances in the beam.

6.2 Experimental

6.2.1 Materials

Low density polyethylene (LDPE) sheets with thickness of 1 mm were purchased from Goodfellow Cambridge Limited (Cambridge, UK) and cut into 20 × 30 mm plates. The samples were ultrasonically cleaned in 5 % detergent in de-ionized water for 30 min, rinsed in de-ionized water, and dried in ambient air for 30 min. The clean, dry samples were then stored in a desiccator. Stainless steel mesh was obtained from McNichols Co. (Atlanta, GA) in sizes mesh 8 and mesh 24. The mesh was cut into 5 × 5 in pieces and

ultrasonically cleaned in acetone for 30 min. The argon and oxygen gases, with purities of 99.997 % and 99.5 %, respectively, were obtained from Praxair (St. Louis, MO). The water used in the Wilhelmy balance method and in the water vapor reactive gas that was added to Ar LTCAT was obtained from a Culligan de-ionizing system attached to in-house distilled water.

6.2.2 LTCAT Reactor Conditions

A detailed description and the operational procedures of the LTCAT reactor were reported in previous investigations[11,13]. The LTCAT reactor consisted of an arc generator, Pyrex glass cross vacuum chamber, and an Edward (Grand Island, NY) High-Vacuum EH500A / E2M80 combination pump. The arc generator was mounted on one port of the cross vacuum chamber and consisted of a narrow channel (2 mm) formed by a series of copper disks that were separated by silicone rubber insulators. A copper needle cathode was placed at the upstream end of the arc generator and the last metal disk was grounded. Before performing each experiment, the copper disks were cooled to 15 °C using an ethylene glycol – water mixture.

For each treatment, the LTCAT reactor was evacuated for 10 min to about 1 mtorr pressure. The leak rate of the reactor was around 0.04 sccm, which was about 0.004 % of the Ar flow rate. Ar flowed throught the narrow channel at 1000 sccm, which created supersonic gas velocity in the narrow channel that forced the glow discharge into the vacuum chamber in the form of a luminous plasma torch. A MDX-5K direct current power supply was used to ignite and sustain the argon discharge inside the arc generator.

Previous studies[12,13] have shown that the electric field inside the arc generator confines most of the charged species and as a result, the discharge torch consists mainly of electronically excited neutral species of argon. Reactive gas, such as O_2 and H_2O vapor can be added to the LTCAT discharge, in which the electronically excited noble gas species transfer energy to the reactive gas species, resulting in dissociation and excitation of the reactive gas molecules. Ionization of the reactive gas molecules and dissociated fragments can be neglected in the discharge vacuum chamber because of the relatively low energy of the electronically excited Ar energy carriers.

The LDPE samples were placed at 21 cm distance from the arc generator outlet and a stainless steel mesh was placed about 1 cm upstream the polymer location or 1 cm downstream the polymer location. In addition, the mesh was either placed at floating potential or at ground potential, depending on the experiment. Treatment times and the flow rates of the reactive gases that were added to the discharges were varied.

6.2.3 Wilhelmy Balance Method

The Wilhelmy balance method was used to examine the surface characteristics of the treated polymers. Section 5.2.4 outlines the theory and method of the dynamic wettabiltiy analysis. A KSV Instruments, Ltd. (Helsinki, Finland) Sigma 70 tensiometer was used to obtain dynamic contact angle measurements of the polymers during several wetting cycles. The stability of the polymer surfaces was examined by observing the *intrinsic hysteresis* or *overshooting* between cycles. Intrinsic hysteresis occurs when the surface during one cycle exhibits greater wettability than in the previous cycle, which is

attributed to mobile hydrophilic functional groups that bend toward the polymer surface during the first wetting, making the surface more wettable for the next wetting cycle. Overshooting is exhibited by a polymer when the treated surface contains loosely-bonded, non-volatile oligomers that display hydrophilic behavior during the initial wetting cycle and wash into the water during immersion, which exposes a more hydrophobic surface layer in the next wetting cycle. Wilhelmy force loops were obtained immediately after treatment, 1 day after treatment, 1 week after treatment, and 2 weeks after treatment. Hydrophobic recovery, when it occurred for a treated polymer, was observed by comparing the immediate Wilhelmy force loop to the loops obtained after allowing the samples to age. The overall stability of a treated polymer surface was gauged from the degree of intrinsic hysteresis, overshooting in the initial force loop, and hydrophobic recovery. A surface is considered stable when each of the three phenomena is minimized.

6.2.4 Optical Emission Spectroscopy

Optical Emission Spectroscopy (OES) was used to examine the photo-emitting species that were present in the glow of the discharges upstream and downstream the mesh screen that was set at floating or grounded potential. The OES equipment was manufactured by Jarrell Ash Corporation (now Thermo Electron in Minneapolis, MN) with a control and data acquisition system from Princeton Instruments, Inc. (Trenton, NJ). The exposure time for the OES spectra was 5 min for all cases.

6.3 Results and Discussion

The effects on the LTCAT discharges and treatments of LDPE substrates from the placement of a stainless steel mesh in the beam at floating or grounded potential were investigated. The types of discharges included Ar LTCAT and Ar LTCAT with reactive gas addition of O_2 or H_2O. Figure 6.1 illustrates the placement of the LDPE substrates and the OES probe with respect to the stainless steel mesh screen.

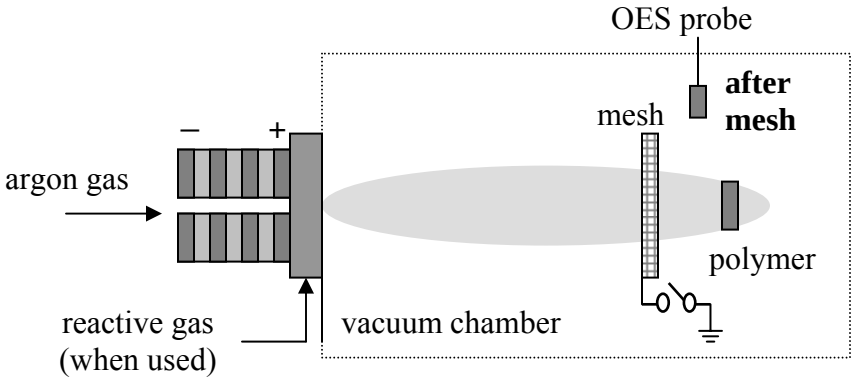

(a) In this configuration, mesh was floating or grounded.

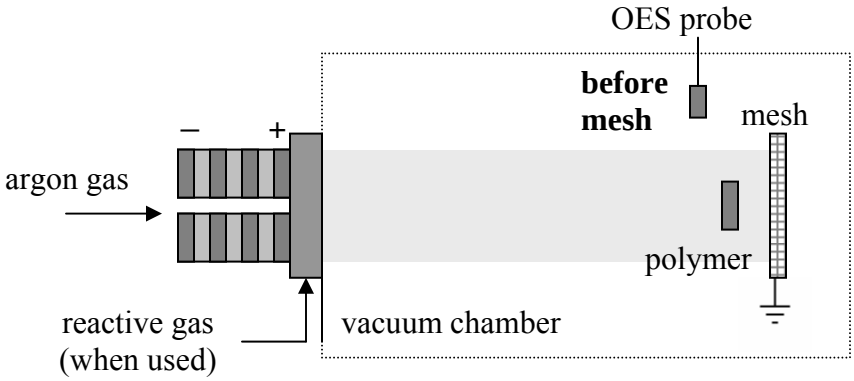

(b) In this configuration, mesh was always grounded.

Figure 6.1. A pictorial representation of the LTCAT configuration, which illustrates the positions of the polymer substrate and OES probe with respect to the stainless steel mesh. In (a), the mesh was placed at floating or grounded potential and in (b), the mesh was grounded.

For the configuration in Figure 6.1 (a) with a floating mesh, both the OES spectra and Wilhelmy loops for the treated polymer surfaces are presented. When a grounded

mesh was placed in the configuration shown in Figure 6.1 (a), however, the glow after the mesh disappeared from both visual inspection and the OES spectra, which showed no significant peaks. Thus, the OES spectra after a grounded mesh are not given, but the Wilhelmy loops of the treated samples placed after the grounded mesh are presented. For the configuration shown in Figure 6.1 (b) with a grounded mesh, the OES spectra of LTCAT and the Wilhelmy force loops of some of the treated samples placed in this position are presented. For comparison, OES spectra and Wilhelmy loops for LDPE substrates treated without the placement of a mesh in LTCAT discharges are also presented. The Wilhelmy force loops for LDPE treated without the mesh were obtained from Section V.

6.3.1 The Effects of Placing a Floating Mesh in LTCAT

The first mesh used in the study had a mesh size 24 (24 holes per linear inch) and was placed upstream from the LDPE sample position (configuration Figure 6.1 (a) with floating mesh). From visible inspection of Ar LTCAT with the stainless steel mesh 24 screen, all of the discharge was reflected and quenched by the mesh and no glow appeared downstream from the mesh. It seems that the size of the openings of the mesh 24 screen was too small to allow significant penetration of the discharge.

A mesh size 8 with larger openings was placed upstream from the LDPE sample position in Ar LTCAT, Ar LTCAT + O_2, and Ar LTCAT + H_2O discharges. Figure 6.2 contains an optical photograph of the effects of the floating mesh placed in the beam of Ar LTCAT discharge.

Figure 6.2. An optical photograph of the effects of placement of a floating stainless steel mesh 8 screen on the visible glow of Ar LTCAT discharge under the conditions of 1000 sccm Ar and 4 A arc current.

It is obvious from Figure 6.2 that the mesh created a significant disturbance in the LTCAT discharge and much of the beam seems to be reflected by the mesh, even though the holes are relatively large (~2.5 mm). OES spectra of the discharges without the mesh and after the floating mesh (configuration Figure 6.1 (a) with floating mesh) were obtained to examine the changes in photo-emitting species induced by the mesh. Figure 6.3 contains OES spectra of (a) Ar LTCAT, (b) Ar LTCAT + 1 sccm O_2, and (c) Ar LTCAT + 1 sccm H_2O vapor discharges obtained without a mesh (gray) and after a floating mesh (black). The OES data indicate that the intensity of electronically excited Ar atoms, Ar^*, after the floating mesh is significantly reduced for all discharges.

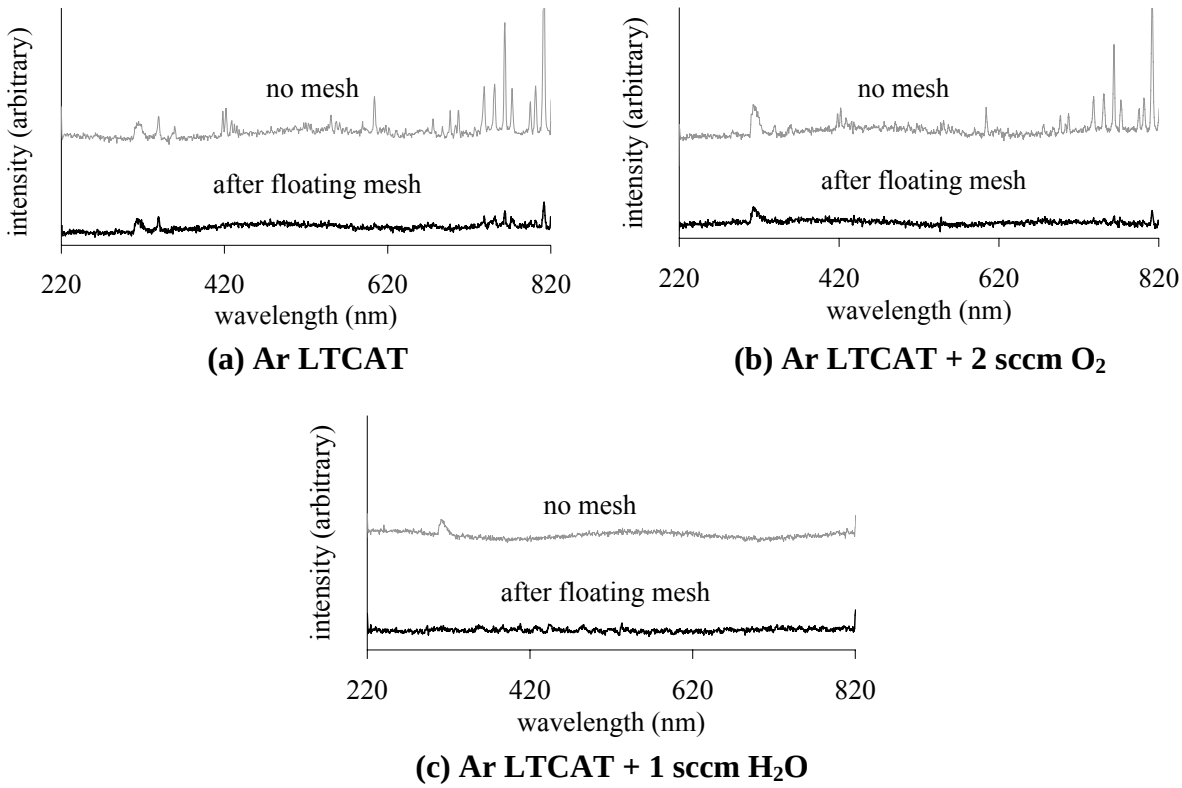

Figure 6.3. The OES spectra of (a) Ar LTCAT, (b) Ar LTCAT + 2 sccm O_2, and (c) Ar LTCAT + 1 sccm H_2O discharges obtained at the sample position without a mesh (gray) and after a floating stainless steel mesh (black). The other LTCAT conditions include 1000 sccm Ar and 4 A arc current. The OES exposure time was 5 min.

In order to clearly elucidate the changes in Ar^* after the floating mesh screen, the normalized intensities for three wavelengths corresponding to Ar^* (420 nm, 762 nm, and 811 nm) were obtained for each discharge using the emission intensities from Ar LTCAT without a mesh. Thus, the normalized intensities for the three chosen wavelengths for Ar LTCAT without a mesh were equal to 1. The comparison of normalized intensities for the three Ar^* wavelengths are shown in Figure 6.4 for Ar LTCAT, Ar LTCAT + 2 sccm O_2, and Ar LTCAT + 1 sccm H_2O. The data show that much of the Ar^* species are significantly reduced by the placement of the floating mesh upstream from the substrate.

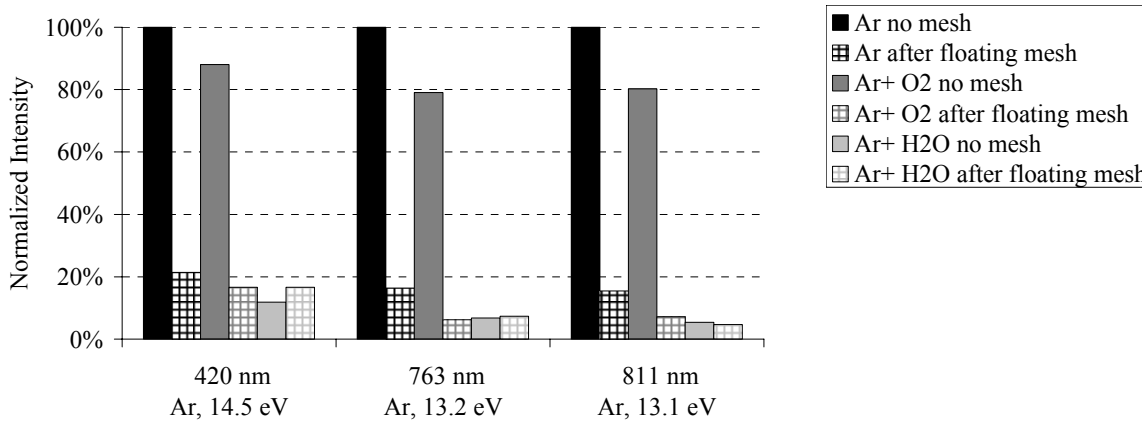

Figure 6.4. A comparison of the normalized intensities of three Ar^* emission wavelengths obtained from OES data given in Figure 6.3 for Ar LTCAT, Ar LTCAT + 2 sccm O_2, and Ar LTCAT + 1 sccm H_2O discharges without a mesh and after a floating, stainless steel mesh. The Ar flow rate, in all cases, was 1000 sccm and the arc current was 4 A.

Some of the discharge passed through the floating mesh, however, and polymer samples were surface treated in this fainter glow region. The effects of treatment time in the Ar LTCAT discharge were examined using Wilhelmy force loops of LDPE surfaces placed after the floating, stainless steel mesh 8 screen (configuration Figure 6.1 (a) with floating mesh) and were compared to those treated without a mesh placement in Figure 6.5. No overshooting was observed for the samples treated after the floating mesh, while all of the samples treated without a mesh exhibited some overshooting. However, the surface wettability was lower using the treatment by the discharge after the floating mesh as indicated by the higher advancing contact angles. Thus, the placement of the floating mesh in front of the sample in Ar LTCAT eliminated surface damage from LMWOM formation for at least up to 20 s treatment time, but the desired wettability enhancement was significantly reduced.

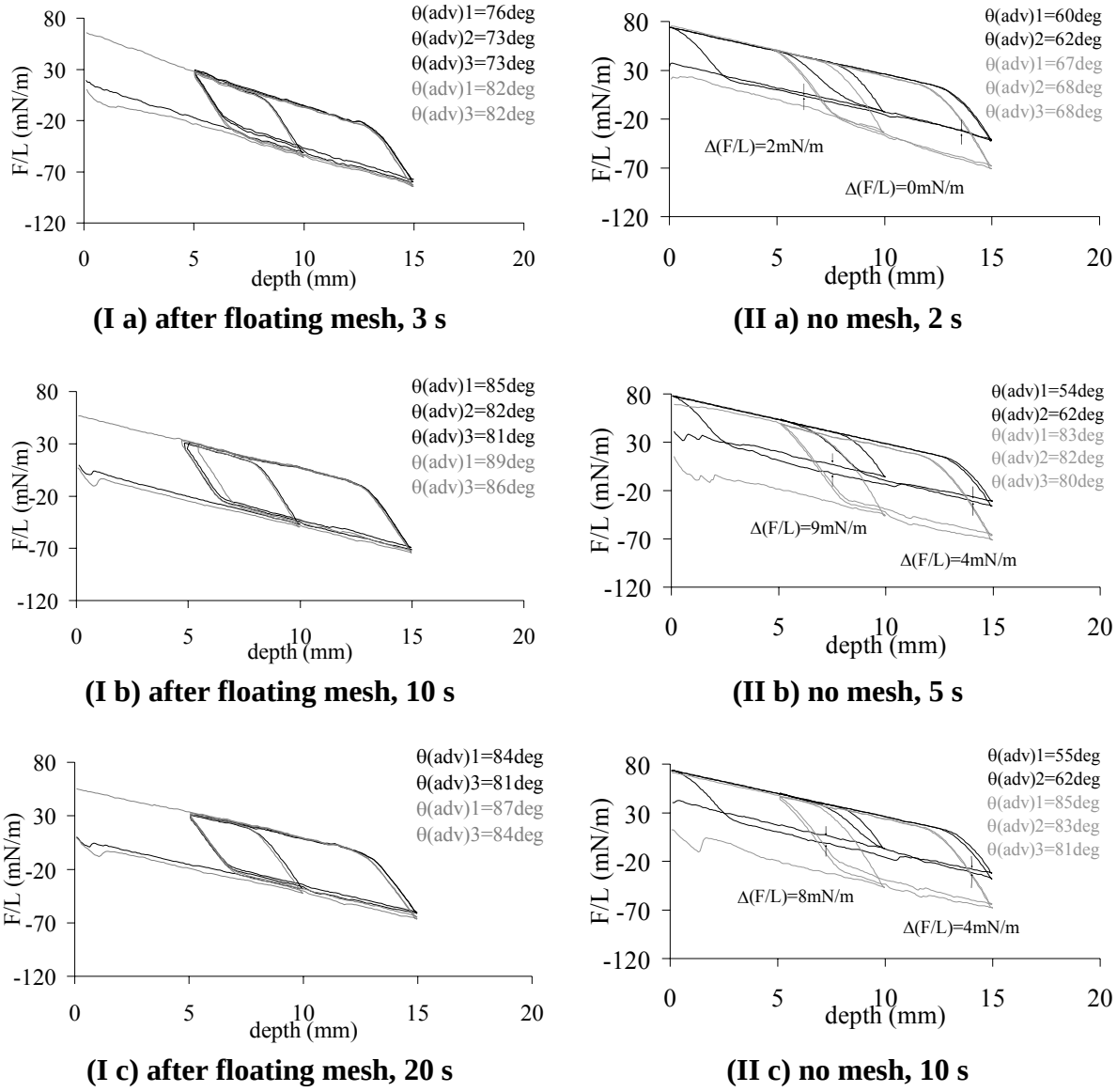

Figure 6.5. The Wilhelmy force loops of Ar LTCAT-treated samples that were placed (I) downstream from a floating stainless steel mesh 8 screen and (II) in a discharge without a mesh with various treatment times. The black lines show the force loops obtained immediately after treatment and the gray lines show the force loops obtained after 2 weeks of aging in ambient air. The other LTCAT conditions included 1000 sccm Ar and an arc current of 4 A. The Wilhelmy force loops obtained without a mesh were obtained from Section V.

The addition of O_2 to the Ar LTCAT discharge with the LDPE substrates placed after the floating stainless steel mesh 8 screen (configuration Figure 6.1 (a) with floating mesh) was investigated and the effects of O_2 flow rate on the dynamic surface

characteristics of the treated samples are shown in the Wilhelmy loops of Figure 6.6. The lower flow rates of 1 sccm and 2 sccm O_2 with the floating mesh did not induce as much damage as in similar discharge conditions without the mesh. However, using the higher flow rate of 7 sccm O_2, the dynamic surface characteristics of the treated LDPE were very similar to those induced by treatments of the same conditions, but without the floating mesh. With lower flow rates of O_2, both the Ar species and the reactive oxygen species contribute to surface modification, due to incomplete quenching of Ar^* by the O_2. At higher flow rates, however, more of the Ar^* species are quenched by O_2 and at some high flow rate, the reactive oxygen species become the main contributors to surface modification effects, including degradation from LMWOM formation. Because the treatment effects are similar using the higher O_2 flow rate in both cases (without a mesh and after a floating mesh), it follows that the reactive oxygen species are not significantly affected by the placement of a floating mesh, unlike the Ar^* species.

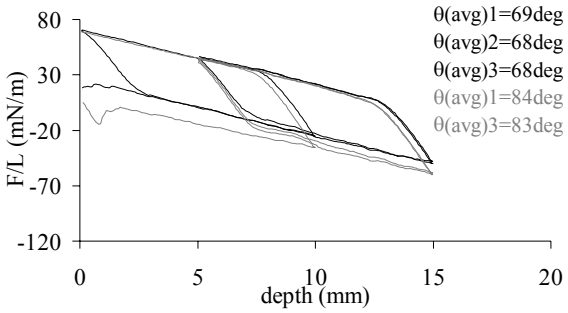

(I a) after floating mesh, 1 sccm O_2

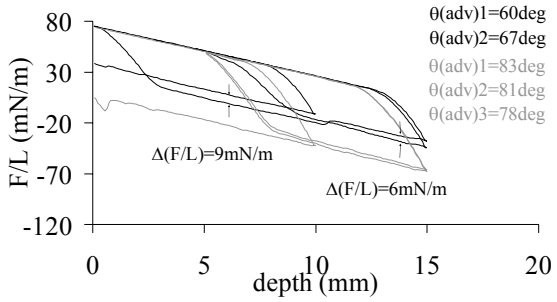

(II a) no mesh, 1 sccm O_2

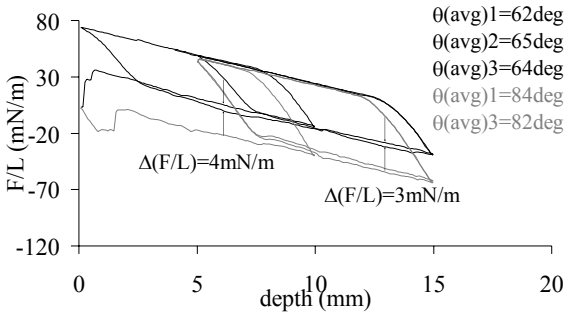

(I b) after floating mesh, 2 sccm O_2

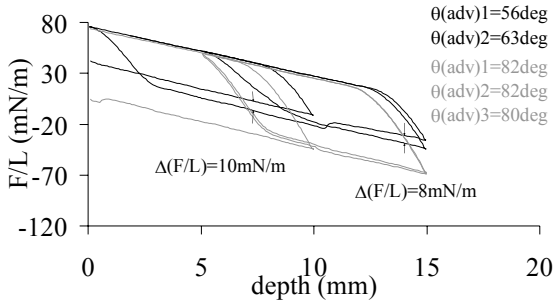

(II b) no mesh, 2 sccm O_2

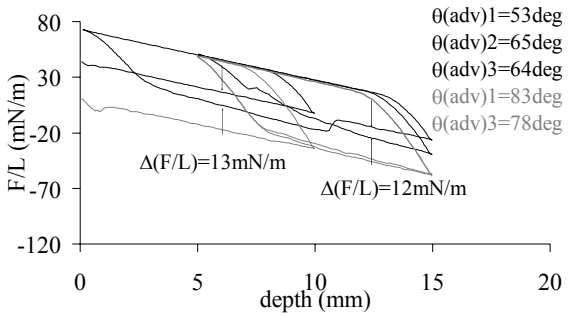

(I c) after floating mesh, 7 sccm O_2

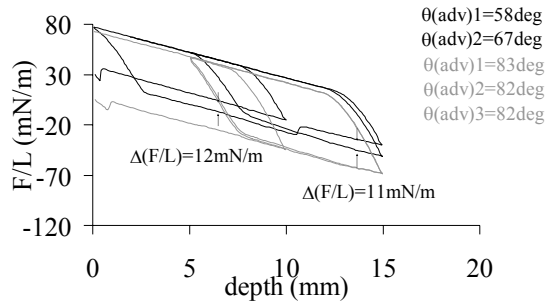

(II c) no mesh, 7 sccm O_2

Figure 6.6. The Wilhelmy force loops of Ar LTCAT + O_2-treated samples that were placed (I) downstream from a floating stainless steel mesh 8 screen and (II) in a discharge without a mesh with various O_2 flow rates. The black lines show the force loops obtained immediately after treatment, and the gray lines show the force loops obtained after 2 weeks of aging in ambient air. The other LTCAT conditions included 1000 sccm Ar, 2 s treatment time, and an arc current of 4 A. The Wilhelmy force loops obtained without a mesh were obtained from Section V.

The treatment time effects were examined using Ar LTCAT + 1 sccm O_2 with the LDPE samples placed after a floating mesh 8 screen (configuration Figure 6.1 (a) with floating mesh) and the data are shown in Figure 6.7.

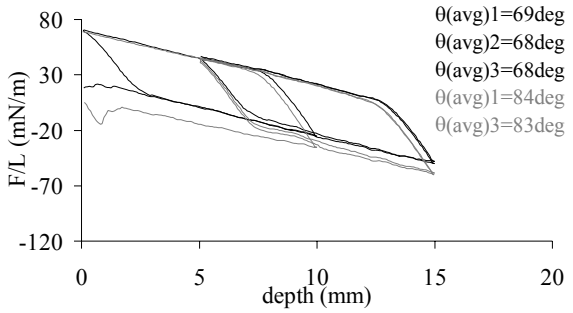

(I a) after floating mesh, 1 sccm O_2, 2 s

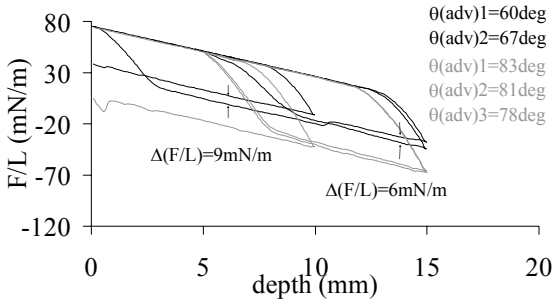

(II a) no mesh, 1 sccm O_2, 2 s

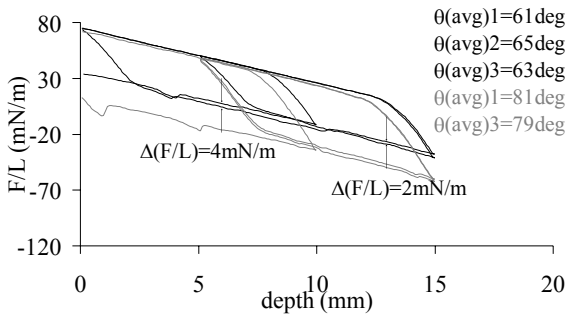

(I b) after floating mesh, 1 sccm O_2, 5 s

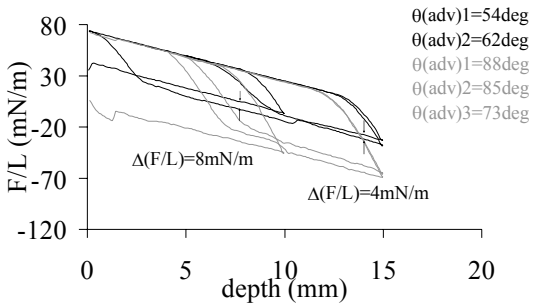

(II b) no mesh, 1 sccm O_2, 5 s

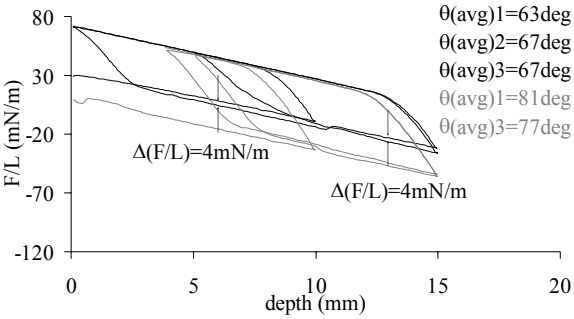

(I c) after floating mesh, 1 sccm O_2, 10 s

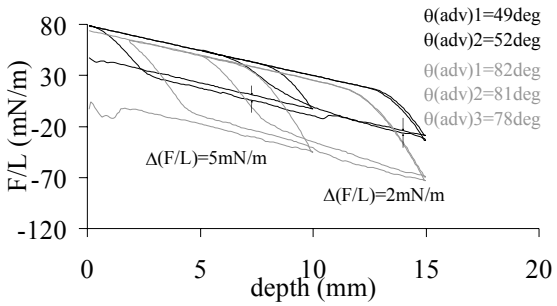

(II c) no mesh, 1 sccm O_2, 10 s

Figure 6.7. The Wilhelmy force loops of Ar LTCAT + O_2-treated samples that were placed (I) downstream from a floating stainless steel mesh 8 screen and (II) in a discharge without a mesh with various treatment times. The black lines show the force loops obtained immediately after treatment, and the gray lines show the force loops obtained after 2 week of aging in ambient air. The other LTCAT conditions included 1000 sccm Ar, 1 sccm O_2, and an arc current of 4 A. The Wilhelmy force loops obtained without a mesh were obtained from Section V.

The Wilhelmy loops show that for the discharges with and without a mesh, increasing treatment time enhanced the wettability, but also resulted in increased surface damage as shown by overshooting. However, less overshooting was observed on the

samples treated in LTCAT after the mesh than without the mesh, which was also less effective in wettability improvement.

A comparison of Ar LTCAT + H_2O treatments of LDPE placed after the floating mesh (configuration Figure 6.1 (a) with floating mesh) to the discharge without the mesh is given in the Wilhelmy loops in Figure 6.8.

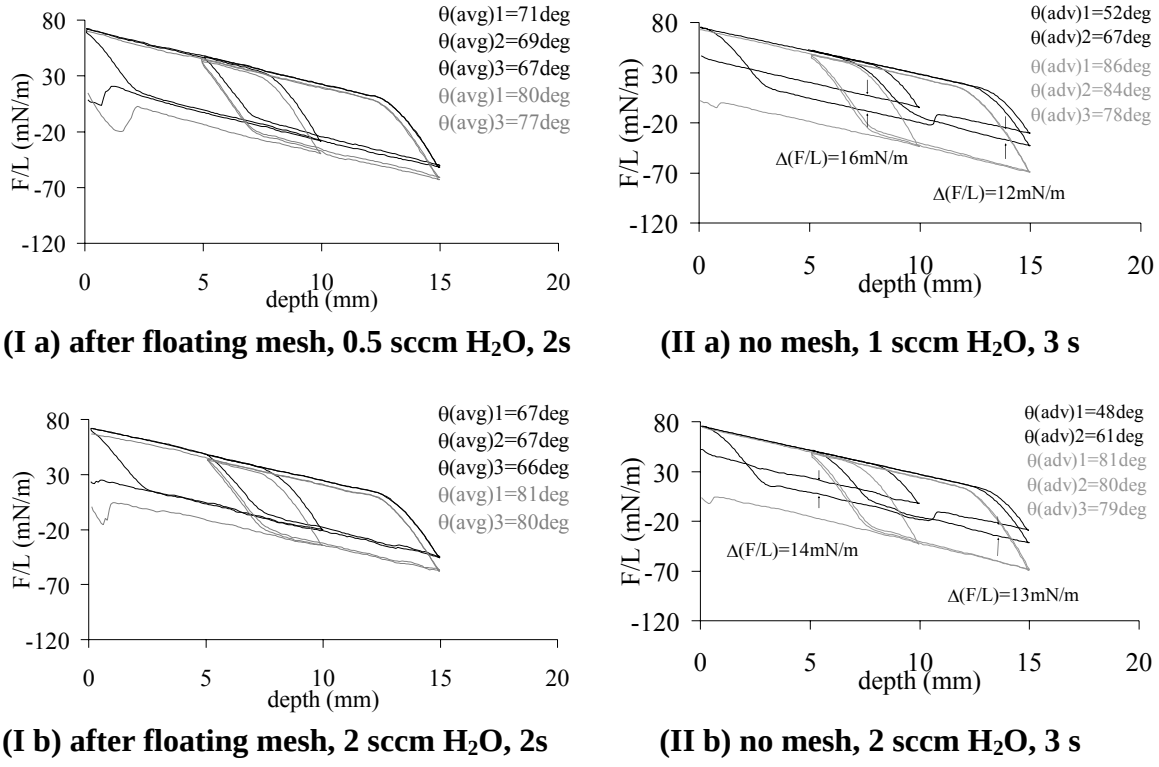

(I a) after floating mesh, 0.5 sccm H_2O, 2s **(II a) no mesh, 1 sccm H_2O, 3 s**

(I b) after floating mesh, 2 sccm H_2O, 2s **(II b) no mesh, 2 sccm H_2O, 3 s**

Figure 6.8. The Wilhelmy force loops of Ar LTCAT + H_2O-treated samples that were placed (I) downstream from a floating stainless steel mesh 8 screen and (II) in a discharge without a mesh with various H_2O flow rates. The black lines show the force loops obtained immediately after treatment, and the gray lines show the force loops obtained after 2 weeks of aging in ambient air. The other LTCAT conditions included 1000 sccm Ar and an arc current of 4 A. The Wilhelmy force loops obtained without a mesh were obtained from Section V.

No damage was induced on the LDPE treated after the floating mesh, unlike the significant damage induced by the discharge without a mesh, but the wettability is only

moderately enhanced. This indicates that the reactive Ar species and H_2O species that induce wettability enhancement and surface damage are significantly affected by the floating mesh.

6.3.2 The Effects of the Grounded Mesh on the LTCAT Discharges

Changing the mesh potential from floating to ground produced significant changes in the nature of the discharge. Instead of a steady, narrow, bright torch in Ar LTCAT, the discharge expanded between the arc generator outlet and the mesh with a decrease in visual glow intensity and a detectable color change. Figure 6.9 contains a comparison of optical photographs of Ar LTCAT, Ar LTCAT + O_2, and Ar LTCAT + H_2O discharges with a floating mesh and a grounded mesh. The OES spectra obtained after the grounded mesh (configuration Figure 6.1 (a) with grounded mesh) did not show any peaks, however, the OES spectra obtained before the grounded mesh (configuration Figure 6.1 (b)) are presented in this section.

(1 a) floating mesh, Ar LTCAT

(1 b) grounded mesh, Ar LTCAT

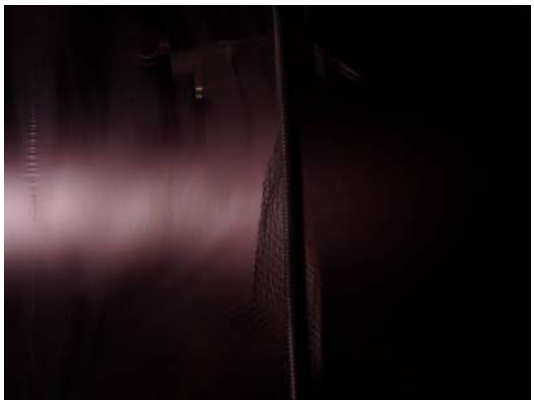

(2 a) floating mesh, 1 sccm O_2

(2 b) grounded mesh, 1 sccm O_2

(3 a) floating mesh, 1 sccm H_2O

(3 b) grounded mesh, 1 sccm H_2O

Figure 6.9. Optical photographs of the effects of placement of a (a) floating and (b) grounded stainless steel mesh 8 screen on the visible glow of (1) Ar LTCAT, (2) Ar LTCAT + O_2, and (3) Ar LTCAT + H_2O discharges. The other conditions include 1000 sccm Ar and 4 A arc current.

Figure 6.10 contains OES spectra from (a) Ar LTCAT, (b) Ar LTCAT + 1 sccm O_2, and (c) Ar LTCAT + 1 sccm H_2O vapor discharges obtained without a mesh (gray) and before a grounded mesh (black, configuration Figure 6.1 (b)).

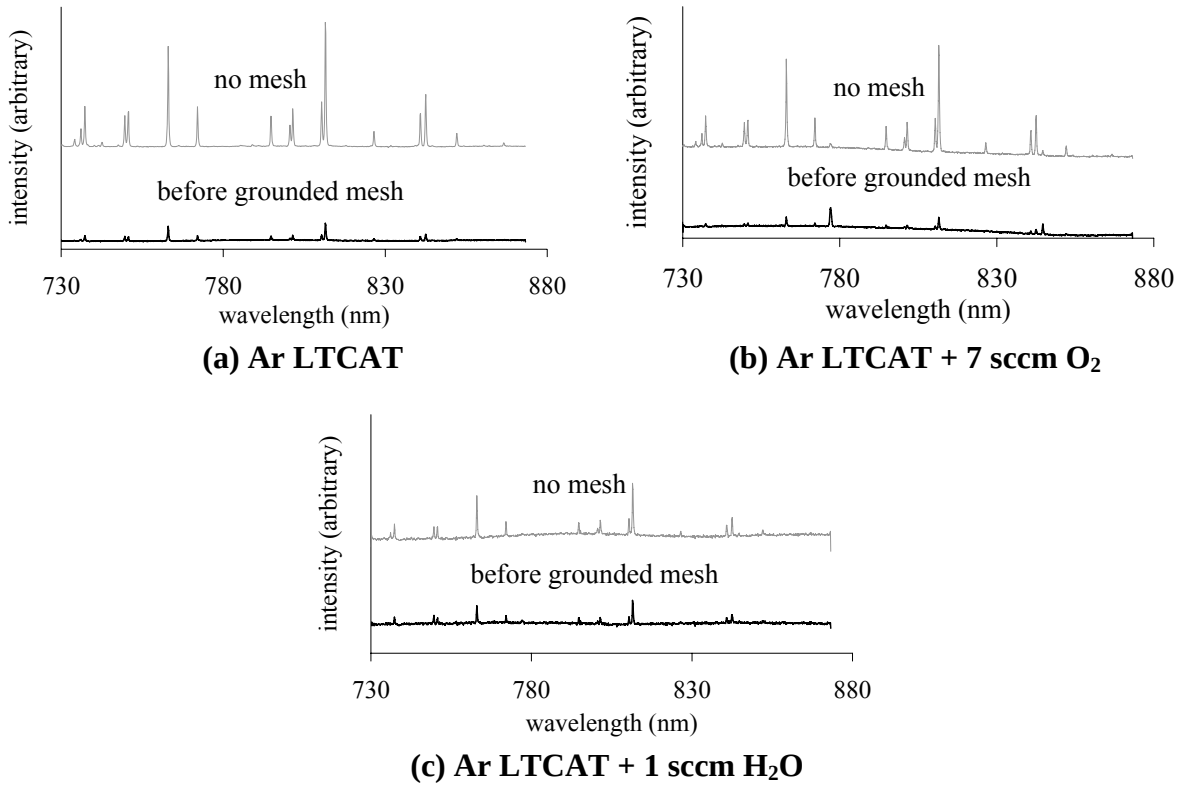

Figure 6.10. The OES spectra of Ar LTCAT (a), Ar LTCAT + 7 sccm O_2 (b), and Ar LTCAT + 1 sccm H_2O (c) discharges obtained at the sample position without a mesh (gray) and before a grounded mesh (black). The other LTCAT conditions include 2000 sccm Ar and 4 A arc current. The OES exposure time was 5 min.

For the Ar^* emission wavelength at 811 nm, the emission intensity obtained by OES from each discharge was normalized using the emission intensity obtained from Ar LTCAT without a mesh, which thus had a normalized intensity equal to 1. For the O emission wavelengths at 777 nm and 844 nm, the emission intensities were normalized using the emission intensities obtained from Ar LTCAT + 7 sccm O_2 before the grounded mesh, which produced the highest emission intensities of the O species for all of the discharges

examined by OES. These normalized intensities of each discharge are compared in Figure 6.11.

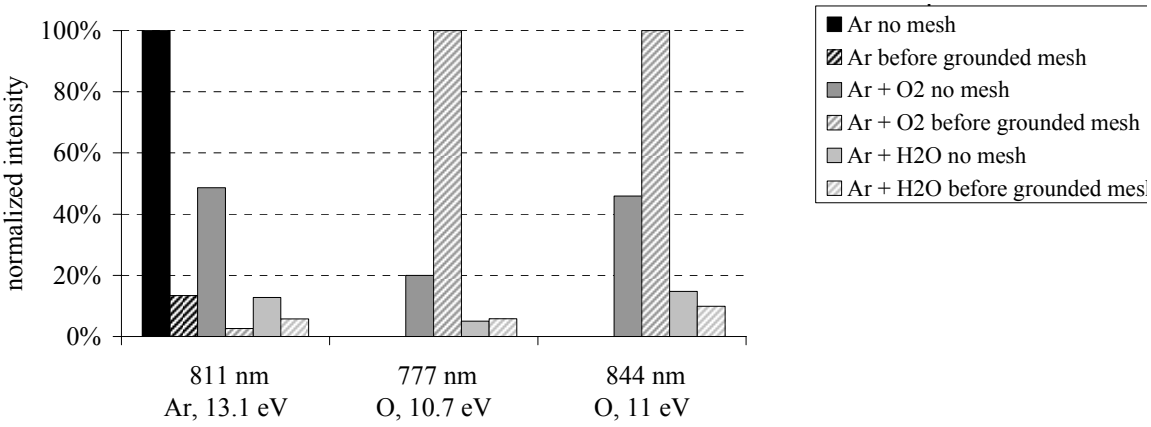

Figure 6.11. A comparison of the normalized intensities of a chosen Ar^* emission wavelength (811 nm) and two O emission wavelengths (777 nm and 844 nm) obtained from OES data given in Figure 6.10 for Ar LTCAT, Ar LTCAT + 7 sccm O_2, and Ar LTCAT + 1 sccm H_2O discharges without a mesh and after a grounded mesh. The Ar flow rate, in all cases, was 2000 sccm and the arc current was 4 A.

Grounding the mesh greatly changed the emission intensities in the discharge, as shown by the decrease in the Ar^* emission intensities. In the case of O_2 addition, the Ar^* emission intensity decreased and the O emission intensities greatly increased. This indicates that when a grounded mesh was added to the discharge of Ar LTCAT + O_2, greater energy transfer to the O_2 occurred. It is possible that the grounded mesh enhanced the number of electrons that escaped from the arc generator, which would have increased the rate of dissociative collisions between electrons and oxygen. Further investigation needs to be performed in order to elucidate the changes in the plasma phase induced by the grounded mesh placement.

Samples were treated in the downstream of the grounded mesh (configuration Figure 6.1 (a) with grounded mesh) for Ar LTCAT, Ar LTCAT + O_2, and Ar LTCAT +

H_2O and in the glow region before the grounded mesh (configuration Figure 6.1 (b)) for Ar LTCAT discharges. For the LDPE treatments after the mesh, comparisons of Wilhelmy force loops from using a grounded and floating mesh are shown for Ar LTCAT in Figure 6.12, Ar LTCAT + O_2 in Figure 6.13, and Ar LTCAT + H_2O in Figure 6.14.

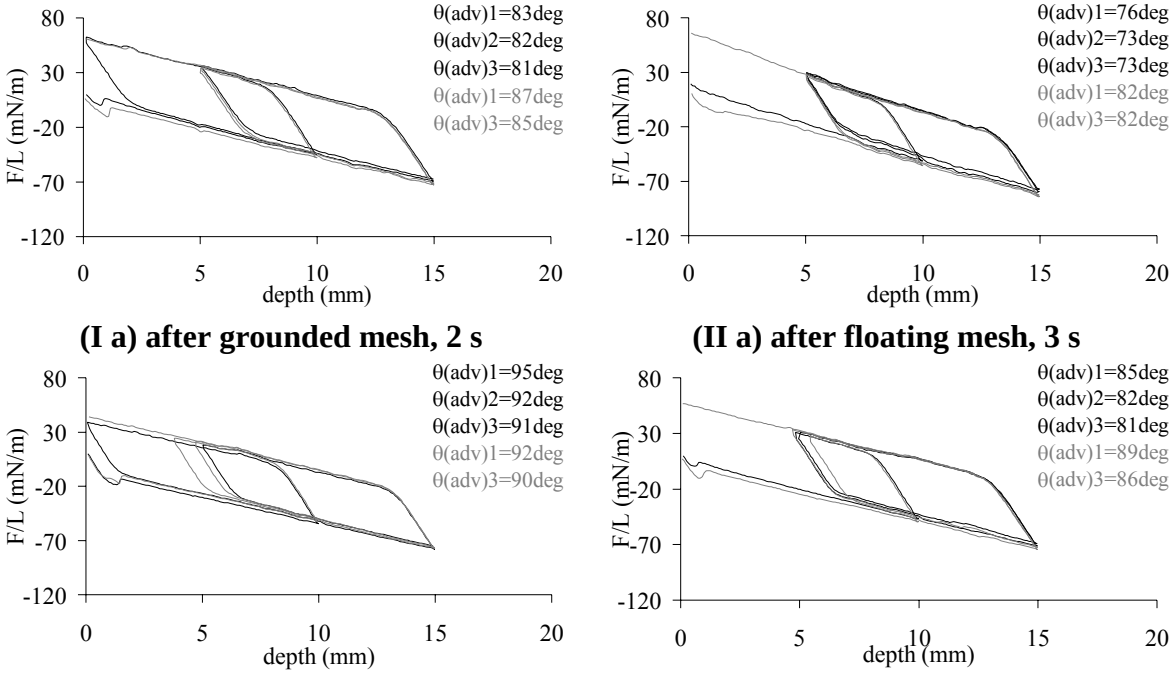

Figure 6.12. The Wilhelmy loops of Ar LTCAT-treated LDPE samples that were placed downstream from (I) a grounded stainless steel mesh 8 screen and (II) a floating stainless steel mesh 8 screen. The black lines show the force loops obtained immediately after treatment and the gray lines show the force loops obtained after 2 week of aging in ambient air. The other LTCAT conditions included 1000 sccm Ar and an arc current of 4 A.

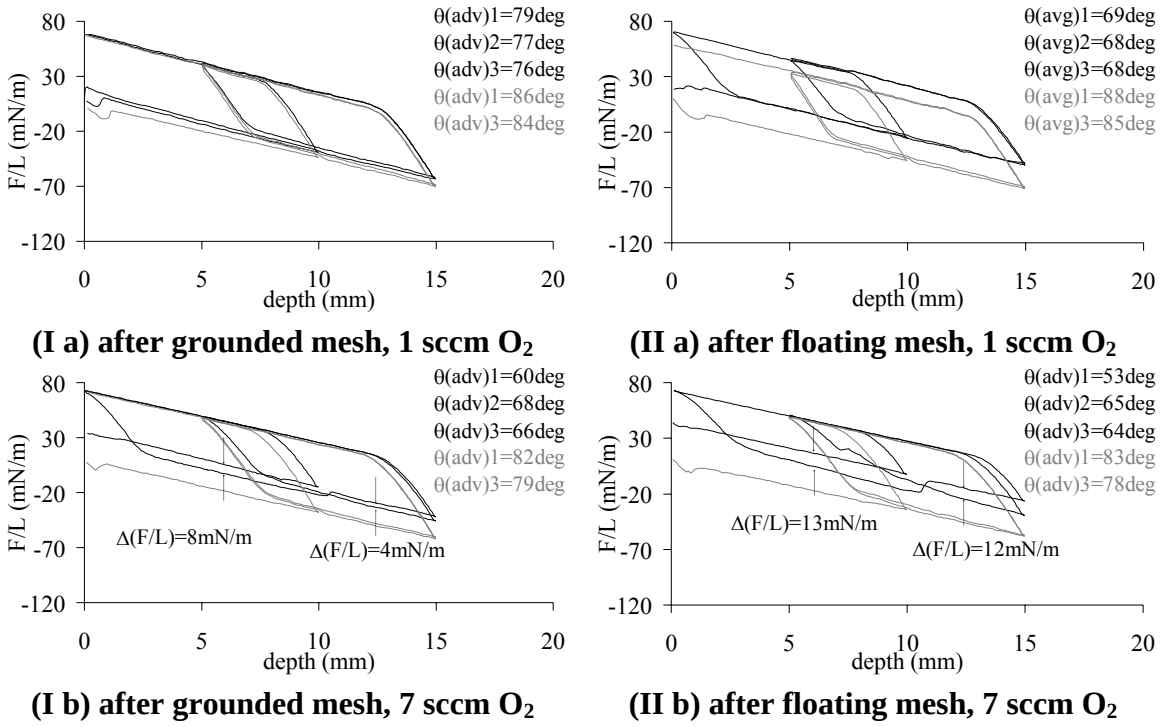

Figure 6.13. The Wilhelmy loops of Ar LTCAT + O_2-treated LDPE samples that were placed downstream from (I) a grounded stainless steel mesh 8 screen and (II) a floating stainless steel mesh 8 screen. The black lines show the force loops obtained immediately after treatment and the gray lines show the force loops obtained after 2 week of aging in ambient air. The other LTCAT conditions included 1000 sccm Ar, an arc current of 4 A, and 2 s treatment time.

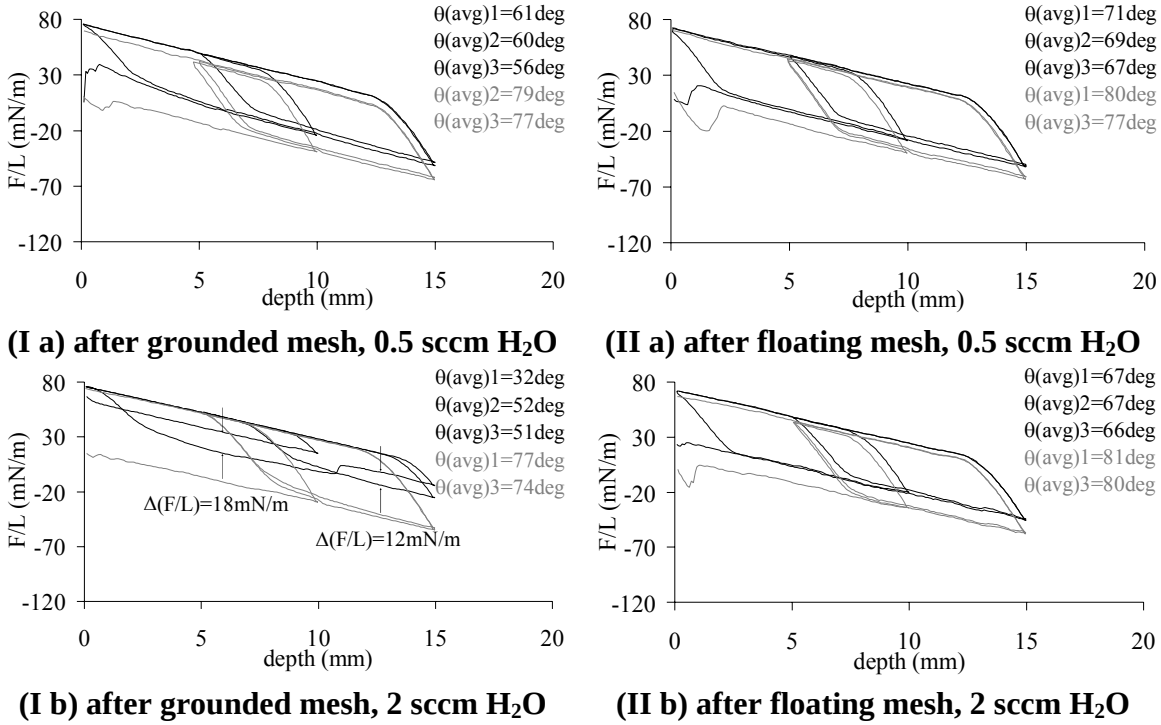

Figure 6.14. The Wilhelmy loops of Ar LTCAT + H_2O-treated LDPE samples that were placed downstream from (I) a grounded stainless steel mesh 8 screen and (II) a floating stainless steel mesh 8 screen. The black lines show the force loops obtained immediately after treatment and the gray lines show the force loops obtained after 2 week of aging in ambient air. The other LTCAT conditions included 1000 sccm Ar, an arc current of 4 A, and 2 s treatment time.

For Ar LTCAT and Ar LTCAT + O_2, the discharges after the floating mesh produced greater wettability on the treated polymer surfaces. However, for O_2 addition, greater surface damage was induced on the polymers placed in the discharge after the floating mesh than after the grounded mesh. For Ar LTCAT + H_2O, however, the effect was reversed; the treatments after the floating mesh were less effective in enhancing the wettability of LDPE surfaces and were also less prone to induce surface damage. Thus, it seems that the grounded mesh inhibited the flux of the reactive Ar and oxygen species to the substrate more significantly than the floating mesh. On the other hand, the greater wettability enhancement and increased surface damage induced on the LDPE placed after

the grounded mesh than the floating mesh in the Ar LTCAT + H_2O discharges indicated a greater penetration of H_2O reactive species through the mesh in the grounded case. Further study of the samples treated after the grounded mesh in the Ar LTCAT + H_2O discharges is presented below.

The effects of H_2O flow rate on the dynamic surface characteristics of the LDPE samples treated after the grounded mesh (configuration Figure 6.1 (a) with grounded mesh) are shown in the Wilhelmy loops of Figure 6.15 and are compared to the results previously obtained without a mesh in Section V. The polymers placed after the grounded mesh achieved significantly greater wettability than the polymers treated in Ar LTCAT + H_2O without a mesh. Furthermore, the treatment after the grounded mesh with 0.5 sccm H_2O induced no surface damage from LMWOM and produced wettability similar to the best condition previously reported for Ar LTCAT (see Figure 6.5 (II a)). However, increasing the flow rate of H_2O induced surface damage, which also increased with increasing H_2O flow rate.

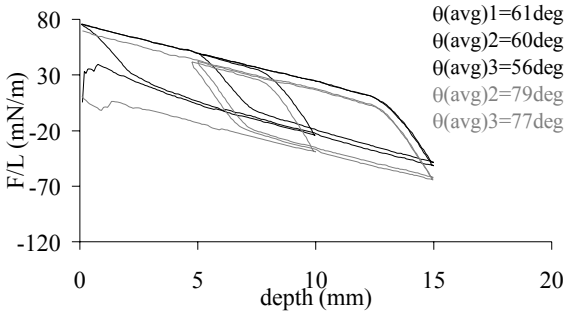

(I a) after grounded mesh, 0.5 sccm H_2O, 2 s

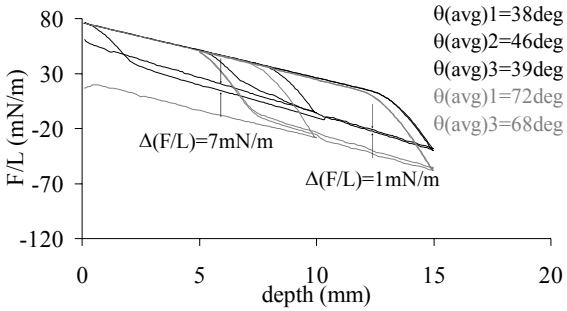

(I b) after grounded mesh, 1 sccm H_2O, 2 s

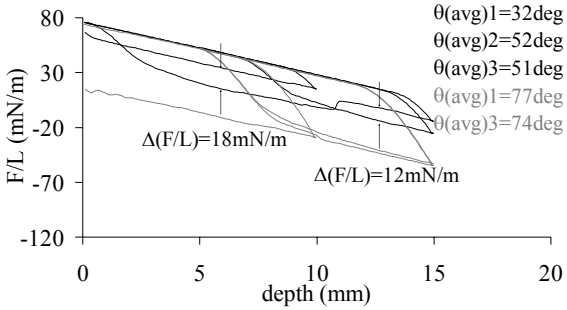

(I c) after grounded mesh, 2 sccm H_2O, 2 s

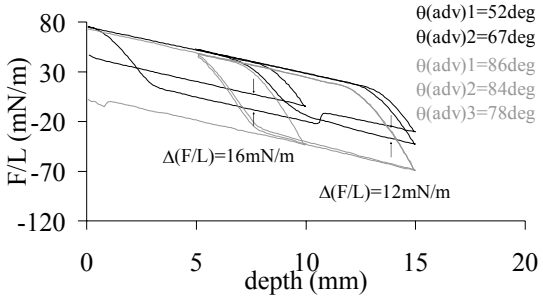

(II b) no mesh, 1 sccm H_2O, 3 s

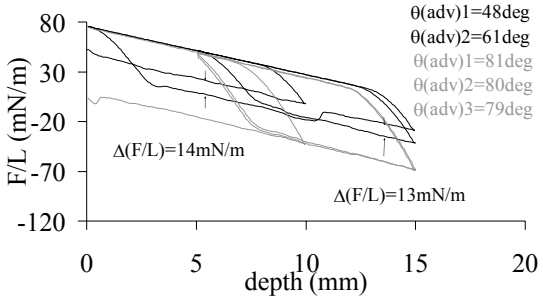

(II c) no mesh, 2 sccm H_2O, 3 s

Figure 6.15. The Wilhelmy force loops of Ar LTCAT + H_2O-treated samples that were placed (I) downstream from a grounded stainless steel mesh 8 screen and (II) in a discharge without a mesh with various H_2O flow rates. The black lines show the force loops obtained immediately after treatment and the gray lines show the force loops obtained after 2 week of aging in ambient air. The other LTCAT conditions included 1000 sccm Ar and an arc current of 4 A. The Wilhelmy force loops obtained without a mesh were obtained from Section V.

The effects of treatment time were observed using Ar LTCAT + 0.5 sccm H_2O discharge with the LDPE samples placed after the grounded mesh 8 screen (configuration Figure 6.1 (a) with grounded mesh) and the results are shown in the Wilhelmy force loops in Figure 6.16. Increasing the treatment time enhanced the wettability of the LDPE surfaces, but at the expense of surface degradation from LMWOM.

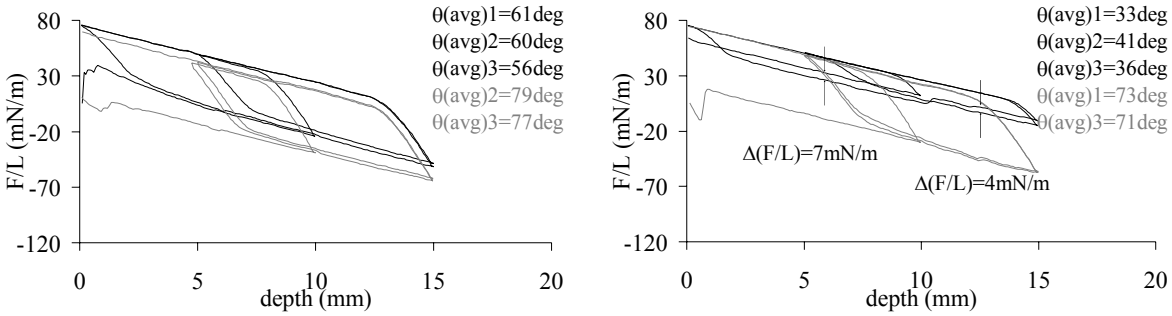

(a) after grounded mesh, 0.5 sccm H_2O, 2 s

(b) after grounded mesh, 0.5 sccm H_2O, 10s

Figure 6.16. The Wilhelmy force loops of Ar LTCAT + H_2O-treated samples that were placed downstream from a grounded stainless steel mesh 8 screen. The black lines show the force loops obtained immediately after treatment, and the gray lines show the force loops obtained after 2 week of aging in ambient air. The other LTCAT conditions included 1000 sccm Ar and an arc current of 4 A.

From visual inspection and OES data, the nature of the discharge emanating from the arc generator between the arc generator outlet and the mesh appeared to have a significantly altered nature when the mesh was grounded, which was not observed with the floating mesh. LDPE samples were placed in this discharge of Ar LTCAT before the grounded mesh (configuration Figure 6.1 (b)) to observe treatment effects of this altered discharge on LDPE samples, the results of which are given in Figure 6.17 and compared with the results obtained without a mesh from Section V.

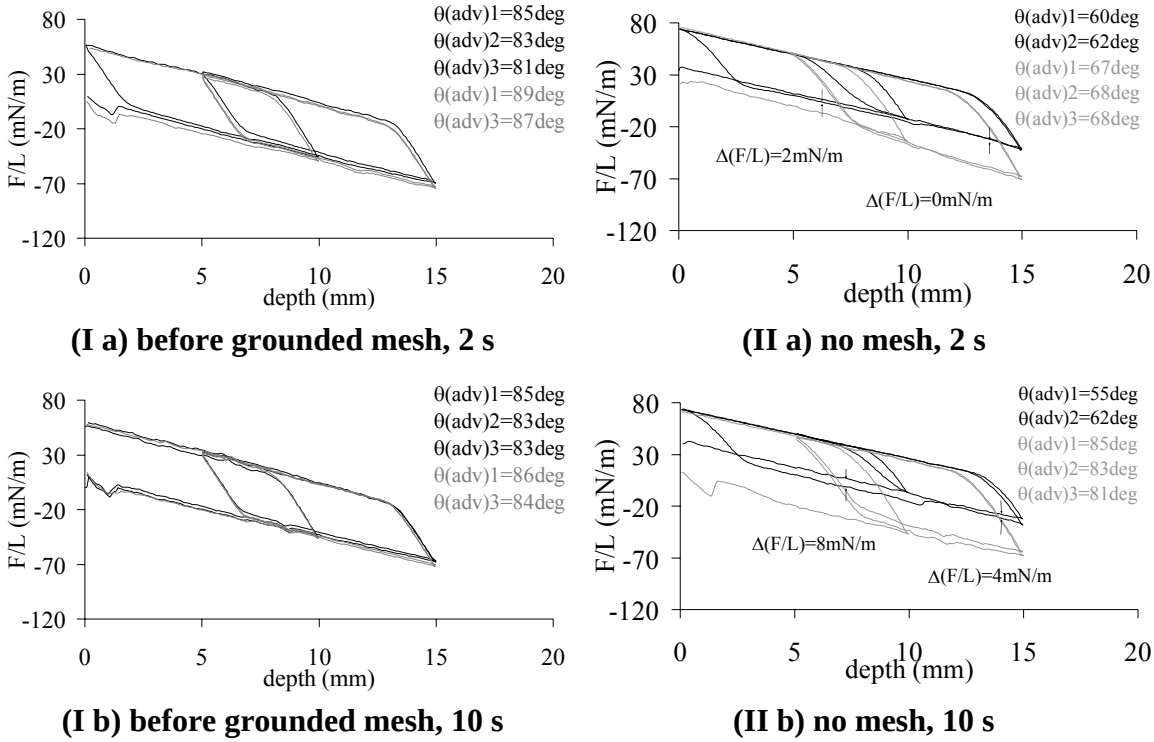

Figure 6.17. The Wilhelmy loops of Ar LTCAT-treated samples that were placed (I) in the discharge created between the arc generator and a grounded, stainless steel mesh 8 screen and (II) in a discharge without a mesh with various treatment times. The black lines show the force loops obtained immediately after treatment and the grey lines show the force loops obtained after 2 weeks of aging in ambient air. The treatment conditions were 1000 sccm Ar and 4 A arc current. The Wilhelmy force loops obtained without a mesh were obtained from Section V.

The Wilhelmy force loops in Figure 6.17 show that the wettability of the treated LDPE samples is significantly reduced with the addition of a grounded mesh in the discharge. This evidence, along with the OES spectra, clearly indicates that placing a grounded mesh in the LTCAT discharge significantly alters the nature of the discharge and possibly changes the plasma density.

6.4 Conclusions

In this study, a stainless steel mesh was placed in the discharges of LTCAT for surface modification of LDPE to distinguish the effects of ions in the discharge from

those of the other species, especially the electronically excited Ar species. However, optical photography and OES data indicated that much of the photo-emitting species were significantly reduced from the placement of the mesh in LTCAT. Furthermore, when the mesh in LTCAT was grounded, the nature of the LTCAT discharge was significantly changed. OES data indicated that in the case of Ar LTCAT + O_2, the emission intensities of O species in the discharge created by the grounded mesh increased, while the Ar peaks were reduced for all discharges. This indicates that the grounded mesh placement resulted in greater energy transfer to the oxygen species, possibly from an increase in the number of electrons released from the arc generator. Further investigation of the changes in the discharge by a grounded mesh could shed more light on the sources of the altered nature of the discharge.

The surface characterization data indicated that placing a floating mesh screen in the Ar LTCAT beam inhibited LDPE surface damage from LMWOM formation, but did not enhance the wettability very effectively. While it is possible that the mesh may have consumed ions in the torch, the reduction of the emission intensities of Ar^* species that reached the samples position was unfavorable for wettability enhancement of LDPE.

The Wilhelmy loops of the LDPE samples treated after the mesh in Ar LTCAT + O_2 discharges revealed that the reactive oxygen species that induce surface modification were not affected by the floating mesh, but were significantly reduced after the grounded mesh, as indicated by poor wettability enhancement. The reactive species in Ar LTCAT + H_2O discharges, however, were greatly reduced after the floating mesh, as indicated by

the decrease in wettability and surface damage on the treated polymers. Samples treated after a grounded mesh in the Ar LTCAT + H_2O discharges, however, exhibited much improved wettability enhancement with less surface damage than LDPE treated without using a mesh and after a floating mesh. For samples treated in the Ar LTCAT discharge before a grounded mesh, the wettability enhancement and induced surface damage were significantly reduced in comparison to the treatments without a mesh.

These findings indicate a most important message, which is that careful consideration needs to take place when applying any such disturbance in a plasma discharge. The nature of the discharge as well as the desirable process outcomes can be significantly altered.

6.5 References for Section VI

1. Gilliam, M.A.; Yu, Q.; *J. Appl. Polym. Sci.* **99** (2005) 2528-2541.

2. Ratner, B.D.; Chilkoti, A.; Lopez, G.P.; in *Plasma Deposition, Treatment, and Etching of Polymers*, R. d'Agostino ed., Academic Press, Boston (1990) 463 – 516.

3. Penn, L.S.; Wang, H.; *Polymers for Advanced Technologies* **5** (1994) 809-917.

4. Wertheimer, M.R.; Martinu, L.; and Liston, E.M.; in *Handbook of Thin Film Process Technology, Volume 2*, Glocker, D.A. ed., Institute of Physics Publishing, Bristol (2002) E3.0:1-E3.0:38.

5. Durand, A.M.; *LE VIDE, Science, Technique, et Applications* **53** (1997) 242 – 252.

6. Weikart, C.M.; Yasuda, H.K.; *J. Polym. Sci.* A **38** (2000) 3028-3042.

7. Gilliam, M.A.; Yu, Q.; Encyclopedia of Chemical Processing, an invited article, in review.

8. Egitto, F.D.; Matienzo, L.J.; *IBM J. Res. Develop.* **38**, No. 4 (1994) 423-439.

9. Truica-Marasescu, F.-E.; Wertheimer, M.R.; *Macromol. Chem. Phys.* **206** (2005) 744-757.

10. Butoi, C.I., Mackie, N.M., McCurdy, P.R., Peers, J.R.D., and Fisher, E.R.; *Plasm. Polym.* **4**, No. 1 (1999) 77-91.

11. Yu, Q.S.; Reddy, C.M.; Meives, M.F.; Yasuda, H.K.; *J. Polym. Sci.: Part A: Polym. Chem.* **37** (1999) 4432 – 4441.

12. Fusselman, S.P. and Yasuda, H.K.; *Plasma Chem. Plasma Process,* **14** (1994) 251 - 275.

13. Yu, Q.S. and Yasuda, H.K.; *Plasma Chem. Plasma Process.* **18** (1998) 461 - 485.

14. H. Yasuda, *Luminous Chemical Vapor Deposition and Interface Engineering*, Marcel Dekker, New York (2005), p.339.

SECTION VII

SURFACE MODIFICATION OF SEVERAL POLYMERS USING A LOW TEMPERATURE CASCADE ARC TORCH

7.1 Introduction

Plasma processes have found wide applications in the surface treatment of polymers to improve their adhesive properties, enhance wettability, biocompatibility, barrier properties, optical reflection, susceptibility to harsh agents, and to reduce friction, among other objectives[1-7]. Plasma techniques offer advantages over other techniques due to the effectiveness and versatility of the treatments and the environmentally benign nature of the plasmas. However, traditional plasma techniques involve surface bombardment by high-energy species, such as ions, electrons, and VUV/UV photons, which can bring about significant degradation on the polymer surfaces. In addition, the complex nature of the plasma makes it difficult to selectively isolate beneficial surface reaction mechanisms and minimize detrimental effects.

Much is still unknown regarding the complex reaction mechanisms at the plasma-polymer interface during plasma surface modification. Consequences of plasma treatments used for chemical modification (excluding deposition processes) include surface functionalization, in which new surface functional groups are created, surface crosslinking by the CASING (Cross-linking via Activated Species of INert Gases) effect, etching of surface material into volatile species, and the scission of surface polymer chains into loosely-bonded oligomers or Low Molecular Weight Oxidized Material (LMWOM)[8]. The degradation of a polymer surface into a layer of oligomers can occur

from bombardment of high energy species that induce chain scission or via the formation and degradation of alkoxy radicals. The alkoxy degradation reaction is shown below, which results in scission of a polymer chain:

alkoxy degradation: $R_1—C—C(O•)—R_2 \rightarrow R_1—C• + R_2—C=O$ (1)

Alkoxy radicals can be formed on polymer surfaces in the presence of oxygen-containing plasmas through several routes originating from reactions with oxidizing species, such as O_2, O, O_3, H_2O_2, HO_2, and OH[9].

Plasma surface modification studies have found that the outcome of the treatment depends on the polymer chemical structure and the polymer's susceptibility to the plasma conditions. For example, some studies have shown that the presence of oxygen in the polymer's chemical structure increases the polymer's susceptibility to degradation[5,10]. On the other hand, aromatic rings in the polymer (both in the backbone and in pendant groups) provide some resistance to etching reactions[10-13]. Polymethylmethacrylate (PMMA) is a polymer that easily undergoes oxidative degradation in a plasma environment[13,14], while polystyrene (PS) is highly stable toward degradation[11,13,15]. Silicon-containing polymers are particularly resistant to photodegradation and oxidative degradation, yet degrade very easily in fluorine-containing plasmas, because of the formation of stable and volatile Si-F compounds[16].

Low Temperature Cascade Arc Torch (LTCAT) plasma provides a beam of mainly electronically excited Ar^* species directed at the polymer surface, making it an ideal glow discharge process for the surface modification of polymers. With the absence of an external electric field in the substrate chamber, the low density of ions that escape the arc generator are not significantly accelerated to the substrate surface. In addition, the application of Ar LTCAT to polymer surfaces induces the CASING effect and any un-reacted surface free radicals that are present after treatment can be quenched by oxygen upon exposure to atmosphere to create hydrophilic moieties. The combination of these two processes results in the creation of new surface functional groups anchored to a stable, cross-linked surface layer[16].

Investigations in our laboratory have involved the application of LTCAT plasma technology to polymer surface modification, which have resulted in successful wettability enhancement with less surface damage than traditional plasma and greater surface stability[6,7]. In addition, LTCAT is a fast and cost-effective treatment that can easily be scaled-up for high throughput in industrial settings. Previous studies have demonstrated the effectiveness of LTCAT in modifying the surfaces of polytetrafluouroethylene (PTFE)[7] and low density polyethylene LDPE[6]. The purpose of this investigation is to uncover the effects of the polymer structure on the outcomes of LTCAT treatments by examining the wettability changes, surface stability, and surface degradation of various treated polymers. The treatments include Ar LTCAT, Ar LTCAT with O_2 addition, and Ar LTCAT with H_2O vapor addition. Polymers that are examined in this study include PS, which contains a stabilizing benzene ring, PMMA and polyoxymethylene (POM),

with oxygen functionalities that may cause enhanced sensitivity to degradation in plasma, and polycarbonate (PC), which contains both benzene rings and oxygen in the backbone. In addition, polymers that exhibit surface cross-linking under radiation are also examined, including nylon-6 and silicone rubber (SR)[17]. The surface changes are examined using static and dynamic wettability, which can be related to other surface characteristics, such as surface energy and adhesive properties.

7.2 Experimental

7.2.1 Materials

The polymeric substrates that were used in the LTCAT treatments consisted of 1 mm thick sheets of PC, POM, PMMA, nylon-6, and SR and 1.2 mm thick sheets of PS, which were purchased from Goodfellow Cambridge Limited (Cambridge, England). The sheets were cut into 1 x 2 cm pieces for the static contact angle measurements and 2 x 2.5 cm for the dynamic analysis. Prior to treatment, all samples were washed in a solution containing 5 % detergent in de-ionized water, which was placed in an ultrasonic bath for 30 min. The samples were then thoroughly rinsed in de-ionized water, dried in ambient air for 1 day, and stored in a dry desiccator. The Ar and O_2 gases were obtained from Praxair (St. Louis, Missouri). The water vapor consisted of de-ionized water obtained from treating in-house distilled water through a Culligan de-ionization system.

7.2.2 LTCAT Treatments

The LTCAT system consisted of an arc generator that created a glow discharge stream into a vacuum chamber. Previous publications have presented detailed schematics and operational procedures of LTCAT[18,19]. The arc generator contained a narrow channel formed by a series of copper disks that were connected by polymer insulators. The arc generator was cooled to 10 ^{o}C prior to starting each experiment. Direct current (4 A) was supplied to the torch and Ar flowed through the narrow channel at a rate of 1000 sccm. The electric field was confined to the arc generator and the species in the glow discharge stream consisted of ground-state neutral species, electronically excited neutral species, Ar^{*}, and a low density of positive ions and electrons. For some trials, reactive gases were added to the treatment chamber, which were activated and dissociated by the Ar^{*} species.

Single samples were placed on a substrate clip at the end of a sliding bar that could be moved into and out of the glow discharge stream. The reactor was pumped down to the base pressure of 1 mtorr before each treatment. Steady discharges were created within seconds of ignition and the samples were immersed in the torch for the desired exposure time. For each type of polymer, 21 sets of experimental conditions were chosen for static analysis, in which the exposure time varied for Ar LTCAT and for Ar LTCAT with reactive gas addition using 3 different reactive gas flow rates for oxygen (1 sccm, 2 sccm, and 7 sccm) and water vapor (1 sccm, 2 sccm, and 10 sccm). The experiments were performed in random order for each polymer.

7.2.3 Wettability and Surface Stability of Polymeric Surfaces

The wettabililty and surface stability of the polymers were determined using static and dynamic contact angle measurements. For the static analysis, a VCA 2500XE system (Advanced Surface Technologies, Inc., Billerica, MD) was used to place a Sessile droplet of 0.3 μL de-ionized water on the surface of the treated polymers and computer software was used to obtain an image of the water droplet. The computer user manually traced the arc that was created by the droplet on the polymer surface and a computer program was used to calculate the two contact angles that the water made with the polymer surface. After obtaining the surface contact angle immediately after treatment, the samples were placed in a beaker of de-ionized water for 4 minutes to allow any surface oligomers, if present, to wash away. The samples were then hung dry in ambient air for 10 minutes before obtaining another contact angle measurement. Static surface analysis was performed at different aging times after treatment to examine any hydrophobic recovery of the treated surfaces. The results of the static analysis were used to determine suitable treatment conditions for each polymer that would be used for the dynamic surface analysis.

Dynamic surface analysis was performed on samples treated using the treatment conditions chosen for each polymer based on the static contact angle data. The Wilhelmy balance method was used with a Sigma 70 modular surface tension/contact angle meter (KSV Instruments, Ltd., Helsinki, Finland) that measured the force exerted on the treated sample during immersion and emersion in de-ionized water. A detailed description of the method is presented in Section 5.2.4.

7.3 Results and Discussion

7.3.1 Static Contact Angles of LTCAT-Treated Polymers

Static contact angle measurements were obtained from the samples that were treated using exposure times of 2, 5, and 10 s for Ar LTCAT, Ar LTCAT + O_2 with O_2 flow rates of 1, 2, and 7 sccm, and Ar LTCAT + H_2O with H_2O flow rates of 1, 2, and 10 sccm. Thus, a total of 21 treatments were performed for each polymer and the measurements were conducted on each treated specimen before and after washing and after aging in ambient air for 2 days, 1 week, and 2 weeks. The static contact angle measurements were used to examine the effects of the LTCAT treatments on the surface wettability, surface damage from oligomer formation, and hydrophobic recovery of the treated polymers. The complete results from the static contact angle analysis are given in the Appendix, while some of the results are presented below. From the static contact angle results, 3 sets of suitable treatment conditions were determined for each polymer for Ar LTCAT, Ar LTCAT + O_2, and Ar LTCAT + H_2O. The conditions were chosen based on a high degree of wettability achieved with minimized surface damage. Samples were treated under the chosen conditions and analyzed using the Wilhelmy balance method. Table 7.1 summarizes the polymer structures and the measured static contact angles of the untreated polymers.

Table 7.1. Chemical Structures and Contact Angles of the Untreated Polymers

Polymer	Repeating Unit	Static Contact Angle (deg)
PS	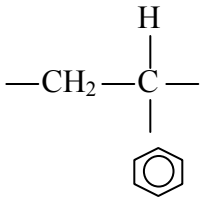	97 ± 3.1
PMMA	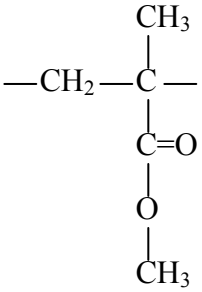	75 ± 2.7
POM	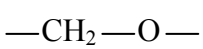	97 ± 2.9
PC	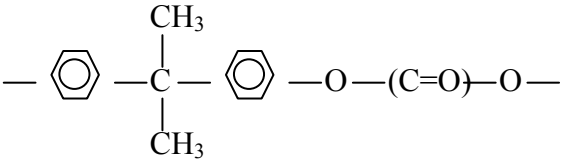	98 ± 1.5
SR	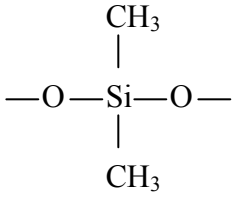	129 ± 2.8
Nylon-6	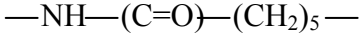	65 ± 1.8

The results from the static contact angle measurements on LTCAT treated polymers are summarized in Figures 7.1 and 7.2. Figure 7.1 contains the treatments using the shortest treatment time (2 s) and the lowest reactive gas addition flow rates, when applied (1 sccm O_2 or 1 sccm H_2O), and Figure 7.2 contains the results from the longest treatment time (10 s) and the highest reactive gas addition flow rates, when applied (7 sccm O_2 or 10 sccm H_2O).

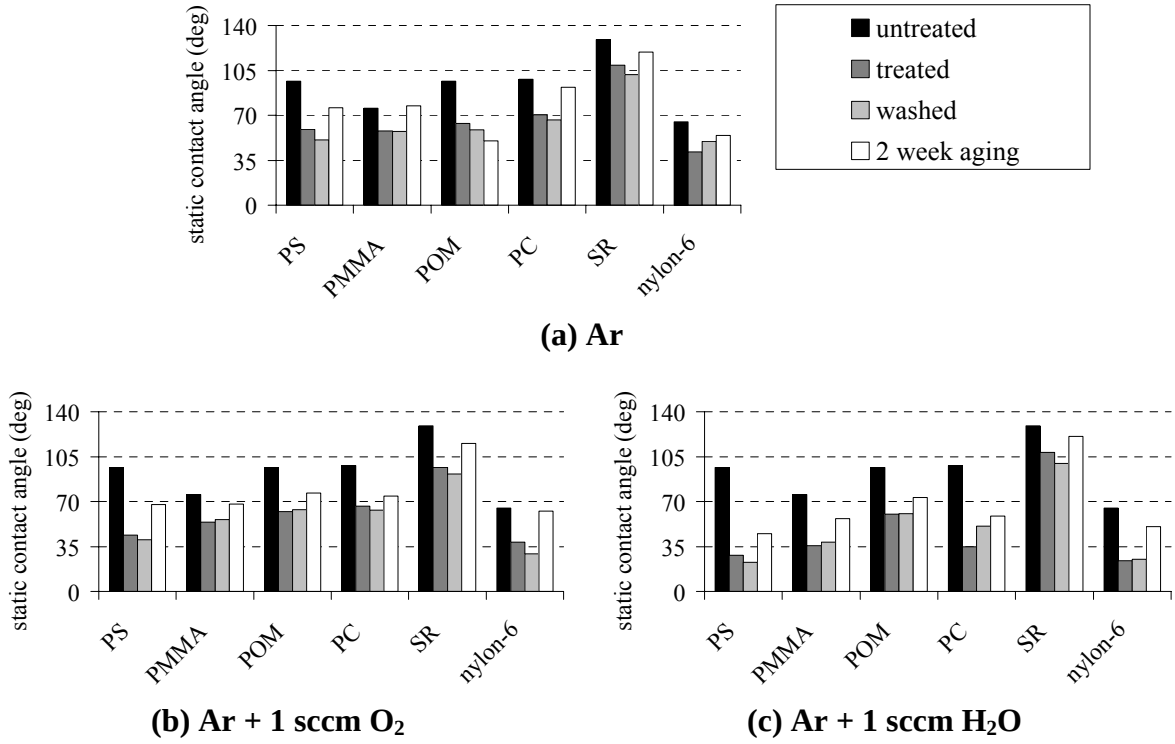

Figure 7.1. The average static contact angles of the six types of polymers treated with (a) Ar LTCAT, (b) Ar LTCAT + 1 sccm O_2, and (c) Ar LTCAT + 1 sccm H_2O. Measurements were obtained from the untreated polymers (black), immediately after treatment (dark gray), after washing in DI water and drying in ambient air (light gray), and after aging in ambient air for 2 weeks (white). The other treatment conditions include 1000 sccm Ar, 4 A arc current, and 2 s treatment time.

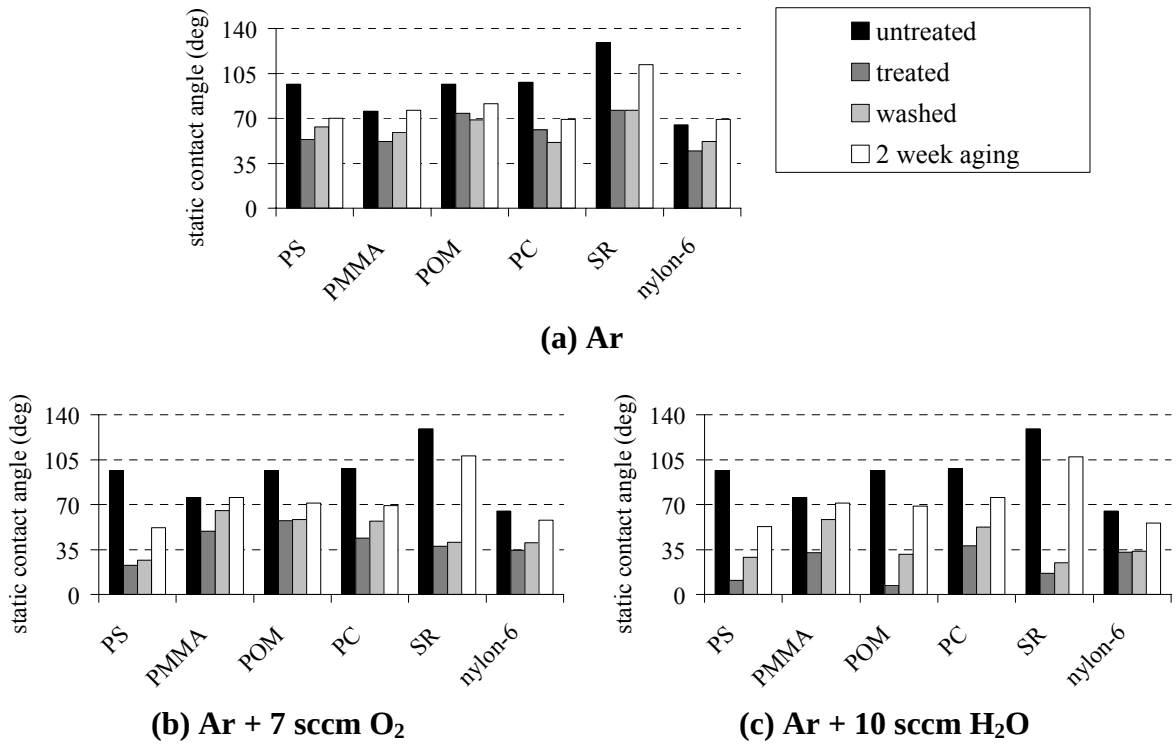

Figure 7.2. The average static contact angles of the six types of polymers treated with (a) Ar LTCAT, (b) Ar LTCAT + 7 sccm O_2, and (c) Ar LTCAT + 10 sccm H_2O. Measurements were obtained from the untreated polymers (black), immediately after treatment (dark gray), after washing in DI water and drying in ambient air (light gray), and after aging in ambient air for 2 weeks (white). The other treatment conditions include 1000 sccm Ar, 4 A arc current, and 10 s treatment time.

The effects of the reactive gas addition on the different types of polymers are further elucidated in Figures 7.3 and 7.4, the data of which were obtained by manipulation of the data from Figures 7.1 and 7.2, respectively. The extent of wettability change is presented in Figures 7.3 (a) and 7.4 (a), which contain the contact angle differences between each treated sample and the corresponding untreated polymer. The degree of surface damage is given in Figures 7.3 (b) and 7.4 (b), which contain the contact angle differences between each washed/dried sample and the corresponding treated sample. The extent of hydrophobic recovery was examined by calculating the contact angle differences between each aged sample and the corresponding washed/dried

sample, which are shown in Figures 7.3 (c) and 7.4 (c). The extent of hydrophobic recovery can also be gauged by the static contact angle difference between the aged sample and the untreated polymer. It should be noted that both previous observations should be used to assess hydrophobic recovery; in some cases, the value in Figures 7.3 (c) or 7.4 (c) is relatively low, but the contact angle after 2 weeks has been completely restored to the value of the untreated polymer, that is, complete hydrophobic recovery occurred.

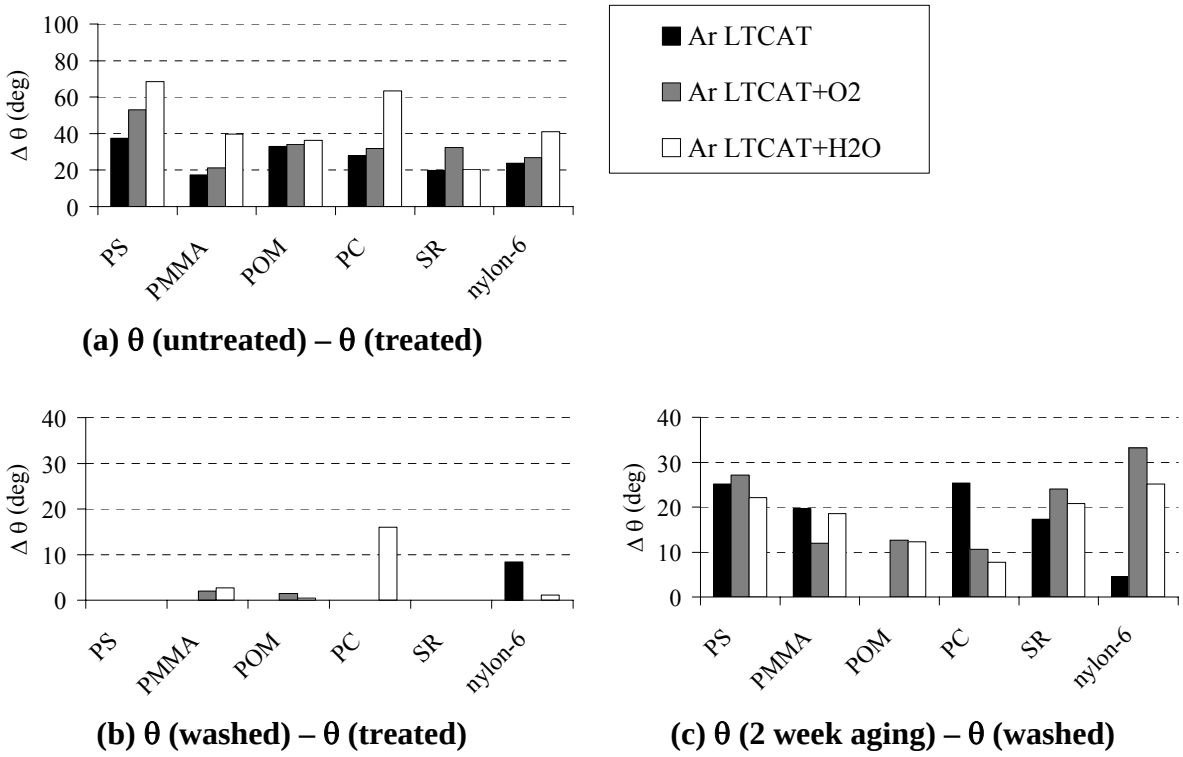

Figure 7.3. The differences in static contact angles, Δ θ, of the six types of polymers treated with Ar LTCAT (black), Ar LTCAT + 1 sccm O_2 (gray), and Ar LTCAT + 1 sccm H_2O (white) with 2 s treatment time. For (a), a higher value represents greater wettability enhancement. The degree of surface damage is evaluated in (b), in which a higher value indicates greater surface damage from LMWOM formation. The chart in (c) gives the extent of hydrophobic recovery, in which a higher value represents greater hydrophobic recovery. The other treatment conditions include 1000 sccm Ar and 4 A arc current.

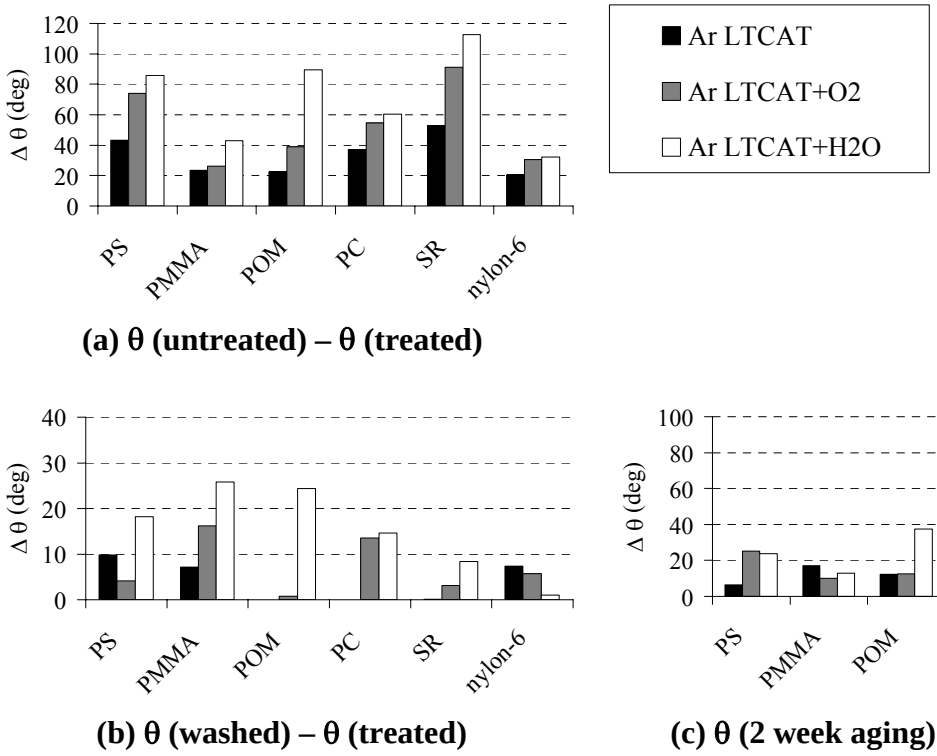

Figure 7.4. The differences in static contact angles, Δ θ, of the six types of polymers treated with Ar LTCAT (black), Ar LTCAT + 7 sccm O_2 (gray), and Ar LTCAT + 10 sccm H_2O (white) with 10 s treatment time. For (a), a higher value represents greater wettability enhancement. The degree of surface damage is evaluated in (b), in which a higher value indicates greater surface damage from LMWOM formation. The chart in (c) gives the extent of hydrophobic recovery, in which a higher value represents greater hydrophobic recovery. The other treatment conditions include 1000 sccm Ar and 4 A arc current.

From Figures 7.1-7.4, some general trends can be observed regarding the Ar LTCAT treatments and those with reactive gas addition. The Ar LTCAT treatments typically enhanced wettability of the polymers without surface damage at the lower treatment times (except for nylon-6, which was damaged by Ar LTCAT for all treatment times). The excellent surface stability that was observed for most of the polymers indicates that the CASING effect induced during Ar LTCAT treatments can occur on various polymeric surfaces. The LTCAT treatments with H_2O vapor addition were the

most effective in enhancing wettability immediately after treatment, followed by the Ar LTCAT + O_2 treatments, and then the Ar LTCAT treatments. However, the extent of surface damage on the treated polymers also followed a similar trend, in which the H_2O vapor addition induced the most surface damage, followed by O_2 addition, and then Ar LTCAT (with mostly no damage for 2 s treatment time). In most cases, increasing treatment time or reactive gas flow rate enhanced wettability, but also increased surface damage. Some of the high energy species that react with the polymer during LTCAT treatments, including ions, induce chain scission and overexposure to them can enhance the degradation effects, resulting in significant surface oligomer formation. Furthermore, the addition of oxygen-containing reactive gases enhances the reaction mechanisms that lead to the alkoxy degradation reaction in Reaction (1) and subsequent chain scission.

Although generalizations were observed regarding the effects of the LTCAT treatments on all of the polymers, the LTCAT treatments affected each polymer in a different manner and those distinctions are discussed below. PS is a polymer that has exhibited relative resistance to degradation during plasma treatments[11,13,15]. The LTCAT treatments of PS enhanced the wettability very greatly and the treated PS samples exhibited resistance to damage with shorter treatment times and lower reactive gas flow rates. Slight damage was induced on PS surfaces using longer treatment times and higher reactive gas flow rates, with moderate hydrophobic recovery in all cases.

PMMA is a polymer that degrades easily in a plasma environment[13,14]. Ar LTCAT treatments of PMMA, however, enhanced the surface wettability without surface

damage using 2 s treatment time, but hydrophobic recovery was nearly complete after 2 weeks aging for most of the conditions. Thus, for application of Ar LTCAT to PMMA, such as for adhesion to another surface, the treated PMMA should be applied immediately after surface treatment due to its short lifetime. PMMA was very sensitive to degradation using higher treatment times and addition of reactive gas, especially at greater flow rates, which induced significant surface damage.

POM can be etched into volatile species very readily in a plasma environment[5], but compared to other polymers, has shown relative resistance to the formation of LMWOM in O_2 and H_2O vapor plasmas. During LTCAT treatments, POM exhibited resistance to surface oligomer formation in Ar LTCAT and Ar LTCAT + O_2, with some surface damage induced during H_2O vapor addition treatments. No C-C bonds are present in the POM polymer chain, so the alkoxy degradation reaction does not occur. Thus, the surface oligomer formation induced during longer treatment times and higher reactive gas flow rate is due to other reaction pathways that lead to chain scission, such as effects from high energy ions. Hydrophobic recovery for POM was moderate after 2 weeks of aging in ambient air for all of the treatment conditions examined.

PC treated by Ar LTCAT exhibited enhanced wettability and surface stability, with no damage observed for all treatment times. For PC treated with Ar LTCAT with reactive gas addition, some surface damage occurred for the higher O_2 flow rates and for all of the H_2O vapor treatments. The hydrophobic recovery of LTCAT-treated PC was moderate after aging for 2 weeks in ambient air.

SR demonstrated great enhancement in wettability from LTCAT treatments using longer treatment times and higher reactive gas flow rates. Although the surface damage induced on SR was generally low, hydrophobic recovery was very high and nearly complete for all treatments, which can be seen from Figures 7.1 and 7.2. Thus, the lifetime of LTCAT treated SR is very short, which must be considered when applying LTCAT treatments to SR surfaces.

The surface of nylon-6 is hydrophilic and the LTCAT treatments lowered the contact angle even further, but not to the extent of some of the other polymers. In addition, LTCAT treatments of nylon-6 induced surface damage for most of the conditions and nearly complete hydrophobic recovery occurred after aging for 2 weeks for most of the conditions applied.

7.3.2 Wilhelmy Data Comparison of LTCAT Treated Polymers

Wilhelmy analysis was performed on each polymer treated with Ar LTCAT, Ar LTCAT + O_2, and Ar LTCAT + H_2O using the conditions chosen from the static contact angle analysis, which are given in Table 7.2. The conditions were chosen based on the enhancement of wettability achieved and the surface stability.

Table 2. Treatment Times and Reactive Gas Flow Rates of Ar LTCAT, Ar LTCAT + O_2, and Ar LTCAT + H_2O Treatments Used for Wilhelmy Analysis of the Treated Polymers. The Other Treatment Conditions Included 1000 sccm Ar and 4A Current.

	Ar LTCAT	**Ar LTCAT + O_2**		**Ar LTCAT + H_2O**	
Polymer	**treatment time (s)**	**O_2 flow rate (sccm)**	**treatment time (s)**	**H_2O flow rate (sccm)**	**treatment time (s)**
PS	2	7	2	10	2
PMMA	2	1	2	1	2
POM	2	1	2	1	2
PC	10	1	5	10	5
SR	15	2	5	1	5
Nylon-6	2	1	2	2	2

Figures 7.5-7.10 contain the Wilhelmy force loops for all 6 polymers, along with the advancing contact angles of the samples that were obtained immediately after treatment (black) and after aging in ambient air for 2 weeks (gray). Overshooting, when present, is indicated by the difference between the average force/length for subsequent cycles, Δ F/L (mN/m).

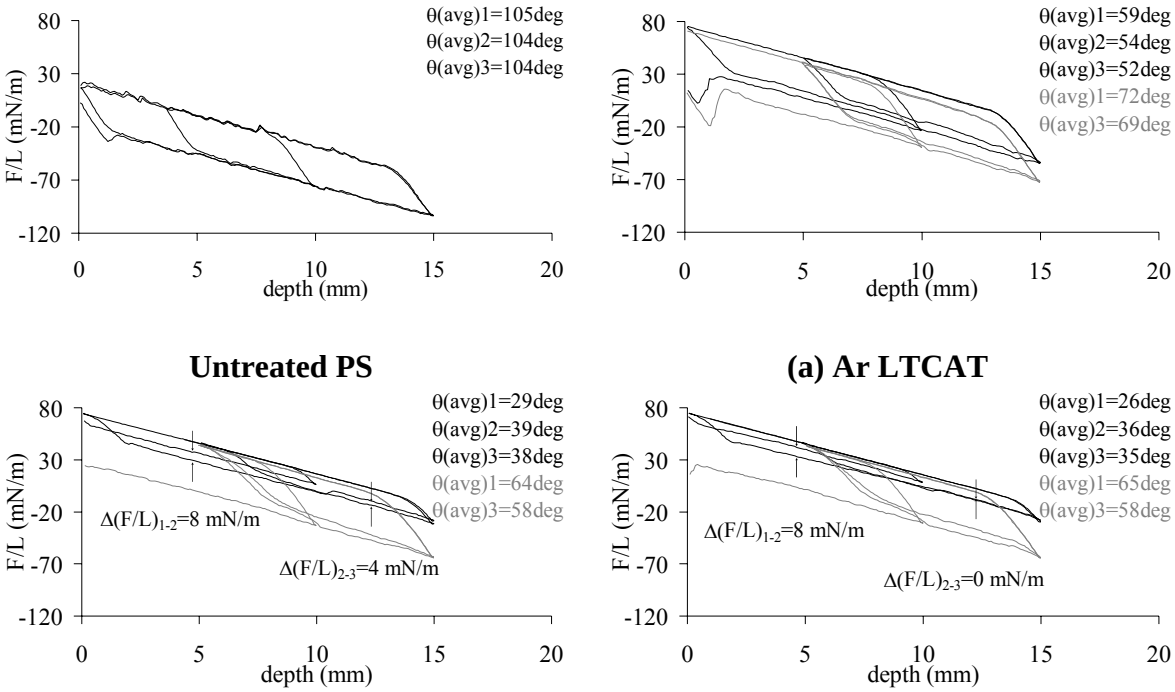

Figure 7.5. The Wilhelmy force loops of untreated PS and Ar LTCAT-treated PS with (a) no reactive gas addition, (b) O_2 addition, and (c) H_2O vapor addition. The black lines show the force loops obtained immediately after treatment and the gray lines show the force loops obtained after 2 weeks of aging in ambient air. The other treatment conditions include 1000 sccm Ar, 4 A arc current, and 2 s treatment time.

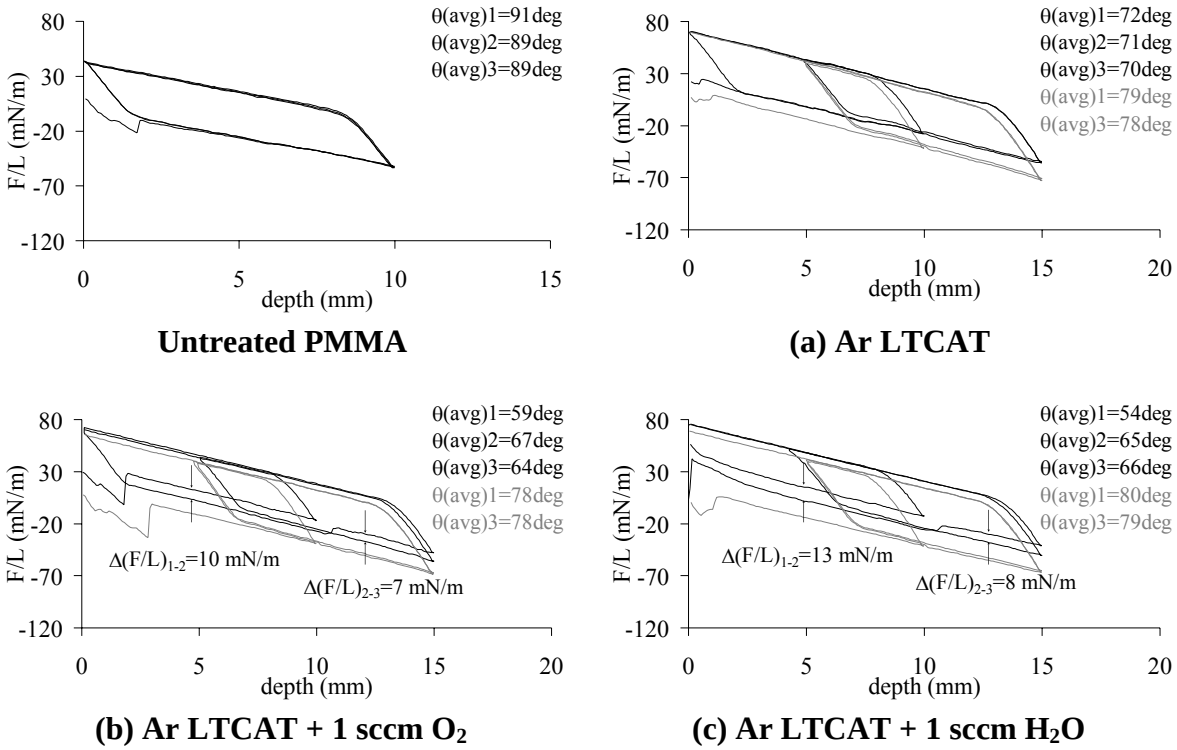

Figure 7.6. The Wilhelmy force loops of untreated PMMA and Ar LTCAT-treated PMMA with (a) no reactive gas addition, (b) O_2 addition, and (c) H_2O vapor addition. The black lines show the force loops obtained immediately after treatment and the gray lines show the force loops obtained after 2 weeks of aging in ambient air. The other treatment conditions include 1000 sccm Ar, 4 A arc current, and 2 s treatment time.

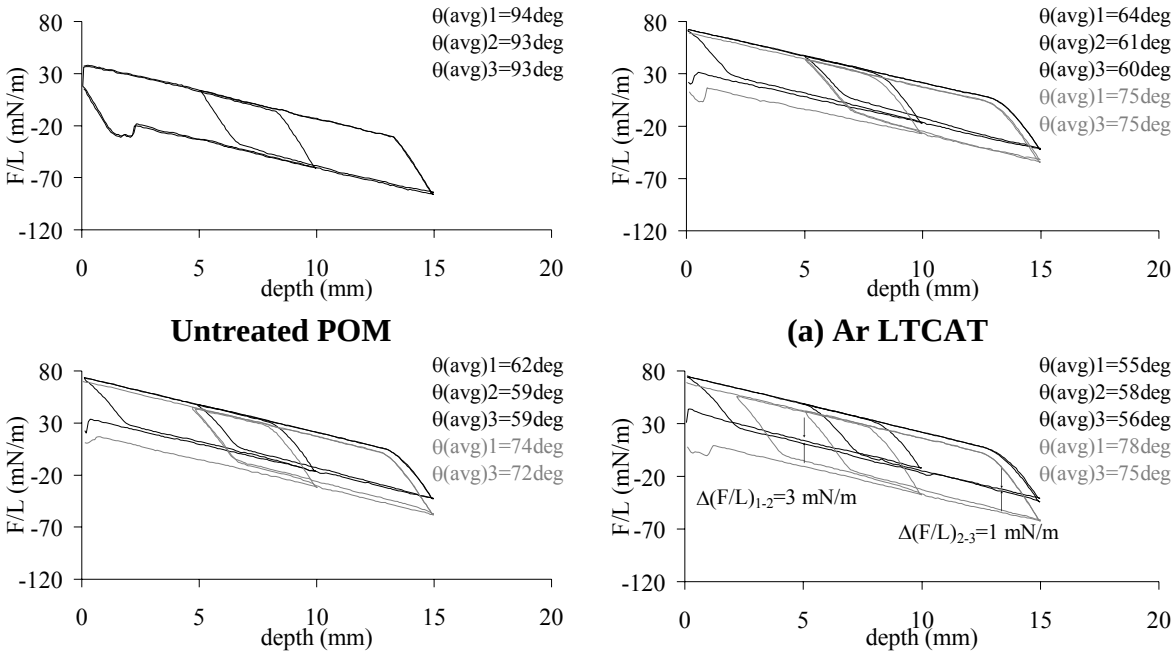

Figure 7.7. The Wilhelmy force loops of untreated POM and Ar LTCAT-treated POM with (a) no reactive gas addition, (b) O_2 addition, and (c) H_2O vapor addition. The black lines show the force loops obtained immediately after treatment and the gray lines show the force loops obtained after 2 weeks of aging in ambient air. The other treatment conditions include 1000 sccm Ar, 4 A arc current, and 2 s treatment time.

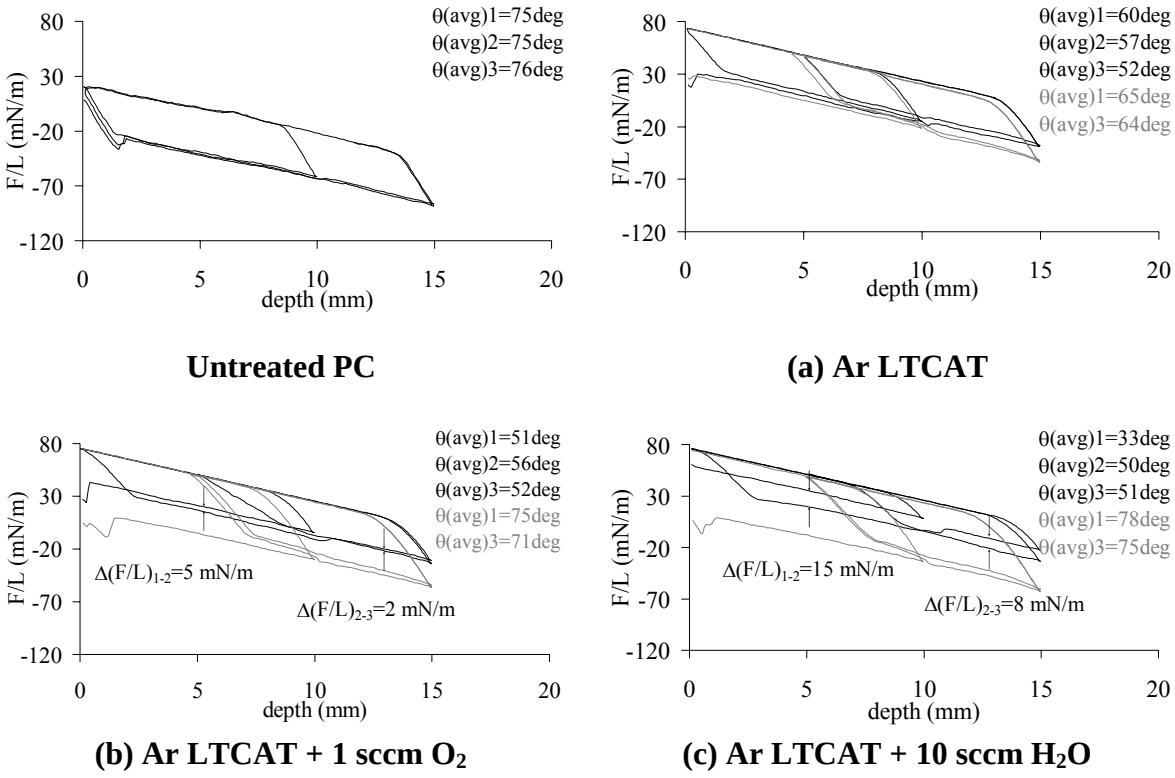

Figure 7.8. The Wilhelmy force loops of untreated PC and Ar LTCAT-treated PC with (a) no reactive gas addition and 10 s treatment time, (b) O_2 addition and 5 s treatment time, and (c) H_2O vapor addition and 5 s treatment time. The black lines show the force loops obtained immediately after treatment and the gray lines show the force loops obtained after 2 weeks of aging in ambient air. The other treatment conditions include 1000 sccm Ar and 4 A arc current.

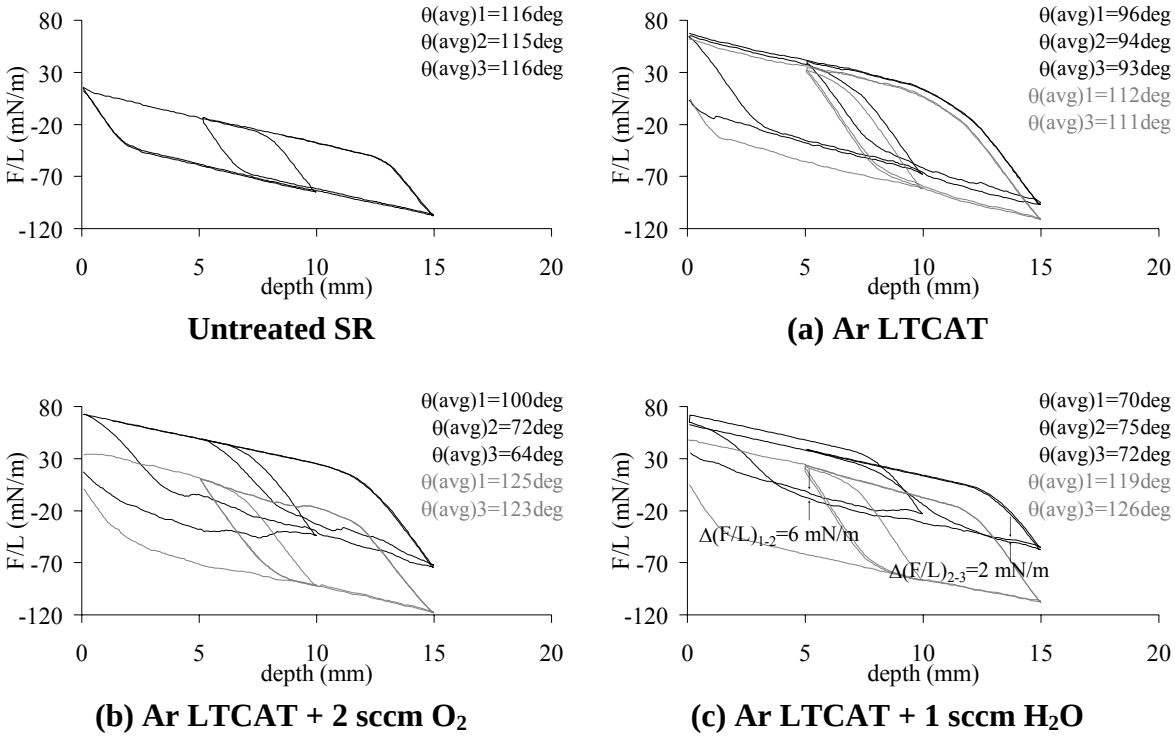

Figure 7.9. The Wilhelmy force loops of untreated SR and Ar LTCAT-treated SR with (a) no reactive gas addition and 15 s, (b) O_2 addition and 5 s, and (c) H_2O vapor addition and 5 s. The black lines show the force loops obtained immediately after treatment and the gray lines show the force loops obtained after 2 weeks of aging in ambient air. The other treatment conditions include 1000 sccm Ar and 4 A arc current.

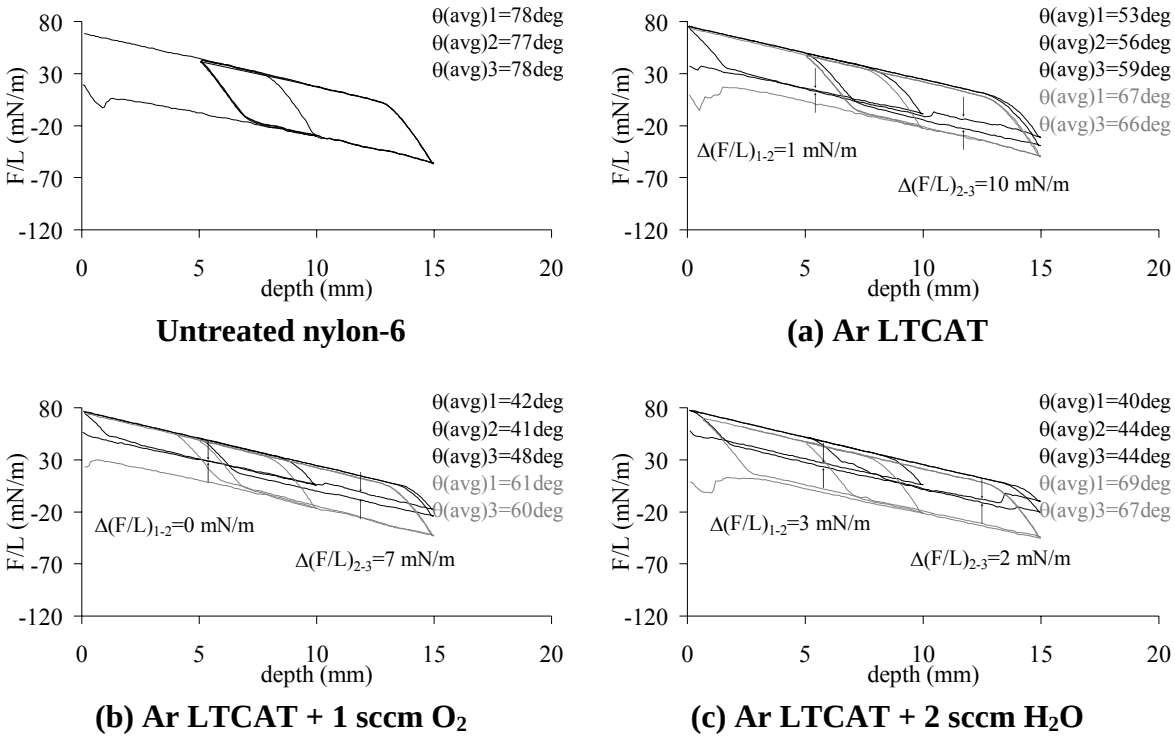

Figure 7.10. The Wilhelmy force loops of untreated nylon-6 and Ar LTCAT-treated nylon-6 with (a) no reactive gas addition, (b) O_2 addition, and (c) H_2O vapor addition. The black lines show the force loops obtained immediately after treatment and the gray lines show the force loops obtained after 2 weeks of aging in ambient air. The other treatment conditions include 1000 sccm Ar, 4 A arc current, and 2 s treatment time.

The Ar LTCAT treatments, in general, enhanced the surface wettability and produced stable surfaces with relatively low hydrophobic recovery, compared to the reactive gas addition treatments. The exception is nylon-6 in Figure 7.10, which exhibited overshooting for all treatments. Figure 7.11 contains the advancing contact angle measurements that were obtained from the Wilhelmy force loops of the untreated polymers (black), cycle 1 of the treated polymers (dark gray), cycle 2 of the treated polymers after drying in ambient air for 10 minutes (light gray), and cycle 1 of the treated polymers after aging in ambient air for 2 weeks.

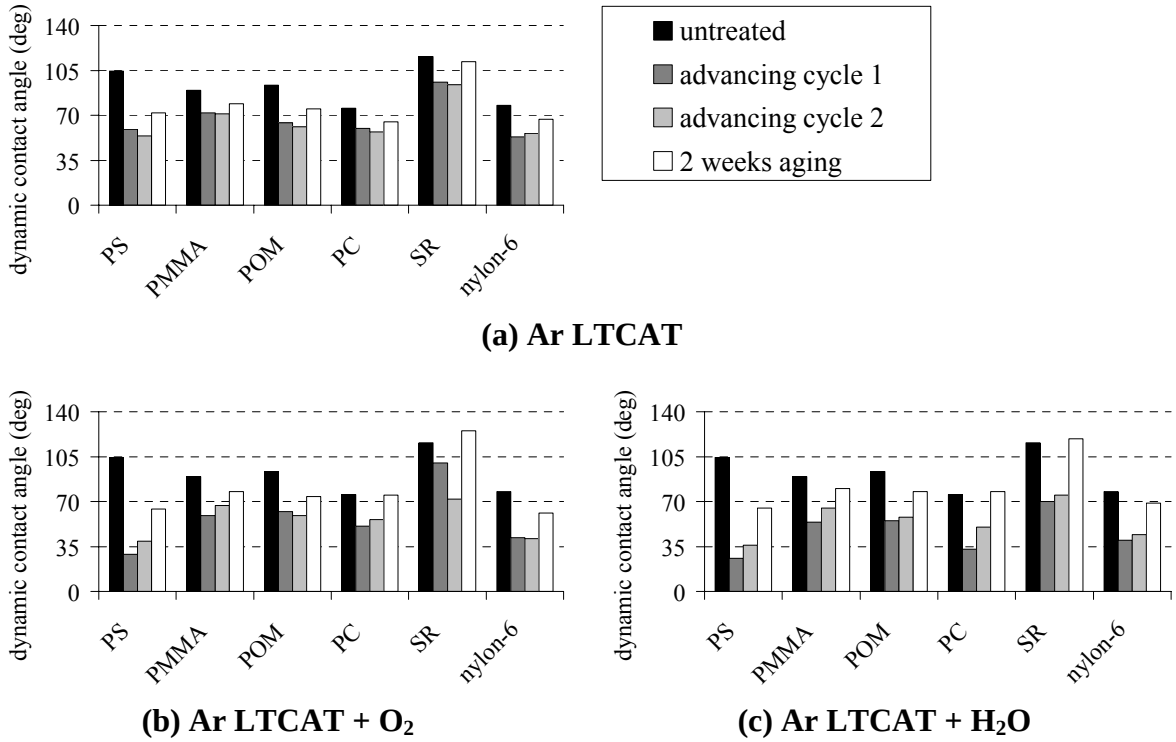

Figure 7.11. The dynamic contact angles of the six types of polymers treated with (a) Ar LTCAT, (b) Ar LTCAT + O_2, and (c) Ar LTCAT + H_2O using the conditions given in Table 7.2. Measurements were obtained from the untreated polymers (black), 1st advancing Wilhelmy cycle of the treated samples (dark gray), 2nd advancing Wilhelmy cycle after drying for 10 min (light gray), and the 1st advancing Wilhelmy cycle after aging in ambient air for 2 weeks (white). The other treatment conditions include 1000 sccm Ar and 4 A arc current.

Figure 7.12 contains a comparison of the extent of intrinsic hysteresis and overshooting that was exhibited by the treated polymers, which was calculated by subtracting the average of F/L in the advancing stage of cycle 2 from the average F/L in the advancing stage of cycle 1. Positive values indicate that intrinsic hysteresis was present due to mobility of surface moieties and negative values correspond to overshooting from washing away of surface oligomers during the first immersion.

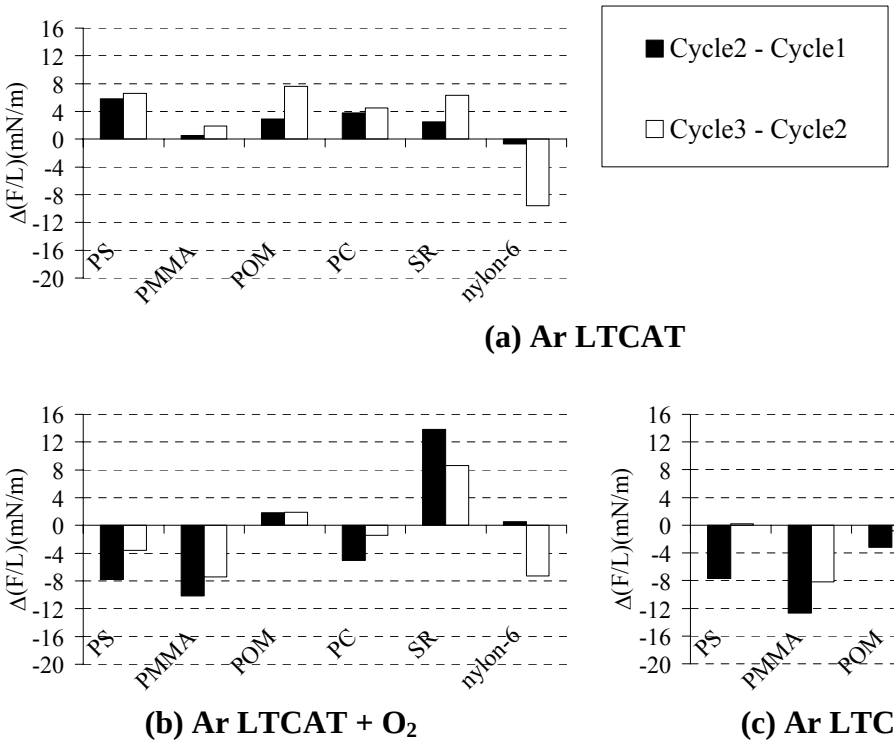

Figure 7.12. The differences in the average values of F/L (mN/m) for Wilhelmy cycles of the polymers treated with (a) Ar LTCAT, (b) Ar LTCAT + O_2, and (c) Ar LTCAT + H_2O using the conditions given in Table 7.2. The Δ(F/L) values were calculated between cycle 2 and cycle 1 (black), in which the polymer sample was allowed to dry in ambient air for 10 min between the cycles. The Δ(F/L) values between cycle 3 and cycle 2 (white) were obtained without a break in motion. A positive value represents intrinsic hysteresis, while a negative value indicates that LMWOM was removed from the treated sample surface between cycles. The other treatment conditions include 1000 sccm Ar and 4 A arc current.

Ar LTCAT-treated PS, POM, PC, and SR exhibited higher surface mobility, in comparison to the others. Interestingly, Ar LTCAT-treated PMMA exhibited the greatest surface stability without damage from oligomer formation. In a traditional plasma environment, volatile species that are ablated from the substrate can contaminate the interface and subsequently react with the substrate. In the case of PMMA, oxygen atoms that are ablated from the side-group can react with polymer chains to form alkoxy radicals and subsequently induce polymer chain scission. In LTCAT, however, the high

flux of neutral species that are directed to the polymer surface can eliminate the contamination by ablated species. Thus, treatment of PMMA by Ar LTCAT minimizes surface contamination and damage from ablated species and results in a stable surface at a lower treatment time (2 s). Nylon-6 is the only polymer in this study that exhibited overshooting during Ar LTCAT treatment.

The dynamic surface analysis results also show that the reactive gas addition treatments were more effective in increasing the polymer surface wettability, especially for H_2O vapor treatments. However, surface damage was also significantly induced by reactive gas addition and generally was highest for H_2O vapor addition. As mentioned previously, reactive gas addition can enhance LMWOM formation through the production of alkoxy radicals and subsequent chain scission. PMMA exhibited the highest overshooting for O_2 addition and the second highest for H_2O vapor addition among the treated polymers. It should be noted that the lowest reactive gas flow rates and treatment times were used for PMMA and POM, unlike the other polymers. Thus, even using very low flow rates of O_2 and H_2O, PMMA underwent significant degradation from oligomer formation. PS, which showed resistance to degradation at lower reactive gas flow rates and treatment times from the static analysis, exhibited overshooting at the higher reactive gas flow rates. Based on the static contact angle results, decreasing the reactive gas flow rates for treatment of PS decreased and eliminated the surface damage. POM showed relative resistance to degradation from LMWOM formation with reactive gas addition and exhibited no overshooting from the oxygen addition treatment. SR also showed some resistance to oligomer formation; however, the polymer is not rigid and did

not completely hold its shape during the Wilhelmy cycles. Thus, the Wilhelmy data for SR contains an added degree of error.

7.4 Conclusions

Ar LTCAT is an energetically mild and effective surface treatment technique that can be applied to various polymers to enhance wettability without surface degradation from LMWOM formation, while maintaining good surface stability. The exception in this study was nylon-6, which was damaged under all treatment conditions. The excellent wettability and surface stability was attributed to the CASING effect combined with the quenching of unreacted surface free radicals upon atmospheric exposure, which resulted in the formation of new hydrophilic functional groups anchored to stable, cross-linked surfaces. Most of the polymers exhibited some extent of surface damage at longer treatment times, which was ascribed to overexposure to high-energy species that induce chain scission and polymer degradation.

The addition of oxygen and water vapor to Ar LTCAT significantly enhanced wettability, but at the cost of greater surface damage from LMWOM formation. The enhanced surface damage was attributed to an increase in alkoxy degradation reactions from the surface reactions with oxygen-containing species, in most cases. Shorter treatment times and lower reactive gas flow rates generally resulted in a decrease in surface damage. However, each polymer exhibited different treatment effects during LTCAT treatments and the treatments should be optimized separately for each polymer and application. Hydrophobic recovery occurred to some extent on all of the polymers

treated by LTCAT. Thus, the lifetime of a treated polymer surface must be considered when applying LTCAT to any polymer.

The surface of PS was readily modified by LTCAT and was resistant to degradation at shorter treatment times and lower reactive gas flow rates. In addition, LTCAT-treated PS surfaces exhibited relatively low hydrophobic recovery. Ar LTCAT treatment of PMMA with 2 s treatment time resulted in wettability enhancement and high surface stability, as indicated by the lowest amount of intrinsic hysteresis. However, PMMA was the most susceptible to degradation with the reactive gas addition treatments. In addition, LTCAT-treated PMMA surfaces exhibited pronounced hydrophobic recovery. POM generally exhibited resistance to degradation from LMWOM formation during Ar LTCAT and Ar LTCAT + O_2 treatments, but not using Ar LTCAT + H_2O. PC had a moderate enhancement of wettability with good surface stability. SR was readily modified by LTCAT, but the treated surfaces had low lifetimes with very high hydrophobic recovery. Nylon-6 experienced surface damage from all of the LTCAT treatments.

7.5 References for Section VII

1. Ratner, B.D.; Chilkoti, A.; Lopez, G.P.; "Plasma Deposition and Treatment for Biomedical Applications" in *Plasma Deposition, Treatment, and Etching of Polymers*, R. d'Agostino ed., Academic Press, Boston (1990) 463 – 516.

2. Penn, L.S.; Wang, H.; "Chemical Modification of Polymer Surfaces: A Review", *Polymers for Advanced Technologies* **5** (1994) 809-917.

3. Wertheimer, M.R.; Martinu, L.; and Liston, E.M.; "Plasma Sources for Polymer Surface Treatment" in *Handbook of Thin Film Process Technology, Volume 2*, Glocker, D.A. ed., Institute of Physics Publishing, Bristol (2002) E3.0:1-E3.0:38.

4. Durand, A.M.; "The Practical Application of Plasma Treatment to Polymer Surfaces for Improved Adhesion", *LE VIDE, Science, Technique, et Applications* **53** (1997) 242 – 252.

5. Weikart, C.M.; Yasuda, H.K.; "Modification, Degradation, and Stability of Polymeric Surface Treated with Reactive Plasmas", *J. Polym. Sci.* A **38** (2000) 3028-3042.

6. Gilliam, M.A.; Yu, Q.; "Surface Modification of Low Density Polyethylene Using a Low-Temperature Cascade Arc Torch", *J. Appl. Polym. Sci.* **99** (2005) 2528-2541.

7. Yu, Q.S.; Reddy, C.M.; Meives, M.F.; Yasuda, H.K.; "Surface Modification of Poly(tetrafluoroethylene) by a Low-Temperature Cascade Arc Torch and Radio-Frequency Plasma", *J. Polym. Sci.: Part A: Polym. Chem.* **37** (1999) 4432 – 4441.

8. Gilliam, M.A. and Yu, Q.; "Low-Temperature Plasma Processes for Polymeric Surface Modification", an invited article to *The Encyclopedia of Chemical Processing* Lee, S., ed., in review.

9. Strobel, M.; Jones, V; Lyons, C.S.; Ulsh, M.; Kushner, M.J.; Dorai, R.; Branch, M.C.; "A Comparison of Corona-Treated and Flame-Treated Polypropylene Films", *Plasma Polym.* **8**, No. 1 (2003) 61-95.

10. Hollander, A.; Kemberg-Sapieha, J.E.; Wertheimer, M.R.; "The Influence of Vacuum Ultraviolet Radiation on Poly(ethylene Terephthalate)", *J. Polym. Sci.* A **34** (1996) 1511-1516.

11. France, R.M.; Short, R.D.; "Plasma Treatment of Polymers: The Effects of Energy Transfer from an Argon Plasma on the Surface Chemistry of Polystyrene and Polypropylene. A High-Energy Resolution X-Ray Photoelectron Spectroscopy Study", *Langmuir* **14** (1998) 4827-4835.

12. Hong, J.; Truica-Marasescu, F.; Martinu, L.; Wertheimer, M.R.; "An Investigation of Plasma-Polymer Interactions by Mass Spectrometry", *Plasma Polym.* **7** (2002) 245-260.

13. Moss, S.J.; Jolly, A.M.; Tighe, B.J.; "Plasma Oxidation of Polymers", *Plasma Chem. Plasma Process.* **6**, No. 4 (1986) 401-416.

14. Hozumi, A.; Masuda, T.; Hayashi, K.; Sugimura, H.; Takai, O.; Kameyama, T.; "Spatially Defined Surface Modification of Poly(methylmethacrylate) Using 172 nm Vacuum Ultraviolet Light", *Langmuir* **18** (2002) 9022-9027.

15. Truica-Marasescu, F.-E.; Wertheimer, M.R.; "Vacuum Ultraviolet Photolysis of Hydrocarbon Polymers", *Macromol. Chem. Phys.* **206** (2005) 744-757.

16. Yasuda, H.K.; *Luminous Chemical Vapor Deposition and Interface Engineering*, Marcel Dekker, New York (2005).

17. Chapiro, A.; *Radiation Chemistry of Polymeric Systems*, John Wiley & Sons, New York (1962).

18. Fusselman, S.P. and Yasuda, H.K.; "Particle Densities and Non-Equilibrium in a Low-Pressure Argon Plasma Jet", *Plasma Chem. Plasma Process,* **14** (1994) 251 - 275.

19. Yu, Q.S. and Yasuda, H.K.; "An Optical Emission Study on Expanding Low-Temperature Cascade Arc Plasmas", *Plasma Chem. Plasma Process.* **18** (1998) 461 - 485.

20. Gilliam, M.A.; PhD Dissertation, University of Missouri-Columbia (2006).

APPENDIX

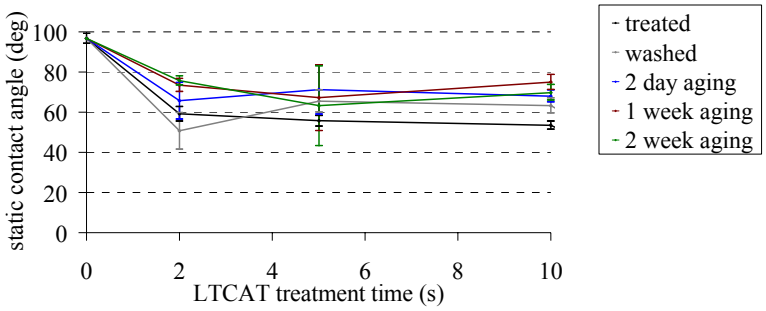

Figure A1. The static contact angle measurements of Ar LTCAT-treated PS obtained immediately after treatment (black), after washing (grey) the treated samples in DI water and allowing them to dry for 10 minutes, and after aging in ambient air for two days (blue), 1 week (red), and 2 weeks (green).

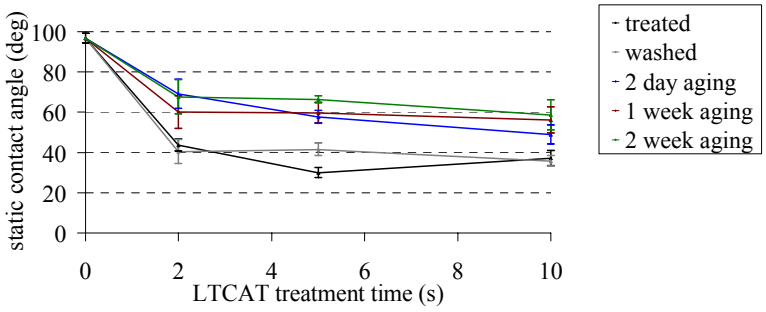

(a) 1 sccm O_2

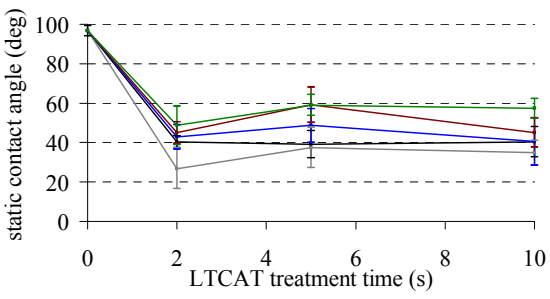

(b) 2 sccm O_2

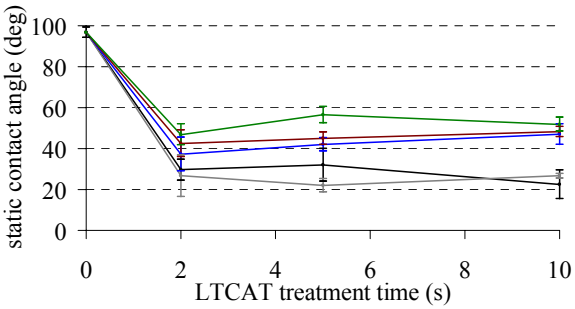

(c) 7 sccm O_2

Figure A2. The static contact angle measurements of Ar LTCAT-treated PS with O_2 addition obtained immediately after treatment (black), after washing (grey) the treated samples in DI water and allowing them to dry for 10 minutes, and after aging in ambient air for two days (blue), 1 week (red), and 2 weeks (green). The oxygen flow rate was varied at 1 sccm (a), 2 sccm (b), and 7 sccm (c).

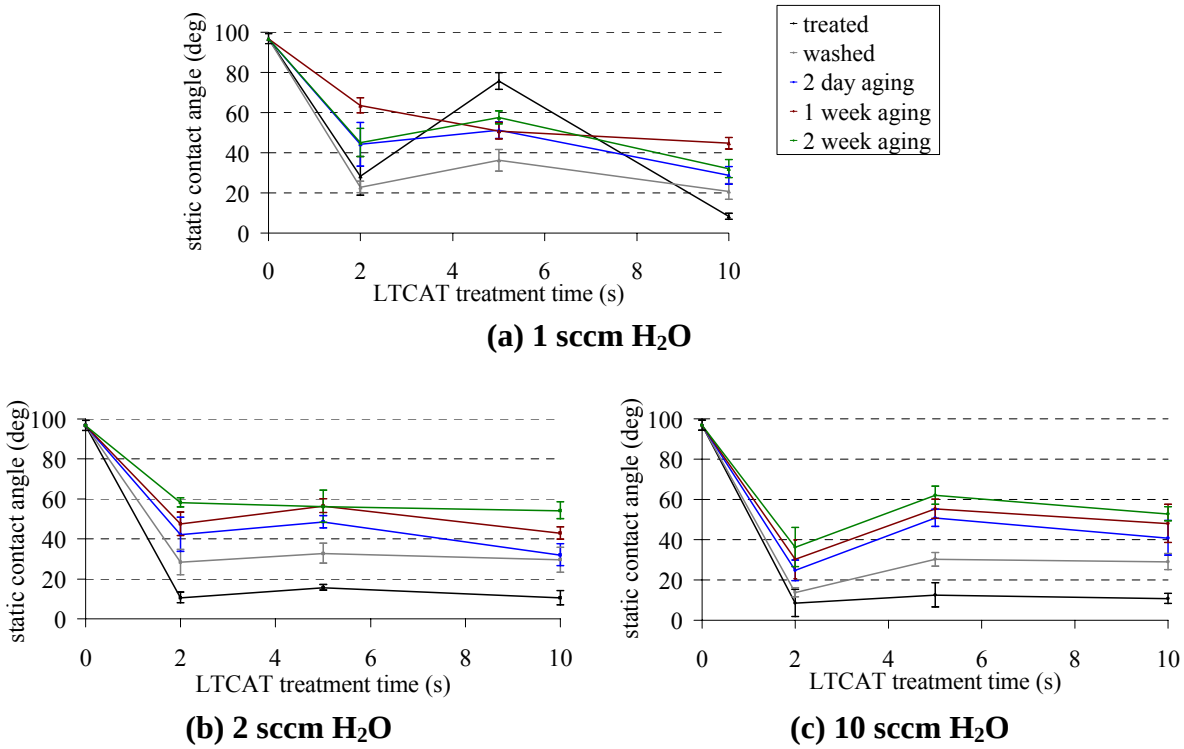

Figure A3. The static contact angle measurements of Ar LTCAT-treated PS with H_2O addition obtained immediately after treatment (black), after washing (grey) the treated samples in DI water and allowing them to dry for 10 minutes, and after aging in ambient air for two days (blue), 1 week (red), and 2 weeks (green). he water vapor flow rate was varied at 1 sccm (a), 2 sccm (b), and 10 sccm (c).

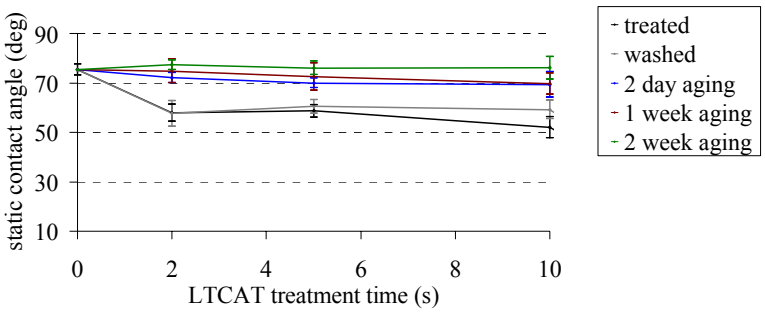

Figure A.4. The static contact angle measurements of Ar LTCAT-treated PMMA obtained immediately after treatment (black), after washing (grey) the treated samples in DI water and allowing them to dry for 10 minutes, and after aging in ambient air for two days (blue), 1 week (red), and 2 weeks (green).

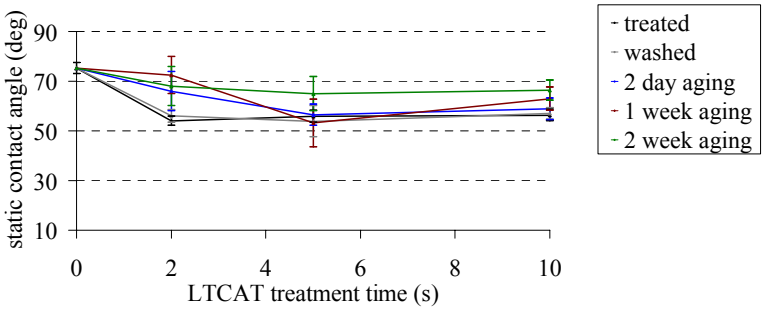

(a) 1 sccm O_2

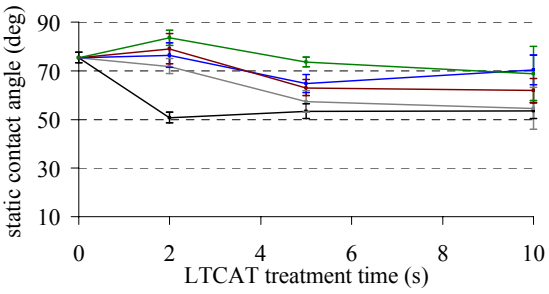

(b) 2 sccm O_2

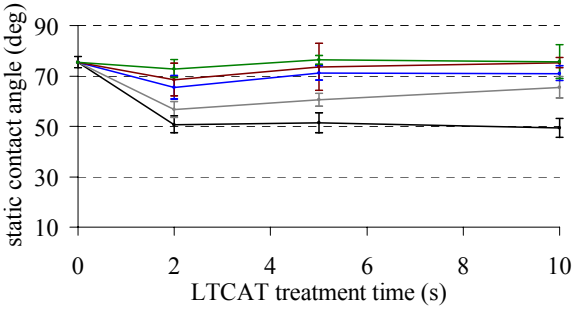

(c) 7 sccm O_2

Figure A.5. The static contact angle measurements of Ar LTCAT-treated PMMA with O_2 addition obtained immediately after treatment (black), after washing (grey) the treated samples in DI water and allowing them to dry for 10 minutes, and after aging in ambient air for two days (blue), 1 week (red), and 2 weeks (green). The oxygen flow rate was varied at 1 sccm (a), 2 sccm (b), and 7 sccm (c).

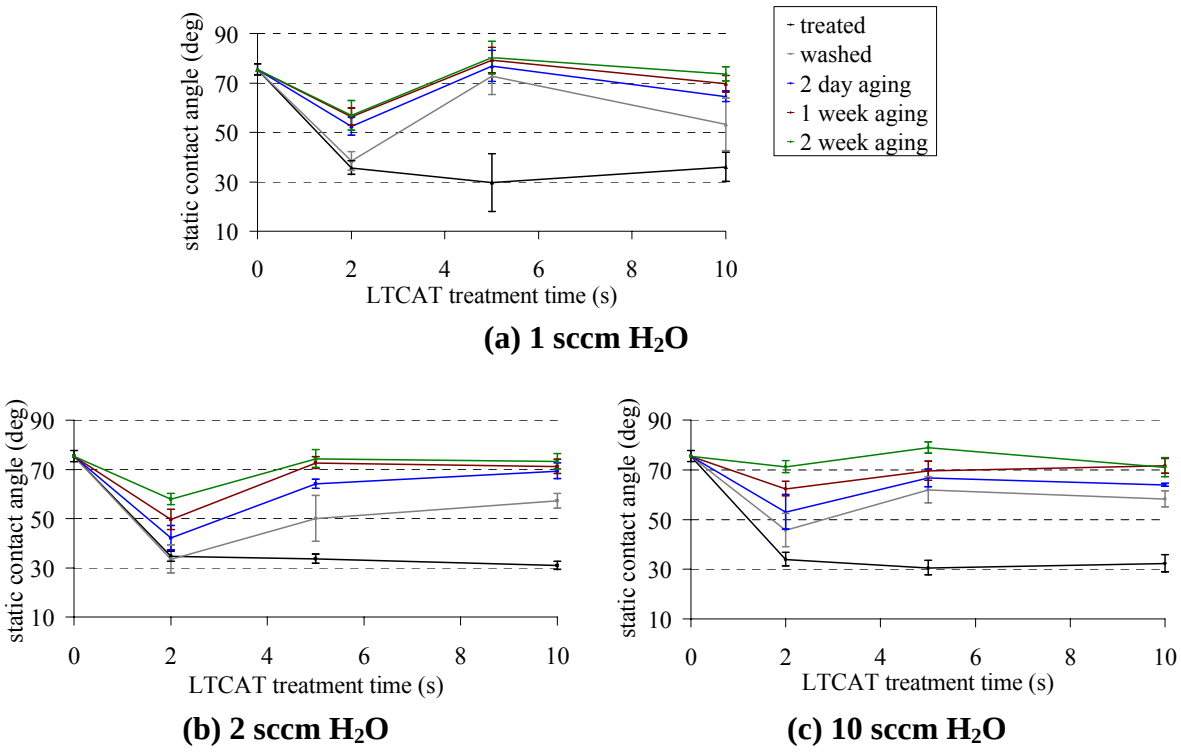

Figure A.6. The static contact angle measurements of Ar LTCAT-treated PMMA with H_2O addition obtained immediately after treatment (black), after washing (grey) the treated samples in DI water and allowing them to dry for 10 minutes, and after aging in ambient air for two days (blue), 1 week (red), and 2 weeks (green). he water vapor flow rate was varied at 1 sccm (a), 2 sccm (b), and 10 sccm (c).

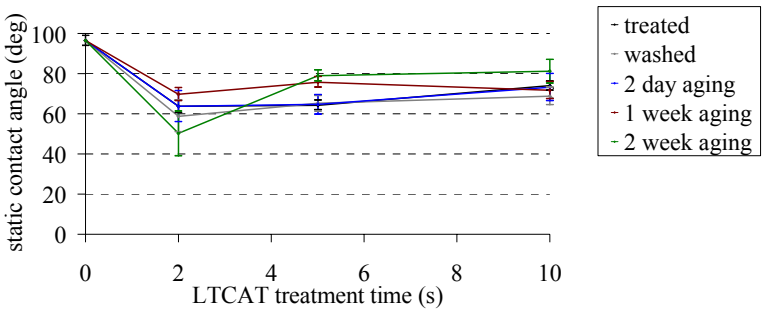

Figure A.7. The static contact angle measurements of Ar LTCAT-treated POM obtained immediately after treatment (black), after washing (grey) the treated samples in DI water and allowing them to dry for 10 minutes, and after aging in ambient air for two days (blue), 1 week (red), and 2 weeks (green).

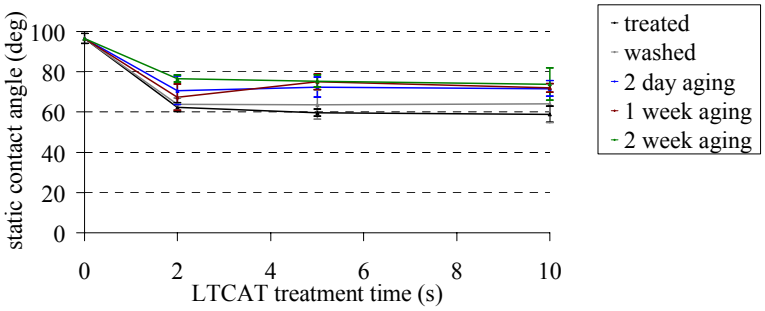

(a) 1 sccm O_2

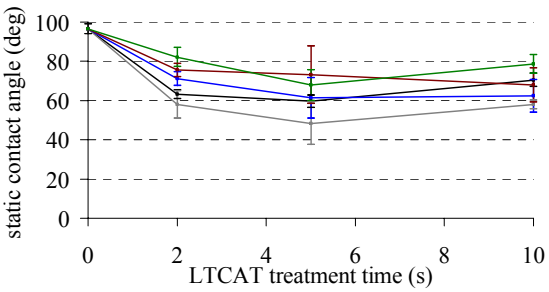

(b) 2 sccm O_2

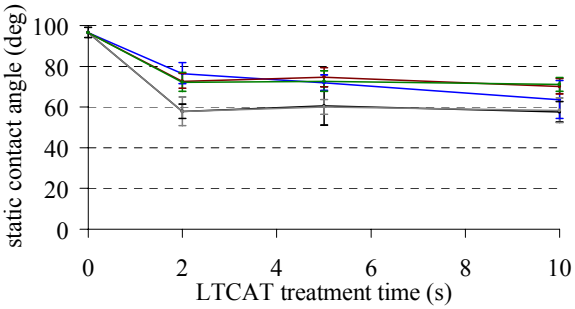

(c) 7 sccm O_2

Figure A.8. The static contact angle measurements of Ar LTCAT-treated POM with O_2 addition obtained immediately after treatment (black), after washing (grey) the treated samples in DI water and allowing them to dry for 10 minutes, and after aging in ambient air for two days (blue), 1 week (red), and 2 weeks (green). The oxygen flow rate was varied at 1 sccm (a), 2 sccm (b), and 7 sccm (c).

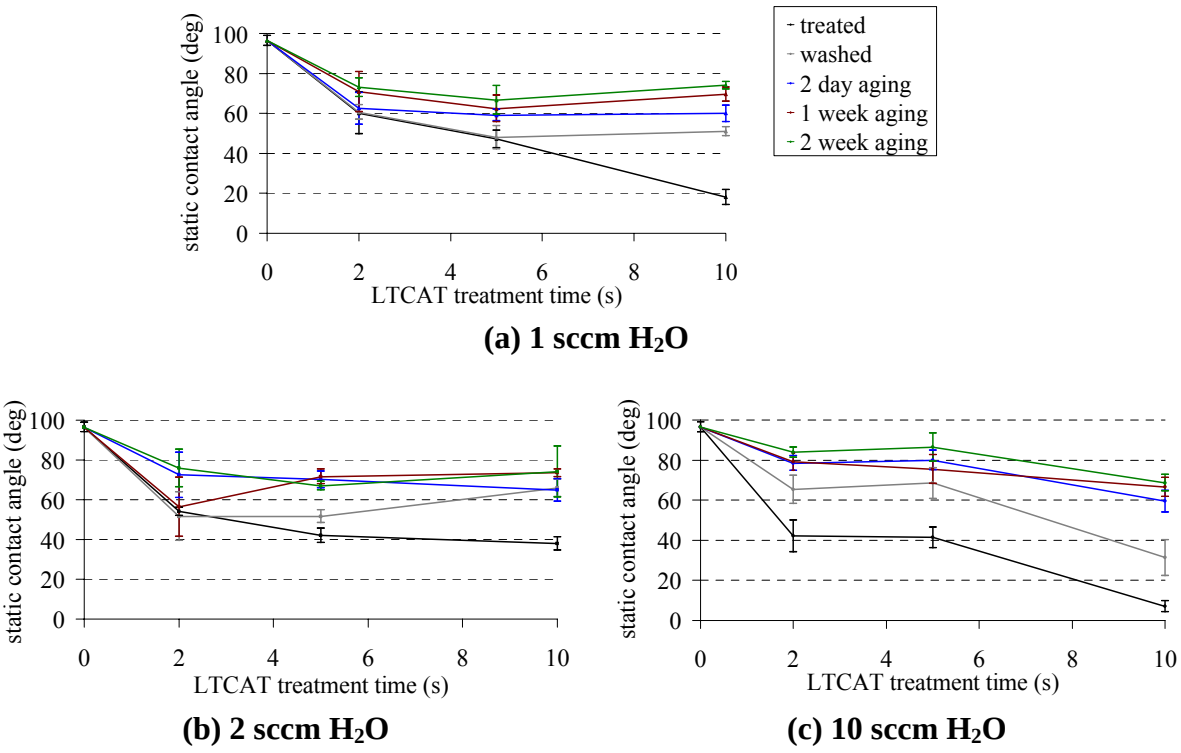

Figure A.9. The static contact angle measurements of Ar LTCAT-treated POM with H_2O addition obtained immediately after treatment (black), after washing (grey) the treated samples in DI water and allowing them to dry for 10 minutes, and after aging in ambient air for two days (blue), 1 week (red), and 2 weeks (green). The water vapor flow rate was varied at 1 sccm (a), 2 sccm (b), and 10 sccm (c).

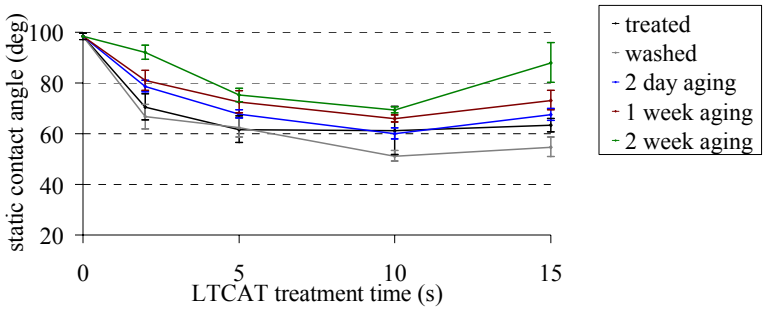

Figure A.10. The static contact angle measurements of Ar LTCAT-treated PC obtained immediately after treatment (black), after washing (grey) the treated samples in DI water and allowing them to dry for 10 minutes, and after aging in ambient air for two days (blue), 1 week (red), and 2 weeks (green).

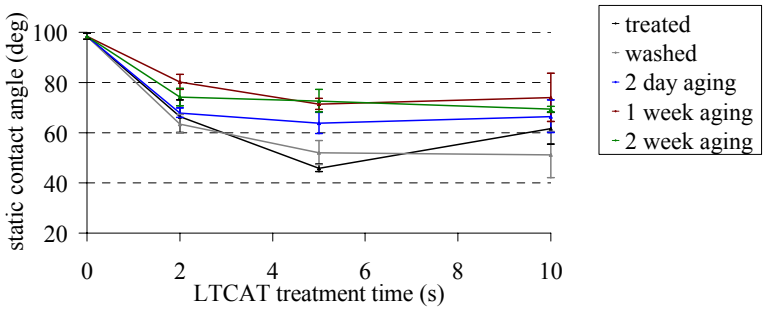

(a) 1 sccm O_2

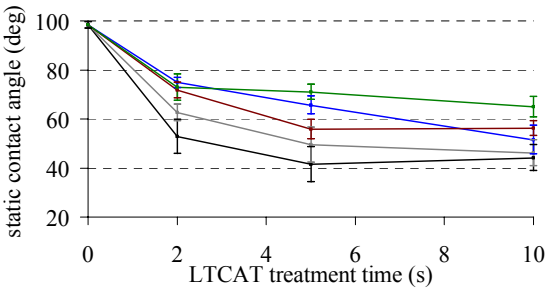

(b) 2 sccm O_2

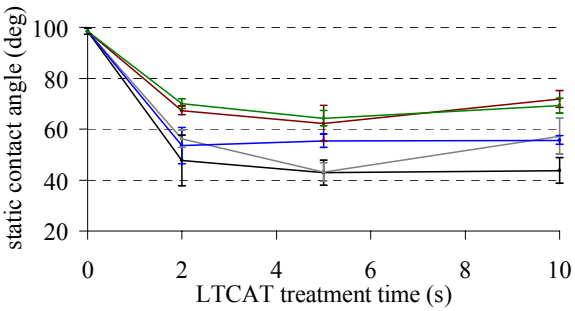

(c) 7 sccm O_2

Figure A.11. The static contact angle measurements of Ar LTCAT-treated PC with O_2 addition obtained immediately after treatment (black), after washing (grey) the treated samples in DI water and allowing them to dry for 10 minutes, and after aging in ambient air for two days (blue), 1 week (red), and 2 weeks (green). The oxygen flow rate was varied at 1 sccm (a), 2 sccm (b), and 7 sccm (c).

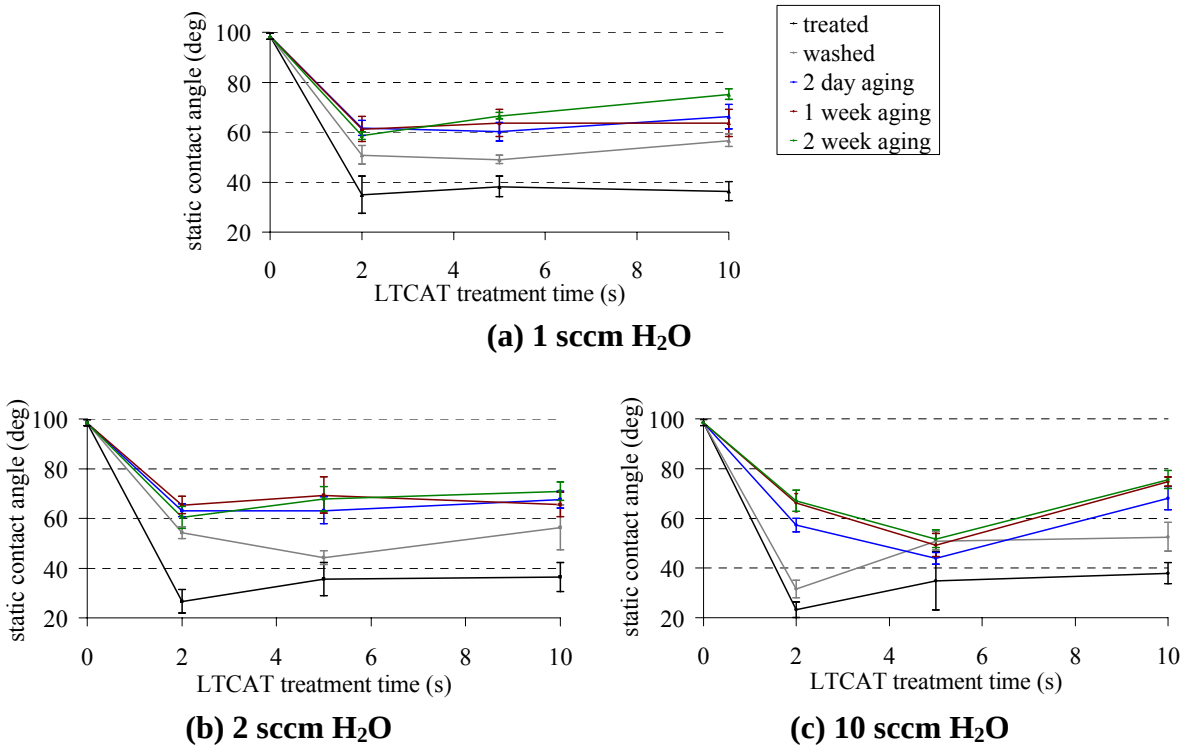

Figure A.12. The static contact angle measurements of Ar LTCAT-treated PC with H_2O addition obtained immediately after treatment (black), after washing (grey) the treated samples in DI water and allowing them to dry for 10 minutes, and after aging in ambient air for two days (blue), 1 week (red), and 2 weeks (green). The water vapor flow rate was varied at 1 sccm (a), 2 sccm (b), and 10 sccm (c).

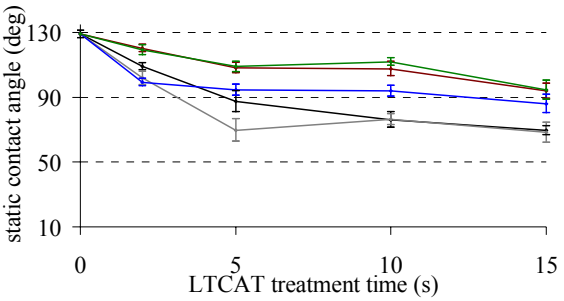

Figure A.13. The static contact angle measurements of Ar LTCAT-treated SR obtained immediately after treatment (black), after washing (grey) the treated samples in DI water and allowing them to dry for 10 minutes, and after aging in ambient air for two days (blue), 1 week (red), and 2 weeks (green).

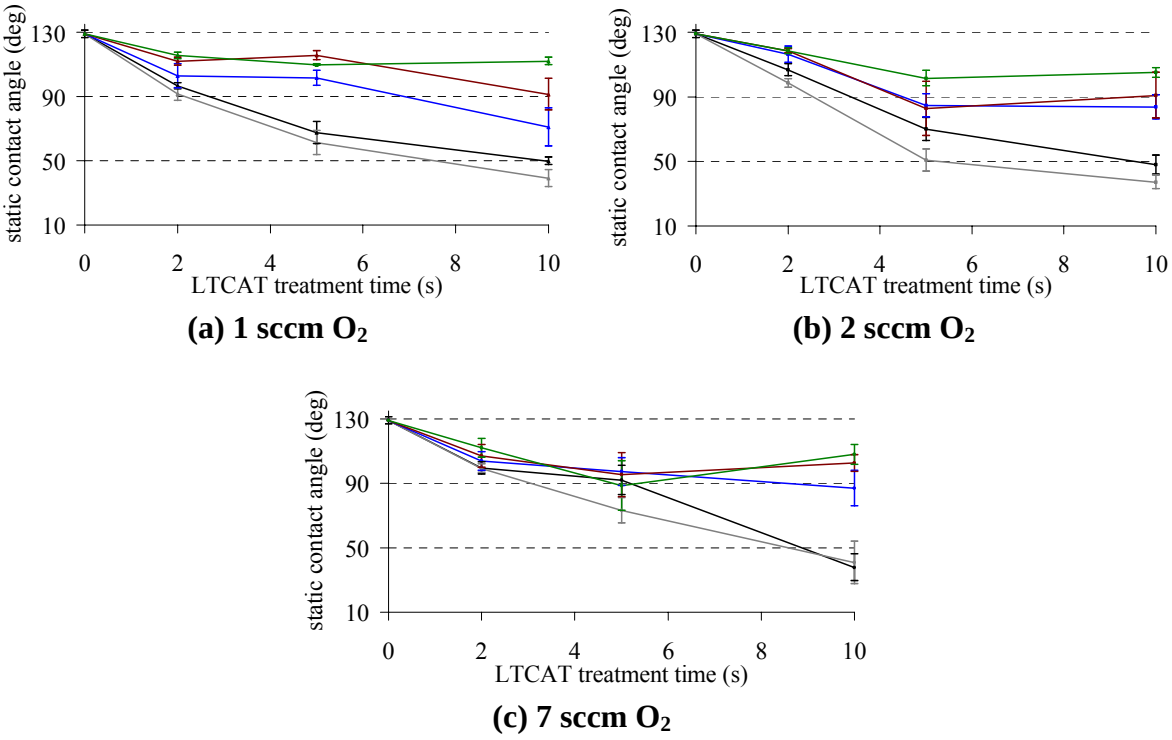

Figure A.14. The static contact angle measurements of Ar LTCAT-treated SR with O_2 addition obtained immediately after treatment (black), after washing (grey) the treated samples in DI water and allowing them to dry for 10 minutes, and after aging in ambient air for two days (blue), 1 week (red), and 2 weeks (green). The oxygen flow rate was varied at 1 sccm (a), 2 sccm (b), and 7 sccm (c).

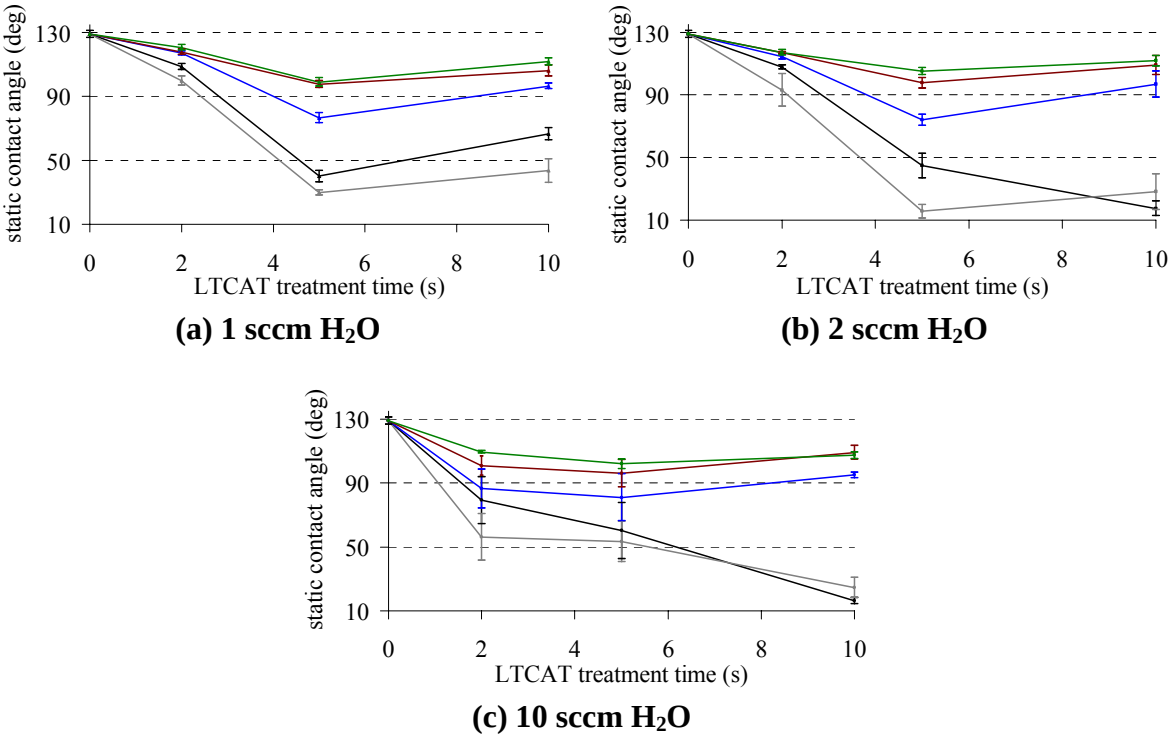

Figure A.15 The static contact angle measurements of Ar LTCAT-treated SR with H_2O addition obtained immediately after treatment (black), after washing (grey) the treated samples in DI water and allowing them to dry for 10 minutes, and after aging in ambient air for two days (blue), 1 week (red), and 2 weeks (green). he water vapor flow rate was varied at 1 sccm (a), 2 sccm (b), and 10 sccm (c).

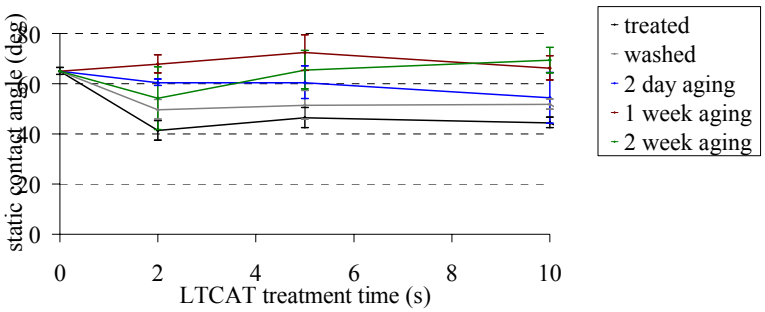

Figure A.16. The static contact angle measurements of Ar LTCAT-treated nylon-6 obtained immediately after treatment (black), after washing (grey) the treated samples in DI water and allowing them to dry for 10 minutes, and after aging in ambient air for two days (blue), 1 week (red), and 2 weeks (green).

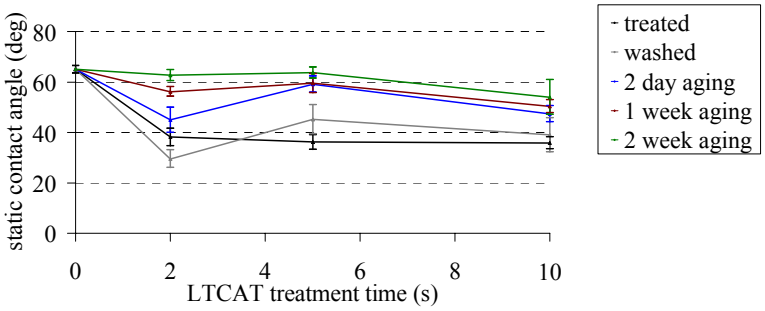

(a) 1 sccm O_2

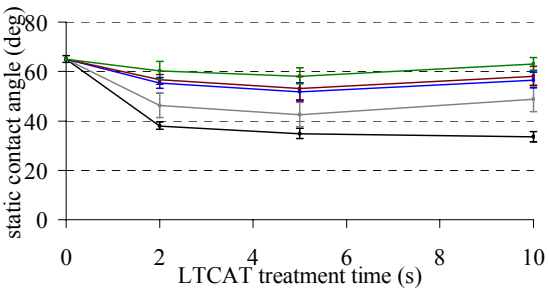

(b) 2 sccm O_2

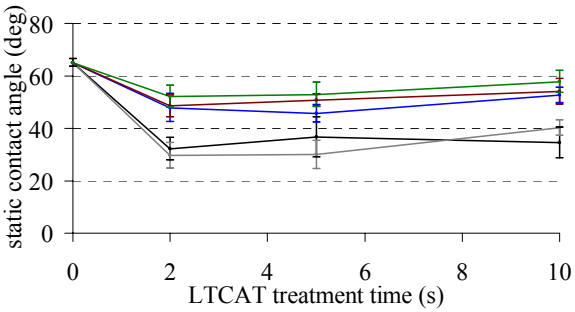

(c) 7 sccm O_2

Figure A.17. The static contact angle measurements of Ar LTCAT-treated nylon-6 with O_2 addition obtained immediately after treatment (black), after washing (grey) the treated samples in DI water and allowing them to dry for 10 minutes, and after aging in ambient air for two days (blue), 1 week (red), and 2 weeks (green). The oxygen flow rate was varied at 1 sccm (a), 2 sccm (b), and 7 sccm (c).

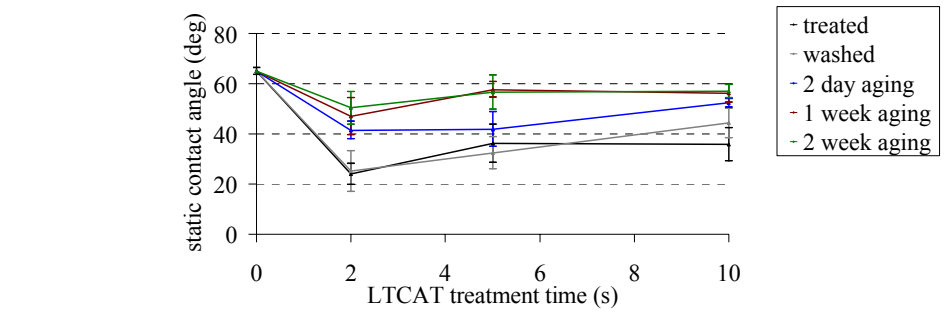

(a) 1 sccm H_2O

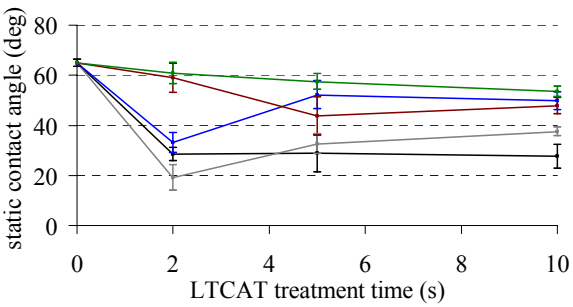

(b) 2 sccm H_2O

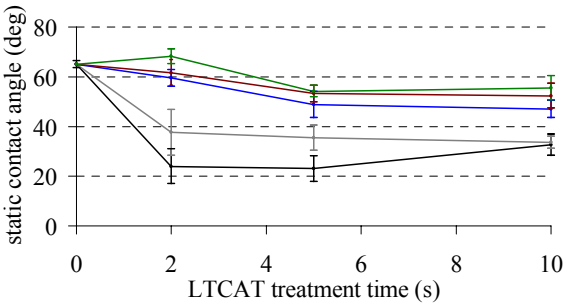

(c) 10 sccm H_2O

Figure A.18 The static contact angle measurements of Ar LTCAT-treated nylon-6 with H_2O addition obtained immediately after treatment (black), after washing (grey) the treated samples in DI water and allowing them to dry for 10 minutes, and after aging in ambient air for two days (blue), 1 week (red), and 2 weeks (green). The water vapor flow rate was varied at 1 sccm (a), 2 sccm (b), and 10 sccm (c).

VITA

Mary Gilliam was born on June 5th 1978 in St. Louis, Missouri, USA. She started undergraduate studies in 1996 at the University of Missouri-Columbia and completed an internship at Anheuser Busch Companies, Inc. from January 2000 – August 2000. In 2001, she received a Bachelor of Science degree in Chemical Engineering from the University of Missouri-Columbia. She received a PhD degree in Chemical Engineering in 2006. In August 2006, she will begin working at Exatec, LLC, a joint venture company owned by General Electric Company and Bayer Corporation.